

## Stress relaxation of near-critical gels

Kurt Broderix,\* Timo Aspelmeier, Alexander K. Hartmann, and Annette Zippelius

*Institute for Theoretical Physics, University of Göttingen, Bunsenstrasse 9, 37073 Göttingen, Germany*

(Received 23 November 2000; published 19 July 2001)

The time-dependent stress relaxation for a Rouse model of a cross-linked polymer melt is completely determined by the spectrum of eigenvalues of the connectivity matrix. The latter has been computed analytically for a mean-field distribution of cross-links. It shows a Lifshitz tail for small eigenvalues and all concentrations below the percolation threshold, giving rise to a stretched exponential decay of the stress relaxation function in the sol phase. At the critical point the density of states is finite for small eigenvalues, resulting in a logarithmic divergence of the viscosity and an algebraic decay of the stress relaxation function. Numerical diagonalization of the connectivity matrix supports the analytical findings and has furthermore been applied to cluster statistics corresponding to random bond percolation in two and three dimensions.

DOI: 10.1103/PhysRevE.64.021404

PACS number(s): 82.70.Gg, 64.60.Ht, 83.80.Sg

### I. INTRODUCTION

The most striking observation in near-critical gels is the anomalous stress relaxation [1] that precedes the transformation of the viscous fluid into an elastic amorphous solid, i.e., the gelation transition. Here, polymer systems are considered, where the viscoelastic behavior is controlled by the concentration  $c$  of cross-links connecting monomers of different molecules. At a critical concentration  $c_{\text{crit}}$  the gelation transition occurs. Viscoelastic studies by several groups have revealed the following characteristic features of stress relaxation. (1) In the sol phase, well below the gelation transition, one observes a stretched exponential decay of the stress relaxation function  $\chi(t) \sim \exp[-(t/\tau^*)^\beta]$ . (2) The time scale  $\tau^* \sim \epsilon^{-z}$  diverges as the critical point is approached. Here  $\epsilon = (c_{\text{crit}} - c)/c_{\text{crit}}$  denotes the distance from the critical point. (3) The viscosity  $\eta$ , which is given as the integral over the stress relaxation function, diverges as  $\eta \sim \epsilon^{-k}$  as the critical point is approached. (4) At the critical point, stress relaxation is algebraic in time:  $\chi(t) \sim t^{-\Delta}$ .

Whereas the stretched exponential decay is characteristic of the sol phase and holds for all cross-link concentrations  $c < c_{\text{crit}}$ , the last three observations refer to critical behavior, as the gel point is approached. If dynamic scaling holds, these findings can be cast in a scaling ansatz for the stress relaxation function  $\chi(\epsilon, t)$ , which depends on time and distance from the critical point  $\epsilon$ ,

$$\chi(c, t) = \epsilon^{z-k} g(t/\tau^*(\epsilon)) \quad (1)$$

with  $\tau^* \sim \epsilon^{-z}$ . Given a certain distance  $\epsilon$  from the gel point, one expects to see a crossover from an algebraic decay at intermediate times to a stretched exponential decay at asymptotically large times. The scaling ansatz implies  $\Delta = (z-k)/z$ . Dynamic scaling as implied by Eq. (1) is well confirmed experimentally [2] for the intermediate time regime where  $\chi(t)$  decays like a power law. However, the values for the exponents scatter considerably. Martin *et al.* [3] and Adolf and Martin [2] find  $\Delta = 0.7 \pm 0.05$  in agreement with the value  $\Delta = 0.7 \pm 0.02$  of Durand *et al.* [4], whereas

Winter and co-workers [5] observe a wide range of exponent values  $0.2 \leq \Delta \leq 0.9$ , depending on molecular weight and stoichiometry. The experimental support for a universal stretched exponential law is weak. Whereas Martin *et al.* confirm the stretched exponential decay and quote  $\beta \approx 0.4$  [3], other studies reveal nonuniversal exponents  $\beta$ . The divergence of the time scale  $\tau^* \sim \epsilon^{-z}$  in the scaling function was determined in viscoelastic measurements as  $z = 3.9 \pm 0.2$  [3,2] and deduced from static measurements of the shear modulus as  $z = 4.0 \pm 0.6$  [6]. The experimental values for  $k$ , the critical exponent of the viscosity, vary in the range  $0.7 \leq k \leq 1.4$ . The origin of the scatter in the experimental data is not clear. One possible explanation is the size of the critical region, which is known to depend on the degree of polymerization. Hence experiments with different samples have to cope with different sizes of the critical region and possibly strong crossover effects.

In this paper we study the simplest dynamic model—Rouse dynamics—in the presence of a time-dependent shear flow by means of analytical calculations and numerical simulations. Within this model, the frequency-dependent stress relaxation is completely determined by the spectral properties of the connectivity matrix  $\Gamma$ , which specifies which monomers are cross-linked. As a function of the total concentration of cross-links  $c$ , one observes in general a percolation transition at a critical concentration  $c_{\text{crit}}$ , such that for  $c < c_{\text{crit}}$  no macroscopic clusters of connected particles exist, whereas for  $c > c_{\text{crit}}$  the system percolates. In the context of gelation the fraction of sites in the macroscopic cluster has been identified with the gel fraction and the percolation transition has been shown to mark the onset of solidification [7].

The connectivity matrix  $\Gamma$  is a positive semidefinite, random matrix, which has been studied in various contexts, e.g., diluted ferromagnets, diffusion in sparsely connected spaces [8], anomalous relaxation in glassy systems, and localization [9]. In all cases the system consists of  $N$  vertices (monomers in the context of gelation) which are connected by  $cN$  edges (cross-links). A given realization of the connectivity matrix can be decomposed into connected components or clusters. Each cluster has one zero eigenvalue that describes the diffusive motion of the center of mass of the cluster. The remaining nonzero eigenvalues determine the stress relaxation function and are discussed in this paper. In the simplest case

\*Deceased.

(mean field) one chooses the edges independently out of all possible  $N(N-1)/2$  edges. The density of eigenvalues can be computed analytically for the above simple distribution and has been discussed in Refs. [8,9] in the percolating regime, i.e.,  $c \geq c_{\text{crit}}$ . In this paper we focus on the range  $c \leq c_{\text{crit}}$ , which corresponds to the sol phase and the critical point. For cross-links of unit strength the spectrum of  $\Gamma$  is shown to consist of  $\delta$  functions only, whereas it is smooth for fluctuating cross-link strength. In both cases the spectrum goes to zero for small eigenvalues as a Lifshitz singularity for all  $c < c_{\text{crit}}$ . The spectrum determines the time-dependent stress relaxation function  $\chi(t)$ . All characteristic features of  $\chi(t)$  as discussed in the first paragraph above are reproduced by the mean-field model. The stretched exponential decay for long times can be traced back to the Lifshitz singularity of the spectrum for small eigenvalues. At the critical point, the spectrum approaches a finite value for small eigenvalues, giving rise to a logarithmic divergence of the static shear viscosity in agreement with previous studies. In mean-field theory the exponents are found to be  $\beta=1/3$ ,  $\Delta=1$ , and  $z=3$ . These results have been confirmed by numerical diagonalization of the connectivity matrix  $\Gamma$ .

The last approach can be extended to finite-dimensional connectivities, corresponding to two- and three-dimensional percolation. The stress relaxation function is found to decay algebraically at the critical point, i.e.,  $\chi(t) \sim t^{-\Delta}$  with  $\Delta \approx 0.74$  ( $d=2$ ) and  $\Delta \approx 0.83$  ( $d=3$ ). In the sol phase one observes a crossover from algebraic decay at intermediate times to stretched exponential decay at long times. The numerically determined spectra can also be used to compute the static shear viscosity. We find for the critical exponent  $k \approx 1.19$  ( $d=2$ ) and  $k=0.75$  ( $d=3$ ). These values are in reasonable agreement with a scaling relation [10] based on an exact correspondence between the viscosity and the resistance of a random resistor network. Using high precision data [11,12] for the conductivity exponent of the latter, one obtains  $k \approx 1.17$  ( $d=2$ ) and  $k \approx 0.71$  ( $d=3$ ).

The paper is organized as follows. In the following section (Sec. II) we introduce the dynamic model and the observables that we want to discuss and that can be related to the spectrum of eigenvalues of the connectivity matrix. In Sec. III we present the analytical calculations for the mean-field distribution of cross-links. We briefly review the derivation of a self-consistent equation for the spectrum, which was previously given by Bray and Rodgers [8]. We then go on to discuss the appearance of Lifshitz tails for small eigenvalues. For cross-links of unit strength the spectrum is shown to consist of a countable set of  $\delta$  peaks. We present an analytical scheme to systematically compute the spectrum by iteration. We also consider cross-links of fluctuating strength, for which the spectrum is continuous and can be obtained by standard numerical means from the self-consistent integral equation. In Sec. IV we present results from a numerical diagonalization of random connectivity matrices. We first compute the spectrum for a mean-field distribution of cross-links and compare it to the analytical results. Next, cluster distributions of random bond percolation in two and three dimensions are considered. Data for the stress relaxation function are presented as well as finite-size scaling plots for

the static shear viscosity. We summarize our results in Sec. V. Some detailed calculations have been deferred to Appendixes.

Our paper is an extension of previous work, in which we discussed the static shear viscosity [10,13] and self-diffusion [14] in the sol phase as well as at the gelation transition. There it was shown that the long time limit of the incoherent scattering function is determined by the zero eigenvalues of the connectivity matrix, and the static shear viscosity is determined by the trace of the Moore-Penrose inverse of the connectivity matrix. Here we focus on the *full* spectrum of eigenvalues, which also determines the decay of the stress relaxation at *finite* times.

## II. MODEL AND OBSERVABLES

We consider a system of  $N$  identical Brownian particles, each characterized by its time-dependent position vector  $\mathbf{R}_i(t)$  ( $i=1, \dots, N$ ) in  $d$ -dimensional space of volume  $V$ , i.e., with density  $\rho=N/V$ .  $M$  permanent cross-links are introduced between randomly chosen pairs of particles  $(i_e, i'_e)$ , resulting in a cross-link concentration  $c=M/N$ . These cross-links are modeled by a harmonic potential

$$U := \frac{d}{2a^2} \sum_{e=1}^M \lambda_e (\mathbf{R}_{i_e} - \mathbf{R}_{i'_e})^2, \quad (2)$$

whose overall strength is controlled by the parameter  $a > 0$ . We use units of energy such that  $k_B T = 1$  and allow for fluctuations in the strength of cross-links by introducing the parameter  $\lambda_e$ . Cross-links of uniform strength correspond to all  $\lambda_e = 1$ . In general each cross-link  $e$  is assigned independently a random strength  $\lambda_e$  according to the distribution  $p(\lambda)$ . The connectivity of the particles is specified by the connectivity matrix

$$\Gamma_{ii'} = \sum_{e=1}^M \lambda_e (\delta_{ii_e} - \delta_{ii'_e})(\delta_{i'i_e} - \delta_{i'i'_e}), \quad (3)$$

in terms of which the potential reads  $U = (d/2a^2) \sum_{i,i'=1}^N \Gamma_{ii'} \mathbf{R}_i \cdot \mathbf{R}_{i'}$ . As usual  $\delta_{ij}$  denotes the Kronecker symbol, i.e.,  $\delta_{ij} = 1$  for  $i=j$  and zero otherwise.

We consider purely relaxational dynamics in an externally applied space- and time-dependent velocity field  $v_{\text{ext}}^\alpha(\mathbf{r}, t)$ :

$$\partial_t R_i^\alpha(t) = - \frac{1}{\zeta} \frac{\partial U}{\partial R_i^\alpha} (t) + v_{\text{ext}}^\alpha(\mathbf{R}_i(t), t) + \xi_i^\alpha(t). \quad (4)$$

Here, Greek indices indicate Cartesian coordinates  $\alpha = x, y, z, \dots$ , and we will always consider a flow field in the  $x$  direction, increasing linearly with  $y$ , i.e.,

$$v_{\text{ext}}^\alpha(\mathbf{r}, t) = \delta_{\alpha,x} \kappa(t) r_y, \quad (5)$$

with a time-dependent shear rate  $\kappa(t)$ . The noise  $\xi$  has zero mean and covariance  $\langle \xi_i^\alpha(t) \xi_{i'}^\beta(t') \rangle = 2\zeta^{-1} \delta_{\alpha,\beta} \delta_{i,i'} \delta(t-t')$ , where  $\delta(t)$  is the Dirac  $\delta$  function. Here, the bracket  $\langle \dots \rangle$  indicates the average over the realizations of the

Gaussian noise  $\xi$ . The relaxation constant is denoted by  $\zeta$ . The probability distribution of cross-link configurations  $\mathcal{G} = \{i_e, i'_e\}_{e=1}^M$  as well as the probability distribution of cross-link strengths will be specified later.

In Ref. [10] we computed the shear viscosity in the sol phase for (macro)molecular units of arbitrary internal connectivity. It was shown that the dependence on the cross-link concentration and in particular the critical behavior near the gelation threshold are the same for all (macro)molecular units, as long as we consider identical units with a finite degree of polymerization. We expect the same universal behavior for stress relaxation on long time scales, which are much larger than the longest internal time scale of a single (macro)molecule. Hence we specialize to the simplest units, namely, Brownian particles.

### A. Relaxation of shear stress

We aim at the computation of the intrinsic shear stress  $\sigma_{\alpha\beta}(t)$  as a function of the shear rate  $\kappa(t)$ . For the simple shear flow (5), a linear response relation

$$\sigma_{xy}(t) = \int_{-\infty}^t d\tau \chi(t-\tau) \kappa(\tau) \quad (6)$$

is valid for arbitrary strengths of the shear rate  $\kappa(t)$ . The linear response or shear relaxation function  $\chi(t)$  is given in terms of the connectivity matrix as explained in detail in Ref. [13],

$$\begin{aligned} \chi(t) &= \frac{\rho}{N} \sum_{i=1}^N \left( [1 - E_0(\mathcal{G})] \exp\left\{ -\frac{2dt}{\zeta a^2} \Gamma(\mathcal{G}) \right\} \right)_{ii} \\ &= \frac{\rho}{N} \text{Tr} \left( [1 - E_0(\mathcal{G})] \exp\left\{ -\frac{2dt}{\zeta a^2} \Gamma(\mathcal{G}) \right\} \right). \end{aligned} \quad (7)$$

The matrix  $E_0$  denotes the projector onto the subspace of zero eigenvalues of  $\Gamma$  (see Ref. [10]). For a time-independent shear rate  $\kappa(t) = \kappa$ , the stress tensor is time independent and related to the shear rate  $\sigma = \rho \eta \kappa$  via the static shear viscosity, given by Ref. [10],

$$\eta = \frac{\zeta a^2}{2dN} \text{Tr} \frac{1 - E_0(\mathcal{G})}{\Gamma(\mathcal{G})}. \quad (8)$$

### B. Self-diffusion

To discuss self-diffusion we set the externally applied velocity field to zero and focus on the incoherent scattering function

$$S(\mathbf{q}, t) := \lim_{T \rightarrow \infty} \left\langle \frac{1}{N} \sum_{i=1}^N \exp\{i\mathbf{q} \cdot [\mathbf{R}_i(t+T) - \mathbf{R}_i(T)]\} \right\rangle \quad (9)$$

and the squared time delayed displacement

$$C(t) := \lim_{T \rightarrow \infty} \left\langle \frac{1}{N} \sum_{i=1}^N [\mathbf{R}_i(t+T) - \mathbf{R}_i(T)]^2 \right\rangle. \quad (10)$$

We note that  $\mathbf{R}_i(t+T) - \mathbf{R}_i(t)$  is a Gaussian Markov process whose distribution in the limit  $T \rightarrow \infty$  is characterized by a vanishing mean and the covariance function

$$\begin{aligned} G_{ii'}(t) &:= \lim_{T \rightarrow \infty} \langle [\mathbf{R}_i(t+T) - \mathbf{R}_i(T)] \cdot [\mathbf{R}_{i'}(t+T) - \mathbf{R}_{i'}(T)] \rangle \\ &= \frac{1}{\zeta} \int_0^t d\tau \left( \exp\left\{ -\frac{2d\tau}{\zeta a^2} \Gamma \right\} \right)_{ii'}. \end{aligned} \quad (11)$$

Performing the integral in Eq. (11) leads to

$$G_{ii'}(t) = \frac{2}{\zeta} \left[ \frac{\zeta a^2}{2d} \frac{1 - E_0}{\Gamma} \left( 1 - \exp\left\{ -\frac{2dt}{\zeta a^2} \Gamma \right\} \right) + t E_0 \right]_{ii'}. \quad (12)$$

The matrix  $\Gamma$  is non-negative by inspection [see Eq. (2)], as it should be to ensure relaxation to equilibrium. The scattering function as well as the time delayed displacement can be expressed in terms of  $G_{ii'}(t)$  via

$$S(\mathbf{q}, t) = \frac{1}{N} \sum_{i=1}^N \exp\{-q^2 G_{ii}(t)\} \quad (13)$$

and

$$C(t) = \frac{1}{N} \sum_{i=1}^N G_{ii}(t). \quad (14)$$

### C. Density of eigenvalues

All dynamic quantities of interest have been expressed in terms of  $\Gamma$ . Accordingly, once we know the eigenvalues  $\{\gamma_{ij}\}_{i=1}^N$  and eigenvectors of this matrix, we can compute dynamic observables for arbitrary times. In the following, we shall discuss the density of eigenvalues

$$D_{\text{tot}}(\gamma) = \lim_{N \rightarrow \infty} \overline{\frac{1}{N} \sum_{i=1}^N \delta(\gamma - \gamma_i)} = \lim_{N \rightarrow \infty} \frac{1}{N} \text{Tr} \delta(\gamma - \Gamma) \quad (15)$$

for several cross-link distributions. Here the overbar denotes the average over cross-link realizations. If one splits off the zero eigenvalues,  $D_{\text{tot}}(\gamma)$  can be written as

$$D_{\text{tot}}(\gamma) = T_0(c) \delta(\gamma) + [1 - T_0(c)] D(\gamma), \quad (16)$$

where  $D(\gamma)$  is normalized to 1 and contains only the non-zero eigenvalues. If we group the particles into clusters, the eigenspace of modes with zero eigenvalues corresponds to vectors that are constant within one cluster [14]. In other words, there is one zero eigenvalue for each cluster and the dimension of the null space is just the number of clusters  $N_{\text{cl}}$ . The weight of zero eigenvalues is simply given by the density of clusters, i.e.,  $T_0(c) = N_{\text{cl}}/N$ .

We restrict ourselves to the density of eigenvalues and do not attempt to compute eigenvectors, which is in general more difficult. Hence, we can compute only observables that can be written as  $(1/N)\sum_{i=1}^N [f(\Gamma)]_{ii}$ , where  $f$  is an arbitrary function of  $\Gamma$ . The incoherent scattering function is not of this form [Eq. (13)], whereas the stress relaxation function is

$$\overline{\chi(t)} = [1 - T_0(c)] \rho \int_0^\infty d\gamma D(\gamma) \exp\left\{-\frac{2t}{\zeta a^2} \gamma\right\}. \quad (17)$$

The zero eigenvalues are not to be included in the integration, due to the term  $1 - E_0$  in Eq. (7). Analogously, the averaged viscosity is given by

$$\overline{\eta} = [1 - T_0(c)] \frac{\zeta a^2}{2d} \int_0^\infty d\gamma \frac{D(\gamma)}{\gamma}. \quad (18)$$

In the same way, the disorder averaged, time delayed displacement is determined by

$$\begin{aligned} \overline{C(t)} = & [1 - T_0(c)] \frac{a^2}{d} \int_0^\infty d\gamma \frac{D(\gamma)}{\gamma} \left(1 - \exp\left\{-\frac{2t}{\zeta a^2} \gamma\right\}\right) \\ & + T_0(c) \frac{2t}{\zeta}. \end{aligned} \quad (19)$$

It can also be expressed as an integral over the time-dependent response function,

$$\overline{C(t)} = \frac{2}{\zeta \rho} \int_0^t d\tau \chi(\tau) + T_0(c) \frac{2t}{\zeta}. \quad (20)$$

### III. MEAN FIELD THEORY

We consider first the simplest distribution of cross-links, which ignores all correlations between cross-links, i.e., the cross-links are chosen independently of each other and each pair  $(i_e, i'_e)$  of particle indices is realized with equal probability. As shown in Ref. [15] the particle clusters exhibit the analog of a percolation transition at a critical cross-link concentration  $c_{\text{crit}} = 1/2$ . Below this concentration there is no macroscopic cluster and almost all finite clusters are trees. The average number of tree clusters  $T_n$  with  $n$  particles is given in the macroscopic limit by

$$\lim_{N \rightarrow \infty} \frac{T_n}{N} = \tau_n = \frac{n^{n-2} (2ce^{-2c})^n}{2cn!}. \quad (21)$$

In particular the total number of clusters per particle is

$$T_0(c) = 1 - c. \quad (22)$$

These results are independent of the distribution of cross-link strengths,  $p(\lambda)$ .

To compute the density of eigenvalues we introduce the resolvent

$$G(\Omega) = \lim_{N \rightarrow \infty} \frac{1}{N} \text{Tr} \frac{1}{\Gamma - \Omega} \quad (23)$$

for complex argument  $\Omega = \gamma + i\epsilon$ ,  $\epsilon > 0$ . In the limit  $\epsilon \rightarrow 0$ , we recover the spectrum from the imaginary part of the resolvent according to

$$D_{\text{tot}}(\gamma) = \frac{1}{\pi} \lim_{\epsilon \downarrow 0} \text{Im} G(\gamma + i\epsilon). \quad (24)$$

It can be inferred from Eq. (15) that, conversely,  $D_{\text{tot}}(\gamma)$  determines  $G(\Omega)$  via

$$G(\Omega) = \int_{-\infty}^{\infty} d\gamma \frac{D_{\text{tot}}(\gamma)}{\gamma - \Omega}. \quad (25)$$

#### A. Disorder average by replicas

Bray and Rodgers [8] have shown how to reduce the computation of  $D_{\text{tot}}(\gamma)$  for cross-links of unit strength (i.e., all  $\lambda_e = 1$ ) to the solution of a nonlinear integral equation. Their derivation is easily generalized to cross-links of strength  $\lambda$  that fluctuates according to a given distribution  $p(\lambda)$ . We restrict ourselves to distributions  $p(\lambda)$  such that

$$\int_0^\infty \frac{d\lambda}{\lambda} p(\lambda) < \infty \quad (26)$$

holds. It will be shown below [see Eq. (37)] that this condition is necessary to ensure a finite viscosity in the sol phase. Following Bray and Rodgers we introduce a generating function

$$Z(\Omega) = \int_{\mathbb{R}^N} \left( \prod_{i=1}^N \frac{d\phi_i}{\sqrt{2\pi}} \right) \exp\left( \frac{i}{2} \sum_{i,j} \phi_i \phi_j (\Omega \delta_{ij} - \Gamma_{ij}) \right), \quad (27)$$

which determines the resolvent, according to

$$G(\Omega) = \lim_{N \rightarrow \infty} \frac{2}{N} \frac{\partial \ln Z}{\partial \Omega}. \quad (28)$$

The average over the disorder is performed with the replica trick, resulting in

$$\begin{aligned} \overline{Z^n} = & \int_{\mathbb{R}^N} \left( \prod_{i=1}^N \prod_{\alpha=1}^n \frac{d\phi_i^\alpha}{\sqrt{2\pi}} \right) \exp\left( \frac{i}{2} \Omega \sum_{i=1}^N \hat{\phi}_i \hat{\phi}_i \right. \\ & \left. + \frac{c}{N} \int_0^\infty d\lambda p(\lambda) \sum_{i,j=1}^N e^{-i\lambda(\hat{\phi}_i - \hat{\phi}_j)^2/2} - cN \right). \end{aligned} \quad (29)$$

We assume that the connectivity is intensive,  $\lim_{N \rightarrow \infty} (c/N) = 0$ , and have introduced the notation  $\hat{\phi}_i = (\phi_i^1, \phi_i^2, \dots, \phi_i^n)$  for  $n$ -times-replicated variables. In the next step one decouples different sites as shown in Ref. [8] and performs a saddle-point approximation for large  $N$ . This gives rise to a self-consistent equation for a function  $g^\Omega(\hat{x})$ ,

$$g^\Omega(\hat{x}) = 2c \int_0^\infty d\lambda p(\lambda) \frac{\int d\hat{y} e^{[i\Omega\hat{y}^2 + 2g^\Omega(\hat{y}) - i\lambda(\hat{y}-\hat{x})^2]/2}}{\int d\hat{y} e^{[i\Omega\hat{y}^2 + 2g^\Omega(\hat{y})]/2}} \quad (30)$$

which in turn determines the resolvent according to

$$G(\Omega) = \lim_{n \rightarrow 0} \frac{i}{n} \frac{\int d\hat{x} \hat{x}^2 e^{[i\Omega\hat{x}^2/2 + g^\Omega(\hat{x})]}}{\int d\hat{x} e^{[i\Omega\hat{x}^2/2 + g^\Omega(\hat{x})]}}. \quad (31)$$

In the last step of the calculation one assumes a replica-symmetric solution for the saddle-point equation:

$$g^\Omega(\hat{x}) = g^\Omega(\rho) \quad \text{with } \rho = \sqrt{\sum_\alpha x_\alpha^2}. \quad (32)$$

The limit  $n \rightarrow 0$  can then be performed resulting in the following nonlinear integral equation for  $g^\Omega(\rho)$  [cf. Eqs. (16,17) in Ref. [8]]:

$$\begin{aligned} g^\Omega(\rho) = & 2c \int_0^\infty d\lambda p(\lambda) \exp\left\{-\frac{i\lambda}{2}\rho^2\right\} \\ & + 2ic e^{-2c} \int_0^\infty d\lambda p(\lambda) \int_0^\infty dx \lambda \rho I_1(i\lambda\rho x) \\ & \times \exp\left\{-\frac{i\lambda}{2}(\rho^2 + x^2) + \frac{i\Omega}{2}x^2 + g^\Omega(x)\right\} \end{aligned} \quad (33)$$

with  $g^\Omega(0) = 2c$ . Here  $I_\nu(z)$  are the modified Bessel functions of the first kind. The solution of Eq. (33) yields the resolvent

$$G(\Omega) = - \int_0^\infty \frac{d\lambda}{\lambda} p(\lambda) + \frac{i}{2c} \int_0^\infty d\rho \rho g^\Omega(\rho) \quad (34)$$

and the density of eigenvalues

$$D_{\text{tot}}(\gamma) = \frac{1}{2c\pi} \lim_{\epsilon \rightarrow 0} \text{Im} \left\{ i \int_0^\infty d\rho \rho g^{\gamma+i\epsilon}(\rho) \right\}. \quad (35)$$

### B. Moments and Lifshitz tails

If all inverse moments  $M_n$  of the density of nonzero eigenvalues  $M_n := \int_0^\infty d\gamma \gamma^{-n} D(\gamma)$ ,  $n \in \mathbb{N}$ , exist, one can derive the following asymptotic expansion of the resolvent:

$$G(\Omega) = \frac{c-1}{\Omega} + \frac{2d\eta}{\zeta a^2} + c \sum_{n=1}^{\infty} \Omega^n M_{n+1} \quad (36)$$

by expanding the denominator in Eq. (25) in a geometric series. As we show in Appendix A, the lowest moments are given explicitly by

$$M_1 = \frac{1}{4c} \left[ \ln\left(\frac{1}{1-2c}\right) - 2c \right] \int_0^\infty \frac{d\lambda}{\lambda} p(\lambda) = \frac{2d\eta}{\zeta a^2} \quad (37)$$

and

$$\begin{aligned} M_2 = & - \frac{(5P_2 - 4P_1^2)}{240c^2} \ln\left(\frac{1}{1-2c}\right) - \frac{8c^3 - 6c^2 - 5c + 1}{30c(1-2c)^3} P_1^2 \\ & - \frac{4c^2 - 3c - 1}{24c(1-2c)^2} P_2 \end{aligned} \quad (38)$$

with  $P_n := \int_0^\infty d\lambda \lambda^{-n} p(\lambda)$ . We are interested in the small eigenvalues that are due to the geometry of the clusters and not due to the appearance of weak links. Hence we confine ourselves to distributions such that weak cross-links are unlikely to occur. More precisely we require

$$\lim_{\lambda \downarrow 0} \frac{\ln|\ln p(\lambda)|}{|\ln \lambda|} > \frac{1}{2}. \quad (39)$$

The divergence of the moments,  $M_1$  and  $M_2$ , suggests a Lifshitz tail of the density of states of the form

$$D(\gamma) \propto \exp\left\{-\left(\frac{\gamma_0(1-2c)^3}{\gamma}\right)^\kappa\right\}, \quad \gamma \downarrow 0, \quad c < \frac{1}{2}, \quad (40)$$

since for positive  $\kappa$  this ansatz implies for the inverse moments

$$M_n \propto (1-2c)^{-3(n-1)}, \quad c \uparrow \frac{1}{2}. \quad (41)$$

Bray and Rodgers have given a heuristic argument in favor of the ansatz (40) with  $\kappa = 1/2$ . They argue that out of all clusters for given  $n$  the linear one has the smallest eigenvalue, namely,  $\gamma_{\min} = \gamma_0 n^{-2}$ . There is just one linear cluster for given  $n$ , so that its contribution to the spectrum is

$$D^{\text{lin}} = \frac{1}{2c} \sum_n (2c e^{(-2c)})^n \delta\left(\gamma - \frac{\gamma_0}{n^2}\right) \sim e^{-\sqrt{\gamma_0/\gamma}}. \quad (42)$$

Arbitrary finite clusters may be attached to the chain without altering the dependence of the smallest eigenvalue on the length of the chain. If a finite cluster of mass  $m_i$  is attached to site  $i$  of the linear chain, the smallest eigenvalue is  $\gamma_{\min} = \gamma_0/m_i n^2$ . Replacing

$$m_i \sim \bar{m} = \frac{\sum_n n \tau_n}{\sum_n \tau_n} = \frac{1}{1-2c} \quad (43)$$

leads to  $\gamma_{\min} = \gamma_0(1-2c)/n^2$ . The number of clusters contributing to  $D(\gamma)$  for small  $\gamma$  is much larger if attachments are taken into account: The probability of finding a chain of length  $n$ , regardless of attachments, is given by  $(2c)^n$ . Hence the density of eigenvalues is estimated as

$$D^{\text{lin}} = \frac{1}{2c} \sum_n (2c)^n \delta\left(\gamma - \frac{\gamma_0(1-2c)}{n^2}\right) \sim \exp\left[-\left(\frac{\gamma_0(1-2c)^3}{\gamma}\right)^{1/2}\right]. \quad (44)$$

Here, we have expanded  $\ln(2c) \sim 2c - 1$  for  $c$  sufficiently close to its critical value  $c_{\text{crit}} = 1/2$  to obtain the Lifshitz tail near criticality. In Appendix A 3 we derive rigorous upper and lower bounds for  $D(\gamma)$ , which prove that  $D(\gamma)$  has indeed a Lifshitz tail of the form  $D(\gamma) \sim \exp[-\sqrt{h(c)/\gamma}]$ . We are unable to derive the dependence of  $h(c)$  on cross-link concentration  $c$ , which is, however, suggested by the lowest order moments (38) and (74).

In the following two subsections we shall discuss two special choices for  $p(\lambda)$ . In the first case all cross-links are of unit strength, giving rise to a point spectrum. In the second case the strength of the cross-links fluctuates according to  $p(\lambda) = \exp(-1/\lambda)/\lambda^2$ . The integral equation (33) simplifies considerably for this distribution and allows for a solution by iteration.

### C. Exact solution of the integral equation for uniform cross-link strengths

For cross-links of unit strength, the integral equation (33) reduces to Eq. (16) in Ref. [8],

$$\begin{aligned} g^\Omega(\rho) &= 2c \exp\left(-\frac{i}{2}\rho^2\right) \left\{ 1 + ie^{-2c} \int_0^\infty dx \rho I_1(i\rho x) \right. \\ &\quad \left. \times \exp\left(\frac{i(\Omega-1)}{2}x^2 + g^\Omega(x)\right) \right\} \\ &= 2c \exp\left(-\frac{i}{2}\rho^2\right) \left\{ 1 - 2c e^{-2c} \int_0^\infty dx J_1(x) \right. \\ &\quad \left. \times \exp\left[\frac{i}{2}(\Omega-1)\frac{x^2}{\rho^2} + g^\Omega\left(\frac{x}{\rho}\right)\right] \right\}. \end{aligned} \quad (45)$$

The second equality follows from a substitution  $x \rightarrow \rho x$  and from the basic relation between the Bessel functions of the first kind  $J_\nu$  and the modified Bessel functions  $I_\nu$ , in particular,  $I_1(x) = -iJ_1(ix)$ .

To get some feeling for the spectrum of eigenvalues, we first consider the case of small  $c$ . We then have predominantly small clusters, i.e., single particles, dimers, trimers, etc. The connectivity matrix of a dimer has eigenvalues  $\lambda_1 = 0, \lambda_2 = 2$ . A linear chain of three particles has eigenvalues  $\{0, 1, 3\}$ , a linear chain of four particles has eigenvalues  $\{0, 2, 2 + \sqrt{2}, 2 - \sqrt{2}\}$ , and a star with three legs has eigenvalues  $\{0, 1, 4\}$ . These are the only trees up to  $\mathcal{O}(c^3)$ . Hence in this order the spectrum consists of  $\delta$  functions at the above eigenvalues, with each cluster contributing to the weight of the  $\delta$  functions according to its frequency of occurrence. Next we show that  $\delta$  functions in the spectrum correspond to Gaussian functions  $g^\Omega(\rho)$ . The ansatz

$$g^\Omega(\rho) = 2ca \exp[-iz(\Omega)\rho^2/2], \quad (46)$$

where  $z = z(\Omega)$  is an arbitrary function of  $\Omega = \gamma + i\epsilon$  with  $\text{Im}\{z\} < 0$  for  $\epsilon > 0$ , leads to  $G(\Omega) = -1 + a/z$ . In the limit  $\text{Im}\{z\} \rightarrow 0$  each zero  $\gamma_i$  of  $\text{Re}\{z(\gamma_i)\} = 0$  gives rise to a  $\delta$  function in the spectrum,

$$D_{\text{tot}}(\gamma) = a \sum_i \frac{\delta(\gamma - \gamma_i)}{|\partial z / \partial \gamma(\gamma_i)|}. \quad (47)$$

Next, we construct an approximation to the integral equation (45) by successive iteration. We start with

$$g_0^\Omega(\rho) := 2c. \quad (48)$$

The first step of the iteration gives

$$\begin{aligned} g_1^\Omega(\rho) &= 2c \exp\left(-\frac{i}{2}\rho^2\right) \left\{ 1 - e^{-2c} \int_0^\infty dx J_1(x) \right. \\ &\quad \left. \times \exp\left[\frac{i}{2}(\Omega-1)\frac{x^2}{\rho^2} + g_0^\Omega\left(\frac{x}{\rho}\right)\right] \right\} \end{aligned} \quad (49)$$

$$= 2c \exp\left(-\frac{i}{2}\frac{\Omega}{\Omega-1}\rho^2\right) \quad (50)$$

since the integral on the right-hand side can be calculated exactly [16]. The spectrum consists of a  $\delta$  function at  $\gamma = 0$ ,  $D_1(\gamma) = \delta(\gamma)$ . The next step of the iteration gives

$$\begin{aligned} g_2^\Omega(\rho) &= 2c \exp\left(-\frac{i}{2}\rho^2\right) \left\{ 1 - e^{-2c} \int_0^\infty dx J_1(x) \right. \\ &\quad \left. \times \exp\left[\frac{i}{2}(\Omega-1)\frac{x^2}{\rho^2} + g_1^\Omega\left(\frac{x}{\rho}\right)\right] \right\} \end{aligned} \quad (51)$$

$$\begin{aligned} &= 2c \exp\left(-\frac{i}{2}\rho^2\right) \left\{ 1 - e^{-2c} \int_0^\infty dx J_1(x) \right. \\ &\quad \left. \times \exp\left[\frac{i}{2}(\Omega-1)\frac{x^2}{\rho^2}\right] \sum_{k=0}^{\infty} \frac{(2c)^k}{k!} \right. \\ &\quad \left. \times \exp\left[-\frac{i}{2}\frac{k\Omega}{\Omega-1}\frac{x^2}{\rho^2}\right] \right\} \end{aligned} \quad (52)$$

by Taylor expansion of the exponential of  $g_1^\Omega(x/\rho)$ . Again, the integrals appearing in Eq. (52) can be computed exactly, yielding

$$g_2^\Omega(\rho) = 2c \sum_{k=0}^{\infty} a_k^{(2)} \exp\left(-\frac{i}{2}z_k^{(2)}\rho^2\right) \quad (53)$$

$$a_k^{(2)} := e^{-2c} \frac{(2c)^k}{k!}, \quad z_k^{(2)} := \left(1 + \frac{1}{\Omega - 1 - k\Omega/(\Omega - 1)}\right). \quad (54)$$

Note that  $\sum_{k=0}^{\infty} a_k^{(2)} = 1$ . In this iteration, the spectrum is given by

$$D_2(\gamma) = \frac{1 - e^{-2c}}{2c} \delta(\gamma) + \sum_{k=2}^{\infty} e^{-2c} \frac{(2c)^{k-1}}{k(k-2)!} \delta(\gamma - k). \quad (55)$$

Next, we consider a general ansatz for  $g_i^{\Omega}$  of the form

$$g_i^{\Omega}(\rho) = 2c \sum_{k=0}^L a_k^{(i)} \exp\left\{-\frac{i}{2} z_k^{(i)} \rho^2\right\}, \quad (56)$$

with  $\sum_{k=0}^{\infty} a_k^{(i)} = 1$ .  $L$  is an arbitrary positive integer and will be allowed to tend to  $\infty$  below. We insert the ansatz (56) into Eq. (45) and use a similar Taylor expansion as above to obtain

$$g_{i+1}^{\Omega}(\rho) = 2c e^{-2c} \sum_{l_0=0}^{\infty} \dots \sum_{l_L=0}^{\infty} \left( \prod_{k=0}^L \frac{(2c a_k^{(i)})^{l_k}}{l_k!} \right) \times \exp\left\{-\frac{i}{2} \left(1 + \frac{1}{\Omega - 1 - \sum_{k=0}^{\infty} l_k z_k^{(i)}}\right) \rho^2\right\}. \quad (57)$$

When we now let  $L \rightarrow \infty$ , we get the expression

$$g_{i+1}^{\Omega}(\rho) = 2c \sum_{\{l_k\}} a_{\{l_k\}}^{(i+1)} \exp\left\{-\frac{i}{2} z_{\{l_k\}}^{(i+1)} \rho^2\right\} \quad (58)$$

with

$$a_{\{l_k\}}^{(i+1)} = e^{-2c} \prod_{k=0}^{\infty} \frac{(2c a_k^{(i)})^{l_k}}{l_k!} \quad (59)$$

and

$$z_{\{l_k\}}^{(i+1)} = 1 + \frac{1}{\Omega - 1 - \sum_{k=0}^{\infty} l_k z_k^{(i)}}. \quad (60)$$

We use the notation  $(l_k)$  to denote a whole sequence of non-negative integers, while  $l_k$  (without parentheses) denotes the  $k$ th element of the sequence. Out of all possible such sequences we only need those with a *finite* number of nonzero elements. This is because  $a_k^{(i)} \rightarrow 0$  as  $k \rightarrow \infty$ , and thus  $\prod_{k=0}^{\infty} (2c a_k^{(i)})^{l_k} / l_k! = 0$  if there were infinitely many nonzero elements in  $(l_k)$ . The set of all sequences with a finite number of nonzero elements is denoted by  $\{(l_k)\}$ . The summation in Eq. (58) thus goes over a countable set and therefore  $g_{i+1}^{\Omega}(\rho)$  is of the same functional form as  $g_i^{\Omega}(\rho)$ . It is easy to see that  $\sum_{\{(l_k)\}} a_{\{l_k\}}^{(i+1)} = 1$  holds also for the next iteration.

Since  $g_2^{\Omega}(\rho)$  is an expression of the form of Eq. (56), it follows by induction that all  $g_i^{\Omega}(\rho)$ ,  $i \geq 2$ , are of the same

form. This observation enables us to write down *fix-point* equations for the coefficients  $a$  and the exponential prefactors  $z$ :

$$a_{\{l_k\}}^{(i+1)} = a_{\{l_k\}}^{(i)} \quad \text{and} \quad z_{\{l_k\}}^{(i+1)} = z_{\{l_k\}}^{(i)}. \quad (61)$$

As shown in Appendix B, these equations can be solved if the indices on the left- and right-hand sides are matched by mapping the sequence  $(l_k)$  that appears as index on the left-hand side onto a simple number  $n = \sum_k l_k M^k$  with some positive integer  $M$ . Afterwards,  $M$  is taken to infinity. In the process, a new structure of the coefficients  $a$  and  $z$  emerges: each pair of coefficients  $(a_i, z_i)$  falls into one of infinitely many ‘‘classes’’ of increasing complexity. The first three classes are given by the following expressions (the upper index denotes the class); the general form can be found in Appendix B:

$$a_0^0 = e^{-2c}, \quad z_0^0 = \frac{\Omega}{\Omega - 1}, \quad (62)$$

$$a_n^1 = e^{-2c} \frac{(2c a_0^0)^n}{n!}, \quad z_n^1 = \frac{\Omega - n z_0^0}{\Omega - 1 - n z_0^0}, \quad (63)$$

$$a_{\{l_k\}}^2 = e^{-2c} \prod_{k=0}^{\infty} \frac{(2c a_k^1)^{l_k}}{l_k!}, \quad z_{\{l_k\}}^2 = \frac{\Omega - \sum_{k=0}^{\infty} l_k z_k^1}{\Omega - 1 - \sum_{k=0}^{\infty} l_k z_k^1}. \quad (64)$$

Note that the expression for a higher class automatically contains all of the lower classes as well if the lower-class expressions are recursively inserted, e.g.,  $a_{1,0,0,\dots}^2 = e^{-2c} (2c a_0^1)^1 / 1! = a_1^1$ . This remains true in the general case. For higher classes, the indices become more complicated, e.g., for class 3 it is necessary to use  $(l_{(k)})$  as index on the left hand side. As a shorthand, however, it is convenient to use the notation  $(l_k)$  or just  $k$  even for the higher classes. It is then understood that  $k$  itself may stand for a more complicated object like a nested sequence. See Appendix B for details.

We mention the result that  $s^m$ , the sum over all  $a$  from classes 0 to  $m$ , is given by

$$s^m := \sum_{\{(l_k)\}} a_{\{l_k\}}^m = e^{-2c} \prod_k e^{2c a_k^{m-1}} = \exp\{-2c(1 - s^{m-1})\}, \quad (65)$$

and

$$s^0 = e^{-2c} \quad (66)$$

As long as  $c < \frac{1}{2}$ , the corresponding fix-point equation  $s = e^{-2c(1-s)}$  has a stable fixpoint at  $s = 1$ , which implies  $\lim_{m \rightarrow \infty} s^m = 1$ , as it should be. The quantity  $1 - s^m$  is therefore a measure for the quality of an approximation that only goes up to class  $m$ . We can conclude that for small  $c$  only a few classes are sufficient whereas for  $c$  close to  $\frac{1}{2}$  consider-

ably more are needed. For  $c > \frac{1}{2}$ , the fix point becomes unstable, indicating that the iteration no longer converges to the full solution of the integral equation due to the appearance of the infinite cluster.

### Implications for the density of states

Making use of the solution just constructed, the resolvent can be written as

$$G(\Omega) = -1 + \lim_{m \rightarrow \infty} \sum_k \frac{a_k^m}{z_k^m}. \quad (67)$$

Here, inclusion of  $a$ 's and  $z$ 's from classes lower than  $m$  in  $a_k^m$  and  $z_k^m$  has been implied as explained above. Analogous to Eq. (47), this results in the exact density of states

$$D_{\text{tot}}(\gamma) = \lim_{m \rightarrow \infty} \sum_k a_k^m \sum_i \frac{\delta(\gamma - \gamma_{ki}^m)}{|\partial z_k^m / \partial \gamma(\gamma_{ki}^m)|}, \quad (68)$$

that is, a sum of  $\delta$  peaks located at the roots  $\gamma_{ki}^m$  of the respective  $z_k^m(\gamma)$  with weight factors  $a_k^m |(\partial z_k^m / \partial \gamma)(\gamma_{ki}^m)|^{-1}$ . It can be proved with Cauchy's integration theorem applied to  $(z_{(l_k)}^m)^{-1}$  and Eq. (64) or the more general expression from Appendix B that  $\sum_i |(\partial z_k^m / \partial \gamma)(\gamma_{ki}^m)|^{-1} = 1$  holds for every  $z_k^m$ . This property guarantees that the total weight of all peaks in the spectrum is 1 (recall that the sum of all  $a$ 's is also 1). There is no continuous part of the spectrum, but this would change for  $c > \frac{1}{2}$  due to the appearance of an infinite cluster.

It is impossible to find the roots of all  $z^m$  but classes 0 and 1 can be solved exactly. We deduce from Eq. (62) that the roots of  $z_n^1$  are located at  $\gamma_{n,1} = 0$  and  $\gamma_{n,2} = n+1$ . The weight factors are easily computed as  $1/(n+1)$  for the peak at 0 and  $n/(n+1)$  for the peak at  $n+1$ . The density of eigenvalues including class 0 and 1 then reads

$$D_{\text{tot}}^1(\gamma) = \frac{e^{2ce^{-2c}} - 1}{2c} \delta(\gamma) + \sum_{k=2}^{\infty} \frac{(2ce^{-2c})^k}{2ck(k-2)!} \delta(\gamma - k). \quad (69)$$

Note that this is different from the result of the second iteration, Eq. (55), although it contains the same peaks.

Another consequence of the exact solution of the integral equation is that the density of states does *not* show scaling behavior with respect to  $c$ , i.e., it cannot be written in the form  $D_{\text{tot}}(\gamma) \sim f(\gamma/\gamma^*(c))$  with some typical  $\gamma^*(c)$ . This follows from the fact that the positions of the peaks are given by the roots of the  $z$ 's, which are independent of  $c$ , and only the weights of the peaks depend on  $c$ . This can obviously never result in an exact scaling form: if scaling were valid, a small change of  $\gamma^*$  would result in a small shift of the peak positions, but they must stay fixed. It will be shown below for fluctuating cross-link strengths that numerical solutions for the eigenvalue density indicate that not even an approxi-

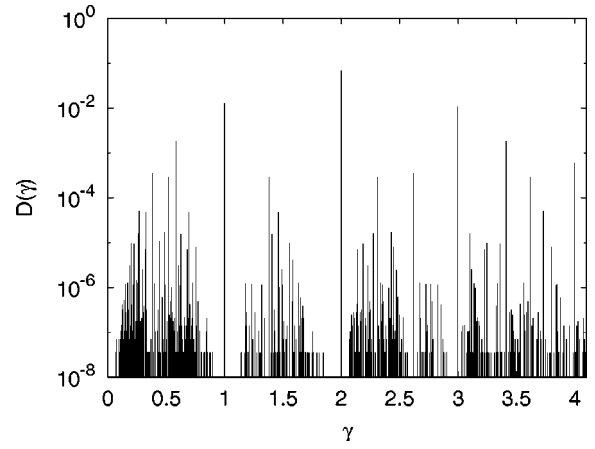


FIG. 1. Numerical simulation of the density of states for  $c=0.1$ .

mate scaling relation holds. This view will furthermore be supported by the results of the numerical diagonalization of random matrices for different types of system.

To conclude the discussion of the density of states for uniform cross-link strengths, the spectrum from the iterative solution of the integral equation is compared with results from numerical diagonalization of  $\Gamma$  (for details see Sec. IV below). Figure 1 shows the numerically computed spectrum for  $c=0.1$ . Note that there is a peak at  $\gamma=1$ , which is not present in Eq. (69). This “missing peak” can be found only in higher classes, e.g., in  $z_{0,1,0,\dots}^2 = \gamma(\gamma-1)(\gamma-3)/(\gamma^3 - 5\gamma^2 + 6\gamma - 1)$ . Other roots that can easily be identified with peaks in the numerical results are at  $2 \pm \sqrt{2}$  (stemming from  $z_{1,1,0,\dots}^2$ ) or at  $5/2 \pm \sqrt{5}/2$  (stemming from  $z_{0,2,0,\dots}^2$ ). Figure 2 shows a direct comparison between the same numerical simulation and a few explicitly calculated peaks from classes up to class 3. The agreement regarding the position of the peaks is excellent but some weight is still missing from some of the peaks. This weight is expected to be

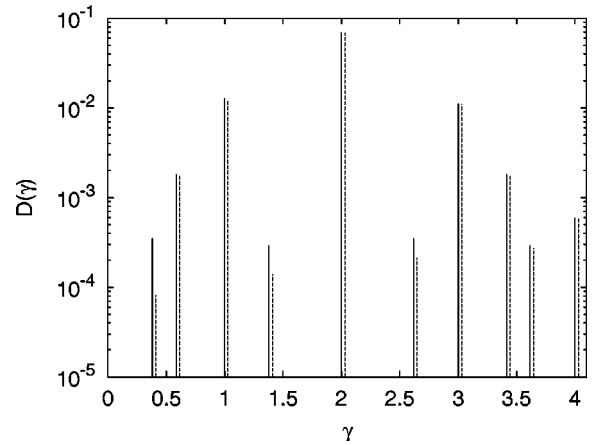


FIG. 2. Comparison between the simulation (solid lines) and some selected peaks calculated from the exact solution (dashed lines) for  $c=0.1$ . The analytical peaks have been slightly shifted to the right for better comparison, otherwise they would be indistinguishable from the numerical peaks.

found in higher classes and/or in different  $z$ 's which happen to have a root at the same position.

#### D. Numerical integration for special $p(\lambda)$

The integral equation (33) simplifies considerably for a special choice of  $p(\lambda)$ , namely,

$$p(\lambda) = \frac{1}{\lambda^2} \exp\left\{-\frac{1}{\lambda}\right\}, \quad (70)$$

implying  $P_n = n!$  Inserting the ansatz  $g^\Omega(\rho) =: f_\Omega(\rho^2/2)$  into Eq. (34) leads to the following representation:

$$G(\Omega) = -1 + \frac{i}{2c} \int_0^\infty dx f_\Omega(x), \quad (71)$$

where  $f_\Omega(x)$  is the solution of the ordinary differential equation (see Appendix A 2 for details)

$$\begin{aligned} f_\Omega(x) &= -ixf_\Omega''(x) + 2c \exp\{-2c + i\Omega x + f_\Omega(x)\}, \\ f_\Omega(0) &= 2c. \end{aligned} \quad (72)$$

This allows one to write down the general term in the asymptotic expansion of  $G(\Omega)$  for small  $\Omega$ . Close to the critical point the lowest order moments are explicitly given by

$$M_1 = \frac{1}{4c} \left\{ \ln\left(\frac{1}{1-2c}\right) - 2c \right\}, \quad c \rightarrow \frac{1}{2}, \quad (73)$$

$$M_2 = \frac{2}{15(1-2c)^3} + \frac{13}{60(1-2c)^2} + \mathcal{O}((1-2c)^{-1}), \quad c \rightarrow \frac{1}{2}, \quad (74)$$

$$\begin{aligned} M_3 &= \frac{47}{240(1-2c)^6} + \frac{16}{105(1-2c)^5} + \mathcal{O}((1-2c)^{-4}), \\ & \quad c \rightarrow \frac{1}{2}, \end{aligned} \quad (75)$$

and

$$\begin{aligned} M_4 &= \frac{5762}{6435(1-2c)^9} + \frac{1159}{720720(1-2c)^8} \\ & \quad + \mathcal{O}((1-2c)^{-7}), \quad c \rightarrow \frac{1}{2}, \end{aligned} \quad (76)$$

giving additional support to the conjecture about the Lifshitz tail Eq. (40).

For a numerical evaluation of  $G(\Omega)$  it is more convenient to rewrite Eq. (33) in the form

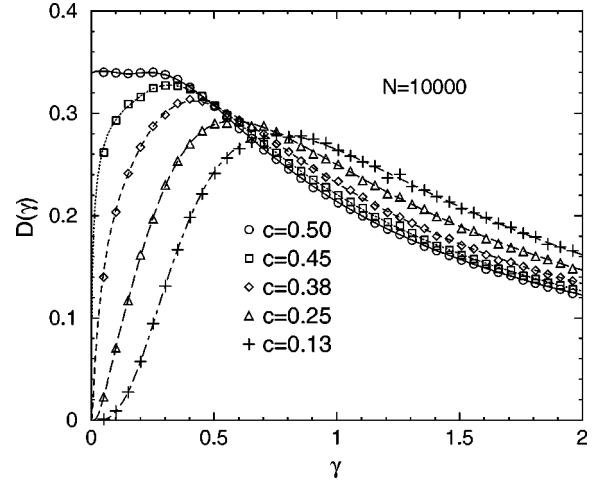


FIG. 3. Density  $D(\gamma)$  of nonzero eigenvalues for the mean-field network for  $p(\lambda)$  given by Eq. (70) for different concentrations  $c$ . The lines are the analytical results [i.e., the results from the numerical solution of Eq. (77)] while the data from the numerical diagonalization are shown by the symbols.

$$\begin{aligned} g^\Omega(\rho) &= 2c \sqrt{2i\rho} K_1(\sqrt{2i\rho}) \\ & \quad + 4ice^{-2c} \rho K_1(\sqrt{2i\rho}) \int_0^\rho d\eta I_1(\sqrt{2i\eta}) \\ & \quad \times \exp\left\{\frac{i\Omega}{2} \eta^2 + g^\Omega(\eta)\right\} \\ & \quad + 4ice^{-2c} \rho I_1(\sqrt{2i\rho}) \int_\rho^\infty d\eta K_1(\sqrt{2i\eta}) \\ & \quad \times \exp\left\{\frac{i\Omega}{2} \eta^2 + g^\Omega(\eta)\right\}, \end{aligned} \quad (77)$$

since in this representation the integrands do not depend on  $\rho$  and the numerical integration thus needs to be done only once per iteration, resulting in time and memory requirements only of the order of the number of integration grid points. This allows for high precision computations of  $g^\Omega(\rho)$ ,  $G(\Omega)$ , and  $D(\gamma)$ .

Figures 3 and 4 show the results for the density of eigenvalues from a numerical integration of Eq. (77) using a Padé approximation in order to extrapolate  $\Omega = \gamma + i\epsilon$  to  $\epsilon = 0$ . There are several noteworthy points to be seen in these figures:

First, we expect to see Lifshitz tails for *all*  $c$ ,  $0 < c < 1/2$ , for asymptotically small  $\gamma$ . Precisely at the critical point  $D(\gamma)$  goes to a constant as  $\gamma \rightarrow 0$ . For cross-link concentrations close to the critical one, we expect to see a crossover between an approximately constant region at intermediate  $\gamma$  to a Lifshitz tail at very small  $\gamma$ . Since small values of  $\gamma$  are hard to access numerically, this crossover makes it difficult to observe the Lifshitz tail, except possibly for small  $c$ . For intermediate  $c$  the data in Fig. 4 can be described approximately by a straight line but with a slope different from  $-\frac{1}{2}$ . This property will be confirmed by the results from the numerical diagonalization presented below.

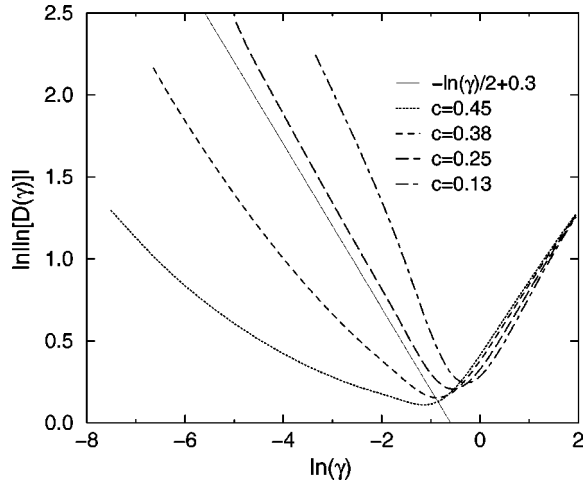


FIG. 4. Double logarithm of the density  $D(\gamma)$  of nonzero eigenvalues as a function of  $\ln \gamma$  for several concentrations  $c$ .

A second remarkable point is that the density of states as seen in Fig. 3 is clearly not suited to a scaling ansatz. There are (at least) two different scales contained in the plot: the first is the drop-off length  $\gamma^0(c)$  which describes the scale on which  $D(\gamma)$  goes to 0 for small  $\gamma$ , the other is the position of the maximum,  $\gamma^{\max}(c)$ . While  $\gamma^0$  goes to 0 for  $c \rightarrow \frac{1}{2}$ ,  $\gamma^{\max}$  evidently does not; these two features together are obviously incompatible with a scaling ansatz of the form  $D(\gamma) \sim f(\gamma/\gamma^*(c))$  with some typical  $\gamma^*$ . This finding is in agreement with the observation from the exact solution for uniform cross-link strength where scaling was not possible either. Here, however, the statement is even stronger since even an approximate scaling relation is ruled out. Note the peculiar feature that a second maximum appears in  $D(\gamma)$  for small  $\gamma$  at the percolation threshold  $c = \frac{1}{2}$ . This is not an artifact and is confirmed by the numerical diagonalization as shown in the figure. It may even indicate the presence of a third scale since the emergence of a maximum can already be suspected in the curves for smaller  $c$ .

### E. Stress relaxation

The characteristic features of the spectrum as discussed above have important consequences for the stress relaxation function. In particular, the Lifshitz tail in the spectrum gives rise to an anomalous long time decay of the stress relaxation function in the sol phase for all  $c < c_{crit}$ . The true asymptotic behavior of  $D(\gamma) \sim \exp[-\sqrt{h(c)/\gamma}]$ , which is proven rigorously in Appendix A 3, implies  $\chi(t) \sim \exp[-(t/\tau^*)^\beta]$  with  $\beta = 1/3$ . However, we are unable to estimate the timescale needed to reach the asymptotic regime. For smaller times, the stress relaxation function is characterized by effective exponents, just as the spectra in Fig. 4 can be fitted to Lifshitz tails with effective exponents that depend on cross-link concentration  $c$ .

The divergence of the time scale  $\tau^*(\epsilon) \sim \epsilon^{-z}$  is determined by the function  $h(c)$ . The expansion of the resolvent for small  $\Omega$  suggests  $z = 3$ . At the critical point the density of eigenvalues is constant as  $\gamma \rightarrow 0$ , implying a logarithmic di-

vergence of the static shear viscosity and  $\chi(t) \sim t^{-\Delta}$  with  $\Delta = 1$ .

The absence of scaling in the density of states is also relevant for the stress relaxation function. The presence of more than one characteristic scale for the eigenvalues implies more than one characteristic time scale for the stress relaxation function. As a consequence, the stress relaxation function does not scale either. This point will be discussed further below in the context of numerical diagonalization of the connectivity matrix. Attempts to scale data for the time dependent stress relaxation function fail (see Fig. 14 below).

## IV. NUMERICAL DIAGONALIZATION

### A. Numerical methods

In this section the eigenvalue densities  $D(\gamma)$  of three different types of random network are studied numerically: mean-field (MF) networks as well as two- and three-dimensional simple square/cubic grids. For the first case, cross-links are allowed for all pairs  $i, j$  of nodes while for the other networks only cross-links between neighboring nodes may appear. For the finite-dimensional grids we apply periodic boundary conditions in all directions. The size of the networks is denoted by  $N$ , with  $N = L^d$  ( $d = 2, 3$ ) for the finite-dimensional cases. For the numerical treatment, we consider random graphs with a fixed number  $M$  of vertices, i.e. the cross-link concentration is  $c = M/N$ . Every cross-link has the same probability of occurrence. For the implementation of the graphs on the computer, the LEDA library [17] was used. Network sizes up to  $N = 10\,000$  (MF),  $N = 3136$  ( $d = 2$ ) and  $N = 4096$  ( $d = 3$ ) were studied. For each system size up to  $10^4$  different realizations of the disorder were considered (1000 for the largest sizes). Different concentrations of the cross-links between 0 and the percolation threshold  $c_{crit}$  were treated, where  $c_{crit}(\text{MF}) = 1/2$ ,  $c_{crit}(d=2) = 1$ , and  $c_{crit}(d=3) \approx 0.7464$  [18].

We consider the same two cases regarding the strength of the cross-links as above: Either all cross-links have the same strength  $\lambda = 1$  or their strengths are distributed randomly with the probability density given in Eq. (70). Numerically, the random values for the strengths of the cross-links are drawn using the inversion method [19]. A random number  $r$  is drawn that is uniformly distributed in  $[0, 1]$ . Then the values of  $\lambda := -1/\ln r$  are distributed according to (70). For testing purposes also some systems were studied where the strengths were uniformly distributed in the interval  $[0.5, 1.5]$ . In all cases no significant deviations of the measurable quantities for different distributions could be observed. The main difference is that for cross-links of unit strength the distribution  $D(\gamma)$  of the eigenvalues is dominated by a sum of  $\delta$  peaks below the percolation threshold while for cross-links of continuous strength the distribution  $D(\gamma)$  is purely continuous (see below).

The numerical method works as follows. Random networks are created, with constant or random cross-link strengths as needed. Then, for each graph the connected components are determined [20]. For each connected component the connectivity matrix is calculated, which is a real symmetric matrix. Therefore, for determining its eigenvalues

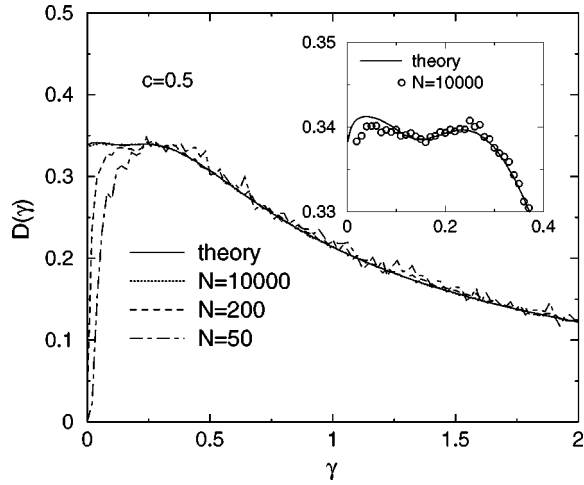


FIG. 5. Density  $D(\gamma)$  of nonzero eigenvalues for the mean-field network at the percolation threshold  $c=0.5$  from numerical diagonalization. The solid line is the analytical result, which is hardly distinguishable from the result for  $N=10\,000$ . The inset magnifies the region  $\gamma \in [0, 0.4]$ , where the numerical results for the largest system size  $N=10\,000$  are shown by circles.

the QR algorithm and the Householder method [21] can be applied. Next, the eigenvalues are sorted in increasing order. Each connected component has one smallest eigenvalue 0. Because of numerical errors usually the smallest eigenvalue is not zero but quite small, depending on the distribution of the strengths of the cross-links. Consequently, the smallest eigenvalue is assigned the value zero. Finally, the eigenvalues of all components are collected, sorted again, and stored for further evaluation for each realization of the network.

### B. Results for the mean-field system

First, we consider the density  $D(\gamma)$  of nonzero eigenvalues for the mean-field network at the percolation threshold  $c=1/2$ . Data for the case  $p(\lambda)=\delta(\lambda-1)$  have already been presented in Fig. 1. Here we consider the case where the strengths of the cross-links are distributed according Eq. (70). In Fig. 5 the resulting density is shown for different system sizes together with the analytical result [obtained from the numerical solution of Eq. (77)]. It can be seen that the size  $N=10\,000$  is already sufficient to reproduce the analytical behavior for a large range of eigenvalues. In particular, the ‘‘dip’’ near  $\gamma=0.15$  is validated by the numerical data (see inset). Because of the finite system sizes, arbitrarily small eigenvalues cannot be found; thus the numerics disagree with the analytical result in that region. Nevertheless, the analytical result  $\lim_{\gamma \rightarrow 0} D(\gamma) > 0$  can indeed be confirmed by extrapolating the numerical data to infinite system size.

The spectrum  $D(\gamma)$  for different cross-link concentrations  $c$  is presented in Fig. 3. Once more, the numerical ( $N=10\,000$ ) and the analytical results agree very well. For small  $\gamma$ , the logarithm of the spectrum should behave as  $\sim -\gamma^{-1/2}$  (Lifshitz tail). Figure 6 shows the logarithm of  $D(\gamma)$  in a double logarithmic plot in complete analogy to Fig. 4. Presumably, the system size of  $N=10\,000$  is still too

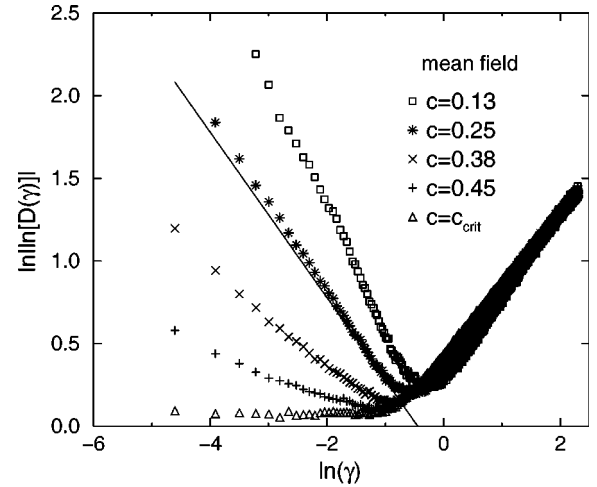


FIG. 6. Double logarithmic plot of  $-\ln[D(\gamma)]$  for different concentrations  $c$  of the mean-field network. The line shows a function  $-\ln(\gamma)/2 + \text{const}$  (Lifshitz tail), which is the behavior predicted by theory.

small in order to observe the asymptotic behavior of the density of states for small eigenvalues.

### C. Results for finite-dimensional systems

Next, we consider three-dimensional systems, which are believed to describe real polymer networks more appropriately. The density of eigenvalues for the case where all cross-links have the same strength,  $p(\lambda)=\delta(\lambda-1)$ , is shown in Fig. 7 for  $N=16^3$  and  $c=0.2$ . As in the mean-field case, a collection of  $\delta$ -peaks is obtained. Since this kind of distribution is more difficult to analyze, we turn again to the model where the strengths of the bonds have the distribution (70). Results for the largest system size  $N=16^3$  and different cross-link concentrations are shown in Fig. 8. Below the percolation transition  $c_{\text{crit}} \approx 0.7464$  the distribution exhibits a maximum and converges to 0 for small eigenvalues, similar

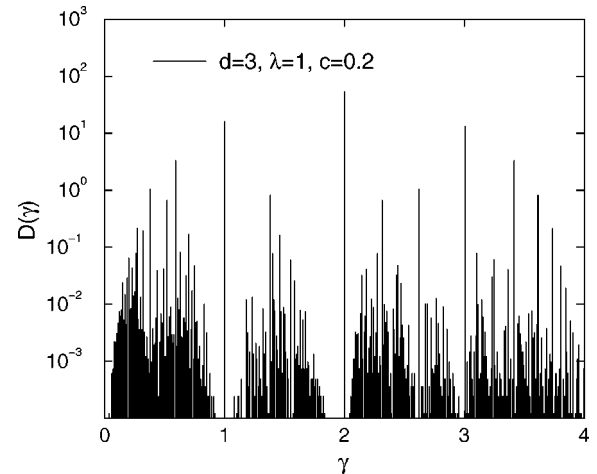


FIG. 7. Density  $D(\gamma)$  of nonzero eigenvalues for the cubic network with all bonds having the same strength  $\lambda=1$  ( $c=0.2, N=16^3$ ). Similar to the case of the mean-field network, a sum of  $\delta$  peaks with strongly varying heights is obtained.

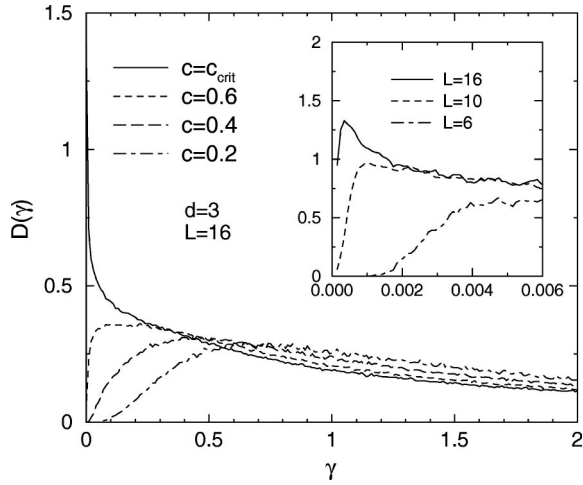


FIG. 8. Density  $D(\gamma)$  of nonzero eigenvalues for the cubic network with  $p(\lambda)$  given by Eq. (70) for different concentrations  $c$ . The inset shows the finite-size dependence at the percolation threshold for small eigenvalues.

to the mean-field case. At the transition,  $D(\gamma)$  diverges as  $\gamma \rightarrow 0$  (see also inset). Below we will show that this behavior changes the divergence of the viscosity near the percolation threshold. The eigenvalue densities for the two-dimensional network look qualitatively similar and are therefore not shown here. The true asymptotic behavior as  $\gamma \rightarrow 0$  is difficult to access, just as in the mean-field case.

The changes in the spectrum as compared to the mean-field case also affect the stress relaxation, which we investigate next. First, the viscosity given by

$$\bar{\eta} = [1 - T_0(c)] \int_0^\infty \frac{D(\gamma)}{\gamma} d\gamma \quad (78)$$

is considered. Here, irrelevant prefactors have been omitted for simplicity; see Eq. (18) for the complete expression. In the numerical calculation we compute

$$\eta = \frac{1}{N} \sum_{\gamma_i > 0} \frac{1}{\gamma_i} \quad (79)$$

for each realization and subsequently average over different realizations of the disorder to obtain  $\bar{\eta}$ . Whereas for the mean-field network the viscosity diverges logarithmically for  $c \rightarrow c_{\text{crit}}$ , for finite-dimensional systems a divergence  $\eta(c) \sim (c_{\text{crit}} - c)^{-k}$  is expected. The reason for the different divergences is the manner in which  $D(\gamma)$  behaves for small  $\gamma$  at the percolation threshold: for the mean-field network,  $\lim_{\gamma \rightarrow 0} D(\gamma)$  is finite, but for the finite-dimensional grids  $D(\gamma)$  diverges as  $\gamma \rightarrow 0$ . The critical exponent  $k$  of the viscosity can be determined from

$$\eta(c, L) = L^{-k/\nu} \tilde{\eta}[(c - c_{\text{crit}})L^{1/\nu}], \quad (80)$$

similar to the usual finite-size scaling relations [22] for the percolation transition. Here  $\tilde{\eta}$  is a universal function and  $\nu$  is the exponent describing the divergence of the correlation length when approaching the percolation transition. The use

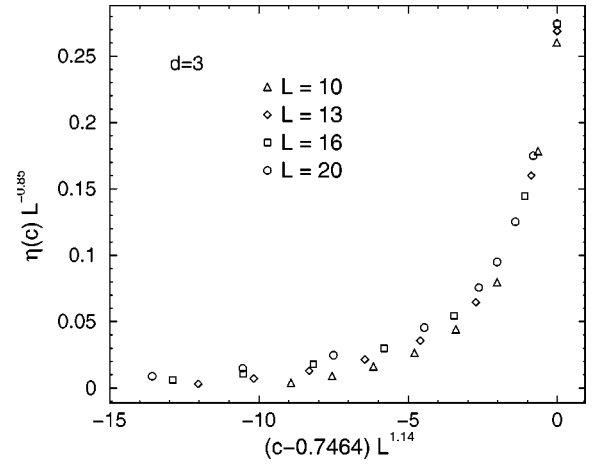


FIG. 9. Finite-size scaling plot of the viscosity  $\eta(c, L)$  for the three-dimensional grid. A scaling behavior of  $\eta(c, L) = L^{-k/\nu} \tilde{\eta}[(c - c_{\text{crit}})L^{1/\nu}]$  is assumed. Using  $\nu = 0.88$  and  $k = 0.75$  the points for  $L = 10, 13, 16, 20$  collapse onto one curve near the critical concentration.

of finite-size scaling enables us to circumvent the problems which are posed by the lack of very small eigenvalues of finite graphs.

By plotting  $\eta L^{k/\nu}$  against  $(c - c_{\text{crit}})L^{1/\nu}$  with correct parameters  $\nu$  and  $k$  the data points for different system sizes and  $c \approx c_{\text{crit}}$  should collapse onto a single curve. We have taken the values  $\nu(d=2) = 4/3$  and  $\nu(d=3) = 0.88$  from the literature [18] and adjusted  $k/\nu$ . The best collapse near  $c_{\text{crit}}$  was obtained with  $k(d=2) = 1.19$  and  $k(d=3) = 0.75$ . The results are presented in Figs. 9 ( $d=3$ ) and 10 ( $d=2$ ). The values we obtained for the different distributions of the cross-link strengths agree within the error bars.

The value of  $k$  for two dimensions agrees very well with the result  $k \sim 1.17$  found previously by Broderix et al. [10], using the high precision simulations of Gingold et al. [12].

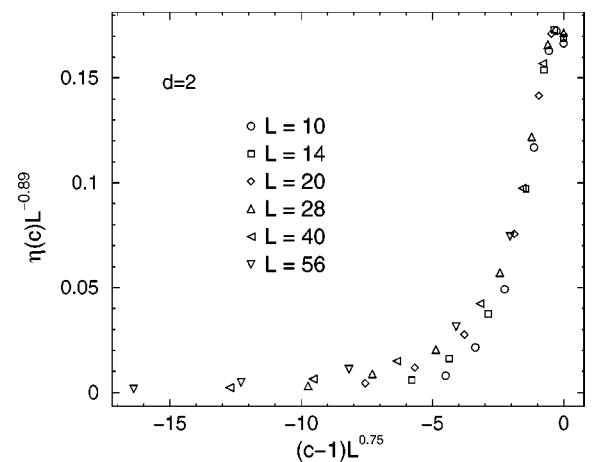


FIG. 10. Finite-size scaling plot of the viscosity  $\eta(c, L)$  for the two-dimensional grid. A scaling behavior of  $\eta(c, L) = L^{-k/\nu} \tilde{\eta}[(c - c_{\text{crit}})L^{1/\nu}]$  is assumed. Using  $\nu = 4/3$  and  $k = 1.19$  the points for  $L = 10, 14, 20, 28, 40, 56$  collapse onto one curve near the critical concentration. Since finite systems are treated, the maximum of  $\eta(c)$  is below the critical concentration  $c_{\text{crit}} = 1$  of the infinite lattice.

The result for the three-dimensional case ( $k=0.75$ ) is slightly worse in comparison with  $k\sim 0.71$  [10,12]. The reason is that here only small system sizes up to  $20^3$  could be treated due to the fact that all eigenvalues are calculated. If one is only interested in  $k$ , it is computationally less expensive to compute the Moore-Penrose inverse of the connectivity matrix. Thereby one might be able to study system sizes as large as those used in Ref. [12]. For the realizations treated here, we have checked other characteristic results concerning the percolation transition, like the critical exponent  $\sigma$ , which describes the behavior of the cluster-size distribution. The finite-size scaling plots have a poor quality for this quantity, too, resulting in a rather low precision of the exponent values. Additionally, we have observed a systematic drift in our results: By including even smaller system sizes, the scaling plot results in  $k=0.89$ , which differs even more from the value obtained before. Consequently, we believe that larger system sizes are needed, to obtain a more reliable result for  $k$  via numerical diagonalization of random connectivity matrices.

Next, the behavior of the stress relaxation function (again omitting irrelevant prefactors and using dimensionless time  $2dt/\zeta a^2 \rightarrow t$ )

$$\chi(t) = [1 - T_0(c)] \int_0^\infty D(\gamma) \exp(-\gamma t) d\gamma \quad (81)$$

was investigated; see Eq. (17) for the complete expression. The functions were obtained by first calculating  $D(\gamma)$  and then numerically integrating it. It would take too much time on the computer to first calculate  $\chi(t)$  for each realization by directly summing up the contributions and then average over the disorder. Here, we have investigated systems with continuously distributed cross-link strengths because they result in continuous eigenvalue densities where it is easier to obtain stable numerical data.

In Fig. 11 the numerical results for the mean-field network, the  $d=2$  and the  $d=3$  models for the largest sizes ( $c=c_{\text{crit}}$ ) are shown. As mentioned before, the numerical simulations are restricted to finite sizes of the networks and to a finite number of realizations of the disorder. Therefore, the eigenvalue densities  $D(\gamma)$  always have a smallest eigenvalue  $\gamma_{\text{min}}$  with  $D(\gamma)=0$  for  $\gamma < \gamma_{\text{min}}$ . Consequently, the long-time behavior is dominated by an exponential decrease  $\exp(-\gamma_{\text{min}}t)$ , irrespective of the true form of  $\chi(t)$ . This results in a negative curvature in the double-logarithmic plot for long times. Thus, in the numerical results, the asymptotic form of the relaxation function is visible only for intermediate times (see Fig. 11). At  $c=c_{\text{crit}}$  a  $\chi(t) \sim t^{-\Delta}$  behavior is expected. By fitting we obtain  $\Delta=1.029(5)$  (mean field),  $\Delta=0.830(2)$  ( $d=3$ ), and  $\Delta=0.741(2)$  ( $d=2$ ). The result for the mean-field case is known exactly to be  $\Delta=1$ . The discrepancy is again due to the finite sizes of the networks: Indeed, we have observed that for smaller networks a value of the exponent is obtained that is even larger. So the result  $\Delta=1$  seems to be confirmed. The value for the three-dimensional grid is compatible with the large range of results obtained in experiments [5].

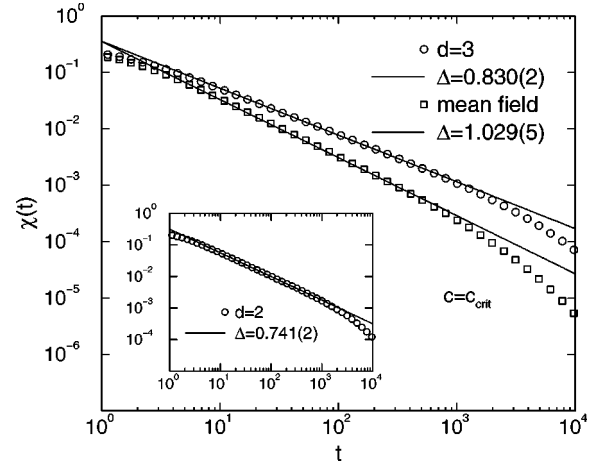


FIG. 11. Stress relaxation function  $\chi(t)$  at the critical concentration  $c=c_{\text{crit}}$  for the three types of model considered here, with continuously distributed strengths of the cross-links in all three cases. Shown are the results for the largest sizes that could be treated with sufficient accuracy. For the part of the long-time behavior which is accessible to the numerical simulations, a  $\chi(t) \sim t^{-\Delta}$  behavior is visible. From fitting we obtain  $\Delta=1.029$  (mean field),  $\Delta=0.830(2)$  ( $d=3$ ), and  $\Delta=0.741(2)$  ( $d=2$ ).

The stress relaxation function  $\chi(t)$  for different concentrations  $c$  of the cross-links is shown in Figs. 12 (mean field) and 13 ( $d=3$ ). In both cases we find exponential decay for the longest times due to finite system size. For intermediate times a stretched exponential behavior  $\chi(t) \sim \exp[-(t/\tau)^\beta]$  is visible. At least for finite system sizes the exponent  $\beta$  seems to be nonuniversal; we find values ranging from  $\beta=0.5$  for small cross-link concentrations down to  $\beta=0.2$  close to the percolation threshold. We suspect that the accessible times are too short to see the true asymptotic behavior, which at least in mean-field theory is known to be a stretched exponential with exponent  $\beta=1/3$ , resulting from the Lifshitz tail in the density of states. For small times  $\chi(t)$  decreases like  $t^{-\Delta}$  and  $\chi(0)=1$  by definition.

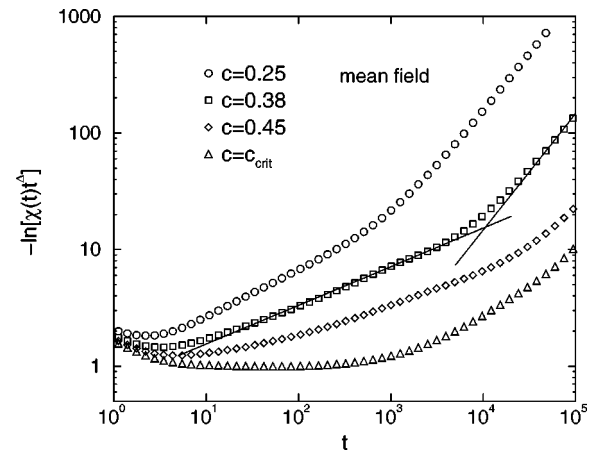


FIG. 12. Rescaled stress relaxation function  $-\ln[\chi(t)t^\Delta]$  as a function of the time for the mean-field network ( $\Delta=1.029$ ) with different concentrations  $c$  of the cross-links. The straight lines correspond to stretched exponentials with exponents  $\beta=0.332$  and  $\beta=1$ .

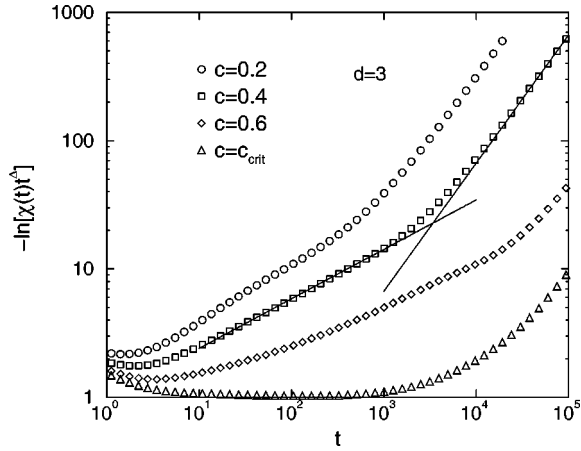


FIG. 13. Rescaled stress relaxation function  $-\ln[\chi(t)t^\Delta]$  as a function of the time for the three-dimensional network ( $\Delta = 0.830$ ) with different concentrations  $c$  of the cross-links. The straight lines correspond to stretched exponentials with exponents  $\beta = 0.386$  and  $\beta = 1$ .

Moreover, this variation of the exponent  $\beta$  makes it impossible to observe a scaling form  $\chi(t) \sim t^{-\Delta} g(t/\tau)$ , where  $\tau$  is a typical time scale that diverges like  $\tau \sim (c_{\text{crit}} - c)^{-z}$  when approaching the percolation threshold. For the mean-field network, the expectations from the Lifshitz tails are  $z = 3$  and  $\Delta = 1$ , while  $g(t)$  is the stretched exponential function, but we have already mentioned that there seems to be no scaling possible due to the existence of more than one scale. In Fig. 14 a scaling plot of  $\chi(t)$  is shown.  $\chi(t)t^\Delta$  is plotted against  $t \times (c_{\text{crit}} - c)^z$  for mean-field networks of different concentrations  $c$ . We have used only the regions below the finite-size asymptotic behavior ( $\beta = 1$ ). It can be seen that the quality of the collapse is rather bad, explained by the variation of  $\beta$  with  $c$ . One might think that near the transition  $c \approx c_{\text{crit}}$  the scaling may be better. But there the collapse is even worse (not shown), because even larger systems are necessary to reach the asymptotic regime for the small eigenvalues, as explained before.

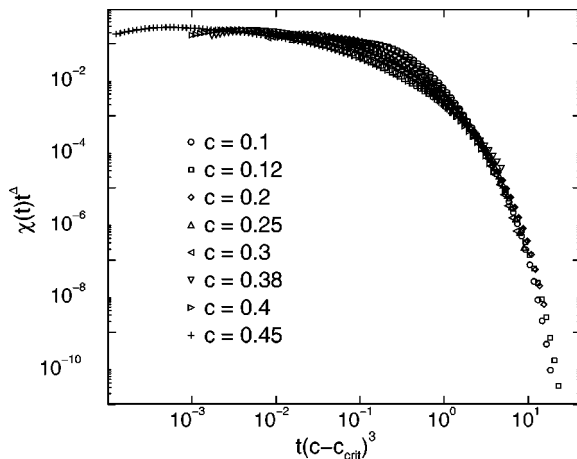


FIG. 14. Scaling plot for the stress relaxation  $\chi(t)t^\Delta$  as a function of  $t(c_{\text{crit}} - c)^z$  for the mean-field network ( $N = 10^4$ , randomly distributed strengths of cross-links) with the values  $\Delta = 1, z = 3$ .

For finite-dimensional systems, the quality of the scaling-plot is similar. Therefore, it is not possible to make a reliable estimate for the dynamical exponent  $z$  in that case.

## V. CONCLUSIONS

Within our model, the dynamics of a cross-linked polymer melt is determined completely by the eigenvalue and eigenvector spectrum of the connectivity matrix  $\Gamma$ . In this paper we have focused on some properties that are determined by the eigenvalues alone (e.g., the stress relaxation function) since the eigenvectors are hard to obtain. We have used three different methods to examine the eigenvalue spectrum: first, the construction of an exact solution for the averaged eigenvalue density for a fixed cross-link strength, second, a very precise numerical solution for the case of varying cross-link strengths, and third, a numerical diagonalization of random connectivity matrices.

The first method allowed for some exact results regarding the eigenvalue spectrum. It could be shown that the eigenvalue spectrum consists of a very complicated but countable set of  $\delta$  peaks, some of which could be calculated and compared with results from numerical diagonalization. Furthermore, we showed that the eigenvalue density does not show (exact) scaling behavior.

The second model of fluctuating cross-link strengths has the advantage that the eigenvalue spectrum becomes a continuous function instead of an inscrutable sum of  $\delta$  peaks. Additionally, it allowed for a fast numerical integration scheme. From these numerical solutions it could be inferred that the expected Lifshitz-tail behavior for small  $\gamma$  seems to set in only for extremely small  $\gamma$ , smaller than is accessible numerically. For this reason, the stress relaxation function does not show a stretched exponential form with exponent  $\beta = \frac{1}{3}$  within the accessible time window. Instead, for the times that could be reached, there seems to be a regime where an apparent stretched exponential with a cross-link concentration-dependent and thus nonuniversal  $\beta$  is observed. Furthermore, in numerical evaluations of the eigenvalue spectrum again scaling could not be observed, not even approximately, since at least two, possibly three or more, different  $\gamma$  scales with different  $c$  dependence could be identified. As a consequence, the stress relaxation function does not scale either.

The third method, numerical diagonalization, confirmed all results obtained so far very well. In particular it showed that the stress relaxation shows stretched exponential behavior with a concentration-dependent exponent  $\beta$  and it showed the failure of scaling of the stress relaxation function. It confirmed, however, the experimental findings that at the critical concentration the stress relaxation function decays algebraically with exponent  $\Delta$ . For the mean-field model, both theory and numerics yield the exponent  $\Delta = 1$ . Furthermore, numerical diagonalization allows for going beyond the mean-field approach. Results were obtained for connectivity matrices on two- and three-dimensional cubic lattices. Unlike the mean-field case, the density of eigenvalues now diverges at the critical concentration as  $\gamma \rightarrow 0$ , and consequently the viscosity shows a power law divergence as

opposed to a logarithmic divergence as seen in the mean-field case. The critical exponent for the viscosity is found to be  $k \approx 1.19$  ( $d=2$ ) and  $k \approx 0.75$  ( $d=3$ ). The exponent  $\Delta$  is found to be  $\Delta \approx 0.74$  ( $d=2$ ) and  $\Delta \approx 0.83$  ( $d=3$ ). These results are comparable to the experimental findings (see the Introduction). If dynamical scaling, Eq. (1), holds, the critical exponent  $z$  is determined by the scaling relation  $\Delta = (z - k)/z$ , which gives  $z \approx 4$ , also in good agreement with experiments.

The Rouse model has some limitations: Excluded volume effects, hydrodynamic interactions, and entanglement are naturally beyond its scope. Hence we consider our work as a first step toward a quantitative analysis of stress relaxation in polymer gels and are presently working on extensions of the dynamic model to include hydrodynamic as well as excluded volume interactions.

### ACKNOWLEDGMENTS

We thank P. Müller for interesting discussions and a careful reading of the manuscript. K.B. obtained financial support from the DFG (Deutsche Forschungsgemeinschaft) under Grant No. Br 1894/1-1, T.A. under Grant No. Zi209/5-1, and A.K.H. under Grant No. Zi209/6-1.

### APPENDIX A: LOW FREQUENCY EXPANSION OF THE RESOLVENT

#### 1. General $p(\lambda)$

The low frequency expansion is derived from an alternative form of the integral equation (33). We start from Eq. (30) and recall an integral representation of the  $n$ -dimensional Laplacian [see also Eqs. (3.47)–(3.51)] in Ref. [13]]

$$\int \frac{d\hat{y}}{(2\pi\Omega)^{n/2}} \exp\left\{-\frac{(\hat{x}-\hat{y})^2}{2\Omega}\right\} f(|\hat{y}|) = \exp\left\{\frac{\Omega}{2}\left(\frac{d^2}{d\rho^2} + \frac{n-1}{\rho}\frac{d}{d\rho}\right)\right\} f(\rho) \Bigg|_{\rho=|\hat{x}|}. \quad (\text{A1})$$

We use this representation in the numerator of Eq. (30) and take the limit  $n \rightarrow 0$ . To evaluate the denominator of Eq. (30) we observe that

$$\lim_{n \rightarrow 0} \int d\hat{x} f_n(|\hat{x}|) = f_0(0) + \mathcal{O}(n). \quad (\text{A2})$$

Both steps taken together lead to the following self-consistent equation for  $g^\Omega(\rho)$ :

$$g^\Omega(\rho) = 2c e^{-2c} \int_0^\infty d\lambda p(\lambda) \exp\left\{\frac{1}{2i\lambda}\left(\frac{\partial^2}{\partial\rho^2} - \frac{\partial}{\rho\partial\rho}\right)\right\} \times \exp\left\{\frac{i\Omega}{2}\rho^2 + g^\Omega(\rho)\right\}, \quad (\text{A3})$$

which is of course equivalent to the integral equation (33), but much better suited for a low frequency expansion.

To that end we rescale variables according to  $x = \sqrt{\Omega}\rho$  and  $\Psi^\Omega(x) = g^\Omega(x/\sqrt{\Omega})$ . The self-consistent equation then reads

$$\Psi^\Omega(x) = 2c e^{-2c} \int_0^\infty d\lambda p(\lambda) \exp\left\{\frac{\Omega}{2i\lambda}\left(\frac{\partial^2}{\partial x^2} - \frac{\partial}{x\partial x}\right)\right\} \times \exp\left\{\frac{i}{2}x^2 + \Psi^\Omega(x)\right\}. \quad (\text{A4})$$

We look for a solution in terms of a power series in  $\Omega$ ,

$$\Psi^\Omega(x) = \sum_{j=0}^{\infty} (\Omega)^j \Psi_j(x). \quad (\text{A5})$$

The resolvent can then be expressed in terms of  $\Psi_j(x)$  as

$$G(\Omega) = -P_1 + \frac{i}{2c\Omega} \sum_{j=0}^{\infty} \Omega^j \int_0^\infty dx x \Psi_j(x) \quad (\text{A6})$$

with  $P_n = \int_0^\infty d\lambda \lambda^{-n} p(\lambda)$  as defined after Eq. (38). The lowest order term obeys the equation

$$\Psi_0(x) = 2c \exp(-2c) \exp\left(\frac{i}{2}x^2 + \Psi_0(x)\right), \quad (\text{A7})$$

which is solved by

$$\Psi_0(x) = -W(-2c \exp(-2c) \exp(ix^2/2)). \quad (\text{A8})$$

Here  $W$  denotes the principal branch of Lambert's  $W$  function, defined as the solution of

$$W(x) \exp[W(x)] = x. \quad (\text{A9})$$

From Eq. (A7) one derives the following property of the lowest order solution:

$$\Psi_0'(x) = \frac{ix\Psi_0(x)}{1 - \Psi_0(x)} \quad (\text{A10})$$

which allows for an exact computation of the integral

$$i \int_0^\infty dx x \Psi_0(x) = -\frac{1}{2} \int_0^\infty dx \frac{d}{dx} [1 - \Psi_0(x)]^2 = 2c(c-1). \quad (\text{A11})$$

The next two terms are given by

$$\Psi_1(x) = \frac{1}{1 - \Psi_0(x)} \frac{P_1}{2i} \left(\frac{d^2}{dx^2} - \frac{d}{x dx}\right) \Psi_0(x), \quad (\text{A12})$$

$$\Psi_2(x) = \frac{-1}{1 - \Psi_0(x)} \left(\frac{d^2}{dx^2} - \frac{d}{x dx}\right) \left(\frac{P_2}{8} + \frac{P_1^2}{1 - \Psi_0(x)}\right) \times \left(\frac{d^2}{dx^2} - \frac{d}{x dx}\right) \Psi_0(x). \quad (\text{A13})$$

The integrals  $\int dx x \Psi_j(x)$  can be performed like Eq. (A11), using the properties of Lambert's  $W$  function. The computations, however, become increasingly tedious, so that higher order terms have been computed only for the special distribution  $p(\lambda)$  (see below).

## 2. Special $p(\lambda)$

We start from Eq. (A3) and introduce the abbreviation  $D_\rho := d^2/d\rho^2 - d/\rho d\rho$ . For the special choice  $p(\lambda) = (1/\lambda^2)\exp(-1/\lambda)$ , one can perform the average over  $p(\lambda)$  analytically,

$$\int_0^\infty \frac{d\lambda}{\lambda^2} \exp\left\{-\frac{(1+iD_\rho/2)}{\lambda}\right\} \exp\left\{\frac{i\Omega}{2}\rho^2 + g^\Omega(\rho)\right\} = \left(1 + \frac{iD_\rho}{2}\right)^{-1} \exp\left\{\frac{i\Omega}{2}\rho^2 + g^\Omega(\rho)\right\}. \quad (\text{A14})$$

The resulting differential equation simplifies, if we introduce the function  $f_\Omega(\rho^2/2) := g^\Omega(\rho)$ ,

$$f_\Omega(\rho^2/2) + i\rho^2/2 f_\Omega''(\rho^2/2) = 2c \exp(-2c) \exp[i\Omega\rho^2/2 + f_\Omega(\rho^2/2)]. \quad (\text{A15})$$

Introducing the new variable  $x = \rho^2/2$  leads to the differential Eq. (72) quoted in the main part of the paper. For the low frequency expansion it is convenient to introduce yet another variable,  $y = \Omega x$ , in terms of which the differential equation for  $h_\Omega(\Omega x) := f_\Omega(x)$  reads

$$h_\Omega(y) - iy\Omega h_\Omega''(y) = 2c \exp(-2c) \exp[iy + h_\Omega(y)]. \quad (\text{A16})$$

The ansatz  $h_\Omega(y) = \sum_{j=0}^\infty (\Omega)^j h_j(y)$  then yields

$$h_n(y) - iy h_{n-1}''(y) = h_0(y) \frac{1}{n!} \frac{d^n}{d\Omega^n} \times \exp\left(\sum_{j=1}^\infty (\Omega)^j h_j(y)\right)_{\Omega=0}. \quad (\text{A17})$$

The left hand side is linear in  $h_n(y)$ , so that Eq. (A17) is easily iterated.

## 3. Proof of the existence of a Lifshitz tail in $D(\gamma)$

The aim of this Appendix is to prove that the density of eigenvalues  $D(\gamma)$  shows a Lifshitz-tail behavior for  $\gamma \rightarrow 0$  and  $c < 1/2$ . For the proof, it is convenient to make use of the eigenvalue distribution function  $F(\gamma) := \int_{-\infty}^\gamma d\gamma' D(\gamma')$ . This can be done without loss of generality because if  $F(\gamma)$  has a Lifshitz tail, so does  $D(\gamma)$ . It will be shown that  $F(\gamma)$  lies between two bounds which, taken together, assert the Lifshitz behavior.

For a given realization of a system with  $N$  vertices (or polymers), the corresponding  $F_N(\gamma)$  can be written, using a decomposition into the  $K$  clusters of the realization,

$$F_N(\gamma) = \frac{1}{N} \sum_{k=1}^K \text{Tr} \Theta(\gamma - \Gamma_k) = \frac{K}{N} + \frac{1}{N} \sum_{k=1}^K \text{Tr}[(1 - E_0^k) \Theta(\gamma - \Gamma_k)], \quad (\text{A18})$$

where  $\Gamma_k$  is the connectivity matrix of the  $k$ th cluster and  $E_0^k$  is the projector on the null space of  $\Gamma_k$ . In the macroscopic limit  $N \rightarrow \infty$ , this yields

$$F(\gamma) = (1-c) \Theta(\gamma) + \sum_{n=1}^\infty \tau_n \langle \text{Tr}[(1 - E_0^n) \Theta(\gamma - \Gamma(\mathcal{T}_n))] \rangle \quad (\text{A19})$$

due to self-averaging. The bracket  $\langle \dots \rangle$  means averaging over the set of all numbered trees  $\{\mathcal{T}_n\}$  of size  $n$  of which there are  $n^{n-2}$ .  $\Gamma(\mathcal{T}_n)$  denotes the connectivity matrix corresponding to the tree  $\mathcal{T}_n$ . The average number of trees of size  $n$  per vertex is denoted by  $\tau_n$  and is given by [15]

$$\tau_n = \frac{n^{n-2}}{2cn!} (2ce^{-2c})^n = \frac{1}{2c\sqrt{2\pi}} n^{-5/2} e^{-nh(c) - f(n)/n} \quad (\text{A20})$$

according to Stirling's formula with  $h(c) = 2c - 1 - \ln(2c)$  and some function  $f(n)$  with  $0 < f(n) < 1$ .

The smallest nonzero eigenvalue of  $\Gamma(\mathcal{T}_n)$  is certainly greater than or equal to the smallest nonzero eigenvalue of the linear cluster with  $n$  vertices, which is proportional to  $n^{-2}$ , i.e.,

$$\Gamma(\mathcal{T}_n) \geq \frac{\alpha}{n^2} \quad (\text{A21})$$

(except for the zero eigenvalue) with some  $\alpha$  independent of  $n$ . This results in

$$\text{Tr}[(1 - E_0^n) \Theta(\gamma - \Gamma(\mathcal{T}_n))] \leq (n-1) \Theta(\gamma - \alpha/n^2) \quad (\text{A22})$$

or

$$F(\gamma) \leq 1 - c + \sum_{n \geq \sqrt{\alpha/\gamma}} (n-1) \tau_n \quad \text{for } \gamma > 0. \quad (\text{A23})$$

For  $\gamma \rightarrow 0$ , the sum can be approximated by an integral,

$$F(\gamma) \leq 1 - c + \frac{1}{2c\sqrt{2\pi}} \int_{\sqrt{\alpha/\gamma}}^\infty n^{-3/2} e^{-nh(c)} \quad (\text{A24})$$

$$\approx 1 - c + \frac{1}{2ch(c)\sqrt{2\pi}} \left(\frac{\gamma}{\alpha}\right)^{3/4} \exp\left\{-h(c) \left(\frac{\alpha}{\gamma}\right)^{1/2}\right\}. \quad (\text{A25})$$

This is the lower bound for  $F(\gamma)$ .

For the upper bound, Eq. (A19) will be used again. Explicitly, one has for  $\gamma > 0$

$$F(\gamma) = 1 - c + \frac{1}{2c} \sum_{n=1}^{\infty} \frac{1}{n!} (2ce^{-2c})^n \times \sum_{\{\mathcal{T}_n\}} \text{Tr}[(1 - E_0^n) \Theta(\gamma - \Gamma(\mathcal{T}_n))] \quad (\text{A26})$$

$$\geq 1 - c + \frac{1}{2c} \sum_{n=1}^{\infty} \frac{1}{n!} (2ce^{-2c})^n \times \sum_{\{\mathcal{L}_n\}} \text{Tr}[(1 - E_0^n) \Theta(\gamma - \Gamma(\mathcal{L}_n))], \quad (\text{A27})$$

where the inner sum has been restricted to the set of *linear* numbered trees  $\{\mathcal{L}_n\}$ . There are  $n!/2$  such linear trees, such that

$$F(\gamma) = 1 - c + \frac{1}{4c} \sum_{n=2}^{\infty} e^{-n[h(c)+1]} \text{Tr}[(1 - E_0^n) \Theta(\gamma - \Gamma(\mathcal{L}_n))]. \quad (\text{A28})$$

Next, the trace, which is a sum of non-negative terms, is estimated by just one of the terms. In particular,  $\text{Tr}[(1 - E_0^n) \Theta(\gamma - \Gamma(\mathcal{L}_n))] \geq \Theta(\gamma - \alpha/n^2)$ , corresponding to the smallest eigenvalue of  $\mathcal{L}_n$ . This finally gives

$$F(\gamma) \geq 1 - c + \frac{1}{4c} \sum_{n \geq \sqrt{\alpha/\gamma}} e^{-n[h(c)+1]} \quad (\text{A29})$$

$$\approx 1 - c + \frac{1}{2c[1+h(c)]} \exp\left\{-\left(\frac{\alpha}{\gamma}\right)^{1/2} [1+h(c)]\right\} \quad (\text{A30})$$

for the lower bound.

The upper and the lower bound together imply

$$\lim_{\gamma \rightarrow 0} \frac{\ln|\ln[F(\gamma) - 1 + c]|}{|\ln \gamma|} = \frac{1}{2} \quad (\text{A31})$$

or, even stronger,

$$\sqrt{\alpha} h(c) \leq -\lim_{\gamma \rightarrow 0} \gamma^{1/2} \ln[F(\gamma) - 1 + c] \leq \sqrt{\alpha} [h(c) + 1], \quad (\text{A32})$$

which is the sought-for Lifshitz-tail behavior.

## APPENDIX B: DETAILS OF THE EXACT SOLUTION OF THE INTEGRAL EQUATION

### 1. Solution of the integral equation

It is not obvious how to solve the fix-point equations 61, because the coefficients of the  $i$ th iteration are labeled by an index, and a subsequent iteration gives rise to coefficients that are labeled by a sequence  $(l_k)$ . We therefore try to map the sequence  $(l_k)$  that appears as index onto a number by writing  $n := \sum_{k=0}^{\infty} l_k M^k$  with some  $M \in \mathbb{N}$ . For this to be a one-to-one map, we need to restrict all  $l_k$  to be  $< M$ . This restriction will be removed later when we let  $M \rightarrow \infty$ . The sequence  $(l_k)$  can be reconstructed from  $n$  by writing  $n$  in the number system of base  $M$ . Let this be indicated by  $l_k = (n)_k^M$ .

The fix-point equations can now be written down as

$$a_n = e^{-2c} \prod_{k=0}^{\infty} \frac{(2ca_k)^{(n)_k^M}}{(n)_k^M!}, \quad (\text{B1})$$

$$z_n = 1 + \frac{1}{\Omega - 1 - \sum_{k=0}^{\infty} (n)_k^M z_k}. \quad (\text{B2})$$

The equations for  $a_n$  can be solved independently from those for  $z_n$ . We start with  $a_n$ . Successively solving the system of equations (B1) by inspection gives

$$a_0 = e^{-2c}, \quad (\text{B3})$$

$$a_n = \begin{cases} e^{-2c} \frac{(2ca_0)^n}{n!} & \text{for } 1 \leq n < M \\ e^{-2c} \prod_{k=0}^{M-1} \frac{(2ca_k)^{(n)_k^M}}{(n)_k^M!} & \text{for } M \leq n < M^M \\ e^{-2c} \prod_{k_0=0}^{M-1} \dots \prod_{k_{M-1}=0}^{M-1} \frac{(2ca_{k_0+Mk_1+\dots+M^{M-1}k_{M-1}})^{(n)_{k_0+Mk_1+\dots}^M}}{(n)_{k_0+Mk_1+\dots}^M!} & \text{for } M^M \leq n < M^{M^2} \end{cases} \quad (\text{B4})$$

$$a_n = \begin{cases} e^{-2c} \frac{(2ca_0)^n}{n!} & \text{for } 1 \leq n < M \\ e^{-2c} \prod_{k=0}^{M-1} \frac{(2ca_k)^{(n)_k^M}}{(n)_k^M!} & \text{for } M \leq n < M^M \end{cases} \quad (\text{B5})$$

$$e^{-2c} \prod_{k_0=0}^{M-1} \dots \prod_{k_{M-1}=0}^{M-1} \frac{(2ca_{k_0+Mk_1+\dots+M^{M-1}k_{M-1}})^{(n)_{k_0+Mk_1+\dots}^M}}{(n)_{k_0+Mk_1+\dots}^M!} \quad \text{for } M^M \leq n < M^{M^2}, \quad (\text{B6})$$

and so on. The coefficient  $a_0$  is obviously independent of all other  $a_n$ . This property will be called ‘‘class 0.’’  $a_1, \dots, a_{M-1}$  depend only on  $a_0$ : this will be termed ‘‘class 1.’’ Analogously,  $a_M, \dots, a_{M^2-1}$  are in class 2 as they depend only on  $a$ 's from classes 0 and 1.

Now we can let  $M$  tend to infinity. Classes 0 and 1 are special (the upper index now denotes the class):

$$a_0^0 = e^{-2c}, \quad (\text{B7})$$

$$a_n^1 = e^{-2c} \frac{(2ce^{-2c})^n}{n!}, \quad n \geq 1. \quad (\text{B8})$$

If we drop the constraint  $n \geq 1$ , Eq. (B8) automatically contains class 0.

For the higher classes, as we are now considering  $M \rightarrow \infty$ , indexing via a number  $n$  is no longer possible. Instead, for class 2, we have to revert to using a finite sequence as index. For class 3, even this is not sufficient and a nested sequence  $(l_{(k_i)})$  is needed:

$$a_{(l_k)}^2 = e^{-2c} \prod_{k=0}^{\infty} \frac{(2ca_k^1)^{l_k}}{l_k!}, \quad \text{length of } (l_k) > 1, \quad (\text{B9})$$

$$a_{(l_{(k_i)})}^3 = e^{-2c} \prod_{\{(k_i)\}} \frac{(2ca_{(k_i)}^2)^{l_{(k_i)}}}{l_{(k_i)}!}. \quad (\text{B10})$$

If the constraint [length of  $(l_k) > 1$ ] is dropped and if the explicit expressions for the  $a$  from the lower classes are recursively inserted, all classes up to class 2 are contained in one formula, Eq. (B9). An analogous statement holds for Eq. (B10).

In general, for class  $m$ , the index will be of the form  $(l_{(k_{\dots(r_i)})})$  with  $m$  nesting levels. The general result is thus

$$a_{(l_{(k_{\dots(r_i)})})}^m = e^{-2c} \prod_{\{(k_{\dots(r_i)})\}} \frac{(2ca_{(k_{\dots(r_i)})}^{m-1})^{l_{(k_{\dots(r_i)})}}}{l_{(k_{\dots(r_i)})}!}. \quad (\text{B11})$$

With the same reasoning as above we can calculate the  $z_n$ . We find the same classes, and the results are

$$z_0^0 = \frac{\Omega}{\Omega - 1}, \quad (\text{B12})$$

$$z_n^1 = \frac{\Omega - nz_0^0}{\Omega - 1 - nz_0^0}, \quad (\text{B13})$$

$$z_{(l_k)}^2 = \frac{\Omega - \sum_{k=0}^{\infty} l_k z_k^1}{\Omega - 1 - \sum_{k=0}^{\infty} l_k z_k^1}, \quad (\text{B14})$$

⋮

$$z_{(l_{(k_{\dots(r_i)})})}^m = \frac{\Omega - \sum_{\{(k_{\dots(r_i)})\}} l_{(k_{\dots(r_i)})} z_{(k_{\dots(r_i)})}^{m-1}}{\Omega - 1 - \sum_{\{(k_{\dots(r_i)})\}} l_{(k_{\dots(r_i)})} z_{(k_{\dots(r_i)})}^{m-1}}. \quad (\text{B15})$$

## 2. Properties of the solution

If one asks for the total weight of a particular peak at, say, some  $\gamma_0$  (up to class  $m$ ), one has to find all finite solutions  $(l_k)$  of the diophantic equation

$$\gamma_0 - \sum_{k=0}^{\infty} l_k z_k^{m-1}(\gamma_0) = 0. \quad (\text{B16})$$

This is possible in some special cases, e.g., for  $\gamma_0 = 1$  in class 2. Since  $z_n^1(1) = 1$ , it follows that Eq. (B16) is satisfied if and only if exactly one entry of  $(l_k)$  equals 1 whereas all the others are 0. Adding up all of the weights yields  $e^{-2c}[(2ce^{-2c} - 1)e^{2ce^{-2c}} + 1]$  as the total weight of  $\delta(\gamma - 1)$  from class 2.

The  $z_{(l_k)}^m$  have several noteworthy properties, most of which are easy to prove by induction over  $m$  and are therefore listed below without proof.

(1)  $z_{(l_k)}^m$  is a rational function of  $\gamma$  with integer coefficients.

(2) The degree of the numerator is the same as that of the denominator.

(3) The coefficient of the highest power is 1 in both numerator and denominator.

(4)  $z_{(l_k)}^m$  is a strictly monotonically decreasing function (except at its poles).

(5) All roots and poles of  $z_{(l_k)}^m$  are located on the non-negative real axis.

(6)  $z_{(l_k)}^m$  has exactly as many poles as roots. Roots and poles alternate, starting with a root at 0.

(7) There is exactly one more root of  $z_{(l_k)}^m$  than there are poles in  $\sum_{k=0}^{\infty} l_k z_k^{m-1}$ .

(8) The sum  $\sum_i |(\partial z_{(l_k)}^m / \partial \gamma)(\gamma_{(l_k),i}^m)|^{-1}$  over all roots  $\gamma_{(l_k),i}^m$  of  $z_{(l_k)}^m$  equals 1. As stated in the text, this can be proved using Cauchy's integration theorem.

Consider now some  $z_{(l_k)}^m$  and choose  $(l_k)$  such that only the  $n$ th entry is nonzero. Then we have

$$z_{0, \dots, 0, l_n, 0, \dots}^m = \frac{\gamma - l_n z_n^{m-1}}{\gamma - 1 - l_n z_n^{m-1}}. \quad (\text{B17})$$

Between two of its poles (see the list of properties above),  $z_n^{m-1}$  is a continuous function that maps one to one onto the real numbers; therefore there exists a  $\gamma_{l_n}^m$  in this interval such that  $z_{(l_k)}^m(\gamma_{l_n}^m) = 0$ . Moreover, when  $l_n \rightarrow \infty$ , the  $\gamma_{l_n}^m$  converge to the root  $\gamma_{n,i}^{m-1}$  of  $z_n^{m-1}$  in this interval. Since  $z_n^{m-1}$  is monotonically decreasing,  $\gamma_{l_n}^m < \gamma_{n,i}^{m-1}$ . This implies that for every peak in the spectrum there are infinitely many other peaks to the left of it in any arbitrarily small interval around this peak. This also applies recursively for each of these satellite peaks. Only the peak at 0 is different: as stated in the list above, all roots of  $z_{(l_k)}^m$  are  $\geq 0$  and thus there are no satellite peaks of  $\delta(\gamma)$ .

[1] J.E. Martin and D. Adolf, *Annu. Rev. Phys. Chem.* **42**, 311 (1991).

[2] D. Adolf and J.E. Martin, *Macromolecules* **23**, 3700 (1990).

[3] J.E. Martin, D. Adolf, and J.P. Wilcoxon, *Phys. Rev. Lett.* **61**, 2620 (1988); *Phys. Rev. A* **39**, 1325 (1989).

[4] D. Durand, M. Delsanti, M. Adam, and J.N. Luck, *Europhys.*

- Lett. **3**, 297 (1987).
- [5] H.H. Winter, Prog. Colloid Polym. Sci. **75**, 104 (1987); F. Chambon and H.H. Winter, J. Rheol. **31**, 683 (1987); J.C. Scanlan and H.H. Winter, Macromolecules **24**, 47 (1991).
- [6] M. Adam, M. Delsanti, and D. Durand, Macromolecules **18**, 2285 (1985).
- [7] P.M. Goldbart, H.E. Castillo, and A. Zippelius, Adv. Phys. **45**, 393 (1996).
- [8] A.J. Bray and G.J. Rodgers, Phys. Rev. B **38**, 11 461 (1988).
- [9] G. Biroli and R. Monasson, J. Phys. A **32**, L255 (1999).
- [10] K. Broderix, H. Löwe, P. Müller, and A. Zippelius, Europhys. Lett. **48**, 421 (1999).
- [11] P. Grassberger, Physica A **262**, 251 (1999).
- [12] D.B. Gingold and C.J. Lobb, Phys. Rev. B **42**, 8220 (1990).
- [13] K. Broderix, H. Löwe, P. Müller, and A. Zippelius, Phys. Rev. E **63**, 011510 (2000).
- [14] K. Broderix, P. M. Goldbart, and A. Zippelius, Phys. Rev. Lett. **79**, 3688 (1997).
- [15] P. Erdős and A. Rényi, Magy. Tud. Akad. Mat. Kut. Int. Kőzl. **5**, 17 (1960); reprinted in *The Art of Counting*, edited by J. Spencer (MIT Press, Cambridge, MA, 1973).
- [16] I.S. Gradshteyn and I.M. Ryzhik, *Table of Integrals, Series and Products* (Academic, New York, 1980).
- [17] K. Mehlhorn and St. Näher, *The LEDA Platform of Combinatorial and Geometric Computing* (Cambridge University Press, Cambridge, 1999); see also <http://www.mpi-sb.mpg.de/LEDA/leda.html>
- [18] D. Stauffer and A. Aharony, *Introduction to Percolation Theory* (Taylor and Francis, London, 1994).
- [19] B.J.T. Morgan, *Elements of Simulation* (Chapman and Hall, London, 1984).
- [20] A. Aho, J.E. Hopcroft, and J.D. Ullman, *The Design and Analysis of Computer Algorithms* (Addison-Wesley, Reading, MA, 1974).
- [21] W.H. Press, S.A. Teukolsky, W.T. Vetterling, and B.P. Flannery, *Numerical Recipes in C* (Cambridge University Press, Cambridge, 1995).
- [22] K. Binder and D.W. Heermann, *Monte Carlo Simulation in Statistical Physics* (Springer, Heidelberg, 1988).

## Density of states of a sparse random matrix

G. J. Rodgers

*Department of Theoretical Physics, The University, Manchester, M13 9PL, United Kingdom*

A. J. Bray\*

*Schlumberger-Doll Research, Old Quarry Road, Ridgefield, Connecticut 06877-4108*

(Received 28 April 1987)

The density of states  $\rho(\mu)$  of an  $N \times N$  real, symmetric, random matrix with elements  $0, \pm 1$  is calculated in the limit  $N \rightarrow \infty$  as a function of the average "connectivity"  $p$ , i.e., of the mean number of nonzero elements per row. For  $p \rightarrow \infty$ , the Wigner semicircular distribution is recovered. For finite  $p$  the distribution has tails extending beyond the semicircle, with  $\rho(\mu) \sim (ep/\mu^2)^{\mu^2}$  for  $\mu^2 \rightarrow \infty$ . Applications to the theory of "Griffiths singularities" in dilute magnets are discussed.

### I. INTRODUCTION

There has been recent interest<sup>1,2</sup> in spin systems in which the exchange interactions are very dilute, but of infinite range, in such a way that the average coordination number is finite. This is achieved by letting the bond occupation probability be  $p/N$ , where  $N$  is the number of sites. Then the mean coordination number is  $p$ .

There are many reasons to study such models. While the finite coordination number is characteristic of systems with short-range interactions, the infinite-range forces lead to exactly soluble models.<sup>1,2</sup> In addition, such models allow one to study the interplay between magnetic order and percolation.<sup>1,2</sup> Finally, the technical problems posed by these models have strong formal similarities with those encountered in many problems of combinatorial optimization, such as graph-partitioning,<sup>3-5</sup> matching,<sup>6</sup> and traveling-salesman<sup>7</sup> problems.

Our own motivation originally arose from the desire to understand the role of Griffiths singularities<sup>8</sup> in both the statics and dynamics<sup>9</sup> of dilute spin systems at temperatures between the critical temperatures of the dilute and non-dilute systems (the "Griffiths phase"<sup>10</sup>). It has been argued<sup>11</sup> that this temperature regime is characterized by unusual behavior of the spectrum of the inverse  $\chi^{-1}$  of the matrix of susceptibilities. In particular  $\chi^{-1}$  should have eigenvalues arbitrarily close to zero, corresponding to localized eigenstates. The phase transition should occur when the eigenstate at the mobility edge goes soft, i.e., when the mobility edge reaches zero eigenvalue.<sup>11,12</sup> It would be very nice to be able to construct an exactly soluble model, such as mean-field theory, exhibiting this effect, and dilute, finitely coordinated, infinite-range models seem promising. Unfortunately, determination of the matrix  $\chi^{-1}$  is itself a difficult nonlinear problem. Therefore, as a first step, we look at the simpler problem of the eigenvalue spectrum of the exchange matrix  $\underline{J}$ . Note that at high temperatures these matrices are related,<sup>11,12</sup> since  $\chi^{-1} = T\underline{I} - \underline{J} + O(1/T)$ , where  $\underline{I}$  is the unit matrix.

While the above considerations provide the authors' personal motivation, the eigenvalue spectrum of a large random matrix is an interesting problem in its own right,

and has a long history.<sup>13</sup> The simplest case is when the elements of the matrix are identically distributed independent random variables with zero mean. For this case one obtains, in the limit of large matrices, the famous "semicircular" distribution of Wigner.<sup>14</sup> We recover this result in the limit that the mean "connectivity"  $p$  (i.e., the mean number of nonzero elements per row) of the sparse matrix tends to infinity. For any finite  $p$ , however, we will show that there are states beyond the semicircle, and that the density of states in the tails of the distribution varies as  $\rho(\mu) \sim (ep/\mu^2)^{\mu^2}$ .

The outline of the paper is as follows. In Sec. II we present the model, and in Sec. III give its formal solution in terms of a nonlinear integral equation. In Sec. IV the integral equation is solved perturbatively to  $O(1/p)$ . The leading term reproduces the semicircle law while the  $O(1/p)$  correction may be interpreted in terms of a shifted band edge. In perturbation theory, however, there are no states at large eigenvalue. To obtain such states it is necessary to extract a nonperturbative contribution from the integral equation, and this is done in Sec. V. Section VI contains a summary and discussion of the results.

### II. THE MODEL

We consider a real, symmetric  $N \times N$  matrix  $\underline{J}$  whose elements  $J_{ij}$  are (up to the symmetry  $J_{ij} = J_{ji}$ ) independent, identically distributed, random variables, with probability distribution

$$P(J_{ij}) = \left[ 1 - \frac{p}{N} \right] \delta(J_{ij}) + \frac{p}{2N} [\delta(J_{ij} - 1) + \delta(J_{ij} + 1)]. \quad (1)$$

For a particular realization of the matrix  $\underline{J}$ , the normalized density of states  $\rho(\mu)$  can be obtained from the Green's matrix

$$\underline{G}(\mu) = (\underline{J} - \mu\underline{I})^{-1} \quad (2)$$

via

$$\rho(\mu) = \frac{1}{N\pi} \text{Im Tr} \underline{G}(\mu + i\delta), \quad (3)$$

where  $\delta$  is a positive infinitesimal.

To compute  $\rho(\mu)$  it is convenient to introduce the generating function

$$Z(\mu) = \int_{-\infty}^{\infty} \left[ \prod_i d\phi_i \right] \exp \left[ \frac{i}{2} \left[ \mu \sum_i \phi_i^2 - \sum_{ij} J_{ij} \phi_i \phi_j \right] \right], \quad (4)$$

where now  $\mu$  contains implicitly a small positive imaginary part which ensures convergence of the integrals. From Eqs. (2)–(4) one obtains

$$\rho(\mu) = \frac{2}{N\pi} \text{Im} \frac{\partial \ln Z}{\partial \mu}. \quad (5)$$

This gives the result for a particular realization of the disorder. To make further progress we invoke the replica method to average over the disorder. The average density of states is obtained from Eq. (5) by replacing  $\ln Z$  by  $[\ln Z]_{\text{av}}$ , where  $[\ ]_{\text{av}}$  indicates a disorder average. The latter may be computed from the replicated generating function  $[Z^n]_{\text{av}}$  via the limit

$$[\ln Z]_{\text{av}} = \lim_{n \rightarrow 0} ([Z^n]_{\text{av}} - 1)/n. \quad (6)$$

### III. THE SOLUTION

Introducing replica variables  $\{\phi_i^\alpha\}$ ,  $\alpha = 1, \dots, n$ , and averaging over the random-matrix elements with the distribution (1) yields, after dropping subextensive terms,

$$Z_n\{W, f\} = \int Dq \exp \left[ -\frac{Np}{2} \left[ \sum_{\alpha, r} b_r (q_\alpha^{(r)})^2 + \sum_{\substack{\alpha, \beta \\ \alpha < \beta}} \sum_{r, s} b_{rs} (q_{\alpha\beta}^{(r,s)})^2 + \dots \right] \right. \\ \left. + N \ln \int \left[ \prod_{\alpha=1}^n d\phi_\alpha \right] \exp \left[ \sum_{\alpha} W(\phi_\alpha) + pg \{\phi_\alpha\} \right] \right], \quad (10)$$

where

$$g\{\phi_\alpha\} = f(0) + \sum_{\alpha, r} b_r q_\alpha^{(r)} (\phi_\alpha)^r \\ + \sum_{\substack{\alpha, \beta \\ \alpha < \beta}} \sum_{r, s} b_{rs} q_{\alpha\beta}^{(r,s)} (\phi_\alpha)^r (\phi_\beta)^s + \dots \quad (11)$$

In the limit  $N \rightarrow \infty$ , the integrals over the auxiliary fields can be evaluated by steepest descents, to give

$$q_\alpha^{(r)} = \langle (\phi_\alpha)^r \rangle_\phi, \\ q_{\alpha\beta}^{(r,s)} = \langle (\phi_\alpha)^r (\phi_\beta)^s \rangle_\phi, \quad (12)$$

etc., where  $\langle \ \rangle_\phi$  is defined by

$$[Z^n]_{\text{av}} = \int_{-\infty}^{\infty} \left[ \prod_{i, \alpha} d\phi_i^\alpha \right] \\ \times \exp \left\{ \frac{i}{2} \mu \sum_{i, \alpha} (\phi_i^\alpha)^2 \right. \\ \left. + \frac{p}{2N} \sum_{i, j} \left[ \cos \left[ \sum_{\alpha} \phi_i^\alpha \phi_j^\alpha \right] - 1 \right] \right\}. \quad (7)$$

To proceed further, it is necessary to decouple the different sites in (7) by the introduction of auxiliary variables ("Hubbard-Stratonovich transformation") in the usual way. To do this we will follow the method of De Dominicis and Mottishaw.<sup>15</sup> Consider generating functions of the form

$$Z_n\{W, f\} = \int D\phi \exp \left[ \sum_{i, \alpha} W(\phi_i^\alpha) \right. \\ \left. + \frac{p}{2N} \sum_{i, j} f \left[ \sum_{\alpha} \phi_i^\alpha \phi_j^\alpha \right] \right], \quad (8)$$

where  $D\phi \equiv \prod_{i, \alpha} (d\phi_i^\alpha)$ ,  $W(\phi)$  is a "weighting function," and the function  $f(\sum_{\alpha} x_\alpha)$  is assumed to have a power-series expansion. Such an expansion can be rearranged in the form

$$f \left[ \sum_{\alpha} x_\alpha \right] = f(0) + \sum_{\alpha} \sum_r b_r x_\alpha^r + \sum_{\substack{\alpha, \beta \\ \alpha < \beta}} \sum_{r, s} b_{rs} x_\alpha^r x_\beta^s \\ + \sum_{\substack{\alpha, \beta, \gamma \\ \alpha < \beta < \gamma}} \sum_{r, s, t} b_{rst} x_\alpha^r x_\beta^s x_\gamma^t + \dots \quad (9)$$

Inserting this expansion in (8), with  $x_\alpha = \phi_i^\alpha \phi_j^\alpha$ , and introducing auxiliary fields  $q_\alpha^{(r)}, q_{\alpha\beta}^{(r,s)}, \dots$  conjugate to  $\sum_i (\phi_i^\alpha)^r, \sum_i (\phi_i^\alpha)^r (\phi_i^\beta)^s, \dots$  yields, up to constants,

$$\langle h\{\phi_\alpha\} \rangle_\phi = \frac{\int D\phi h\{\phi_\alpha\} \exp F\{\phi_\alpha\}}{\int D\phi \exp F\{\phi_\alpha\}}, \quad (13)$$

$$F\{\phi_\alpha\} = \sum_{\alpha} W(\phi_\alpha) + pg \{\phi_\alpha\} \quad (14)$$

for an arbitrary function  $h$ .

At this point we can use Eq. (12) to substitute for the "order parameters"  $\{q\}$  in Eq. (11). The function  $g\{\phi_\alpha\}$  can then be expressed in terms of  $f\{\phi_\alpha\}$  as

$$g\{\phi_\alpha\} = \left\langle f \left[ \sum_{\alpha} \phi_\alpha \psi_\alpha \right] \right\rangle_\psi, \quad (15)$$

which is a nonlinear integral equation for  $g\{\phi_\alpha\}$ .

Note the generality of the above approach. If  $Z_n$  is regarded as the replicated partition function for a spin system with "spin variables"  $\{\phi_i\}$ , then  $W(\phi)$  specifies the spin weight function, while  $f(x)$  characterizes the bond distribution.

The random-matrix problem under consideration here is specified by  $W(\phi) = (i/2)\mu\phi^2$ , and  $f(x) = \cos(x) - 1$ . Inserting these into Eq. (15), and using (13) and (14), gives an explicit equation for  $g\{\phi_\alpha\}$  which can be written compactly by treating  $\phi = (\phi_1, \dots, \phi_n)$  as a vector in the  $n$ -dimensional replica space:

$$g(\phi) = \frac{\int d^n \psi [\cos(\phi \cdot \psi) - 1] \exp F(\psi)}{\int d^n \psi \exp F(\psi)}, \quad (16)$$

$$F(\psi) = \frac{i}{2} \mu \psi^2 + p g(\psi). \quad (17)$$

It is clear that Eq. (16) possesses a solution in which  $g(\phi)$  is a function of  $x = |\phi|$  only, and we will just consider this solution, i.e., we will not pursue the possibility that rotational symmetry in the replica space is spontaneously broken. The angular integrals in Eq. (16) may then be evaluated in  $n$ -dimensional polar coordinates, and the  $n \rightarrow 0$  limit taken, to give

$$g(x) = -x \int_0^\infty dy \exp \left[ \frac{i}{2} \mu y^2 + p g(y) \right] J_1(xy), \quad (18)$$

where  $J_1$  is the Bessel function of order 1.

Equation (18) is our central result. It remains to extract the average density of states  $[\rho(\mu)]_{av}$  [which we will henceforth call simply  $\rho(\mu)$ ] from  $g(x)$ . Using Eqs. (5)–(7) one obtains

$$\rho(\mu) = \frac{1}{n\pi} \text{Re} \sum_\alpha \langle (\phi_\alpha)^2 \rangle_\phi = \frac{1}{n\pi} \text{Re} \langle \phi^2 \rangle_\phi. \quad (19)$$

From Eq. (16) one has

$$g(\phi) = -\frac{1}{2} \langle (\phi \cdot \psi)^2 \rangle_\psi + \dots = -\frac{1}{2n} \phi^2 \langle \psi^2 \rangle_\psi + \dots,$$

the last equality following from rotational invariance. Thus if

$$g(x) = -\frac{1}{2} a_2(\mu) x^2 + O(x^4)$$

then

$$\rho(\mu) = \frac{1}{\pi} \text{Re} a_2(\mu). \quad (20)$$

In Sec. IV, Eq. (18) is solved perturbatively in  $1/p$ , while in Sec. V the leading nonperturbative term is extracted. Equation (18) has many similarities to the analogous equation derived by Kim and Harris<sup>16</sup> for the density of states of a random hopping model on a Cayley tree, and we will follow closely their method of analysis below.

#### IV. THE LARGE- $p$ EXPANSION

In order to facilitate and systematize the large- $p$  expansion it is convenient to make the following changes of variable:

$$x^2 = 2is/\mu, \quad y^2 = 2iu/\mu, \quad \mu^2 = pE^2, \quad (21)$$

$$g(x) \equiv g \left[ \left[ \frac{2is}{\mu} \right]^{1/2} \right] = \frac{1}{p} \gamma(s), \quad (22)$$

and to replace  $J_1$  in (18) by its power-series expansion, to obtain

$$\gamma(s) = \frac{s}{E^2} \int_0^\infty du \exp[-u + \gamma(u)] \times \sum_{r=0}^\infty \left[ \frac{su}{pE^2} \right]^r \frac{1}{r!(r+1)!}. \quad (23)$$

The fact that  $\mu$  has a positive imaginary part means that the integration contour should end up in the fourth quadrant. This will be important for extracting the nonperturbative part in Sec. V. For the purposes of the perturbative treatment, however, one can take the integration contour to be the positive real axis. Note that if

$$\gamma(s) = b_1(\mu)s + O(s^2)$$

then

$$\rho(\mu) = -\frac{\mu}{\pi p} \text{Im} b_1(\mu). \quad (24)$$

To derive the  $1/p$  expansion we observe that higher powers of  $s$  in the expansion (23) of  $\gamma(s)$  are associated with higher powers of  $1/p$ . Therefore we write

$$\gamma(s) = p \sum_{r=1}^\infty b_r \left[ \frac{s}{p} \right]^r, \quad b_r = \sum_{l=0}^\infty \frac{b_r^{(l)}}{p^l}.$$

Substituting into (23), expanding the right-hand side as a power series in  $1/p$ , integrating term by term, and equating coefficients of  $s^r/p^{r+1}$ , gives

$$b_1^{(0)} = \frac{1}{E^2(1-b_1^{(0)})}, \quad (25)$$

$$b_1^{(1)} = \frac{1}{E^2} \left[ \frac{b_1^{(1)}}{(1-b_1^{(0)})^2} + \frac{2b_2^{(0)}}{(1-b_1^{(0)})^3} \right], \quad (26)$$

$$b_2^{(0)} = \frac{1}{2E^4(1-b_1^{(0)})^2}, \quad (27)$$

etc. Note that, according to (24), the density of states is determined solely by  $b_1$ . From (25)–(27) one finds

$$b_1^{(0)} = \frac{1}{2} \left[ 1 - \left[ 1 - \frac{4}{E^2} \right]^{1/2} \right], \quad (28)$$

$$b_1^{(1)} = \frac{E^2}{16} \left[ 1 - \left[ 1 - \frac{4}{E^2} \right]^{1/2} \right]^{-4} \left[ 1 - \frac{4}{E^2} \right]^{-1/2}. \quad (29)$$

These results can now be inserted into (24) to give

$$\rho(\mu) = \frac{2}{\pi \mu_c^2} (\mu_c^2 - \mu^2)^{1/2} \times \left[ 1 + \frac{1}{p} \left[ 1 - \frac{4\mu^2}{\mu_c^2} \right] + O \left[ \frac{1}{p^2} \right] \right], \quad (30)$$

where

$$\mu_c^2 = 4[p + 1 + O(1/p)],$$

and  $\rho(\mu) = 0$  for  $\mu^2 > \mu_c^2$ . The leading term is the "semicircle" law derived by Wigner for the nondilute random matrix. The  $O(1/p)$  correction leads to a shift in the band-edge location  $\mu_c$ , but does not lead to any states at large eigenvalue. Note that the normalization  $\int \rho(\mu) d\mu = 1$  is satisfied order by order in perturbation theory.

## V. THE NONPERTURBATIVE TERM

The leading nonperturbative contribution to  $\rho(\mu)$  is computed via a saddle-point evaluation of the integral in Eq. (23), using the lowest-order approximation for  $\gamma(s)$ , following the method of Kim and Harris.<sup>16</sup> The idea is to pick up the leading contribution to the imaginary part of the coefficients  $\{b_r\}$  in the regime  $\mu^2 > \mu_c^2$ , where they are entirely real in perturbation theory. The lowest-order approximation,  $\gamma_0(s)$ , is obtained by letting  $p \rightarrow \infty$  in the argument of the exponential in (23), i.e., by putting  $\gamma(s) = b_1 s$  in the right-hand side of (23) to give

$$\gamma_0(s) = p \left[ \exp \left[ \frac{s}{pE^2(1-b_1)} \right] - 1 \right]. \quad (31)$$

Now we set

$$\gamma(s) = \sum_{K=1}^{\infty} B_K s^K / p^{K-1}. \quad (32)$$

While at this point the  $B_K$ 's are the same as the  $b_K$ 's of Sec. IV, the use of upper-case symbols here is intended to avoid subsequent confusion. Putting (32) in (23) gives

$$B_K = a_K \int_C du \exp \left[ -u + \sum_{r=1}^{\infty} B_r u^r / p^{r-1} \right] u^{K-1}, \quad (33)$$

where

$$a_K = \frac{1}{E^{2K}} \frac{1}{(K-1)!K!}. \quad (34)$$

Choosing the integration contour  $C$  as shown in Fig. 1, where  $u^*$  is the saddle point of the integrand, gives

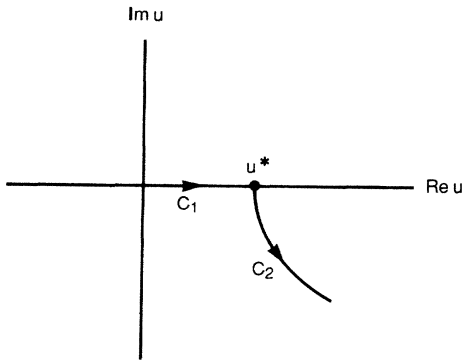


FIG. 1. Integration contour used to extract the nonperturbative contribution to the density of states. The point  $u^*$  is the saddle point of the integrand in Eq. (36).

$$B_K = a_K \int_{C_1} du \exp \left[ -u + \sum_{r=1}^{\infty} B_r u^r / p^{r-1} \right] u^{K-1} + a_K \int_{C_2} du \exp[-u + \gamma_0(u)] u^{K-1}, \quad (35)$$

where we have inserted the lowest order approximation (31) in the integral along  $C_2$ .

We wish to compute the leading nonperturbative contribution to each  $B_K$ , i.e., the contribution proportional to the first power of the (exponentially small) integral

$$I = \int_{C_2} du \exp[-u + \gamma_0(u)]. \quad (36)$$

Since it will turn out that the saddle point  $u^*$  is of order  $p$  for large  $p$ , contributions to  $B_K$  involving the integral along  $C_2$  are of order  $p^{K-1}I$ . Hence we have to keep track of all the  $B_r$ 's in Eq. (35). Now set  $B_K = B_K^{(0)} + B_K^{(1)} + \dots$ , where now (and in contrast to Sec. IV)  $B_K^{(0)}$  is the *perturbative* contribution to  $B_K$ , while  $B_K^{(1)}$  is the *nonperturbative contribution of order  $I^1$* . To leading order in the nonperturbative contribution, we require only  $B_K^{(0)}$  and  $B_K^{(1)}$ . Expanding (35) to leading order in  $B_K^{(1)}$ ,  $K \geq 2$ , and dropping higher-order perturbative corrections, yields

$$B_K = a_K \int_{C_1} du \exp[-(1-b_1)u] u^{K-1} \times \left[ 1 + \sum_{r=2}^{\infty} B_r^{(1)} u^r / p^{r-1} \right] + a_K \int_{C_2} du \exp[-u + \gamma_0(u)] u^{K-1}. \quad (37)$$

Recalling that  $B_K^{(1)}$  is of order  $p^{K-1}I$ , and retaining only the leading terms for  $p \rightarrow \infty$ , we obtain

$$B_K^{(1)} = a_K \int_{C_2} du \exp[-u + \gamma_0(u)] u^{K-1}, \quad K \geq 2. \quad (38)$$

The case  $K=1$  must be treated separately, since  $\int_{C_1}$  and  $\int_{C_2}$  in Eq. (37) give comparable contributions

$$B_1^{(1)} = E^{-2} \int_{C_1} du \exp[-(1-b_1)u] \sum_{r=2}^{\infty} B_r^{(1)} u^r / p^{r-1} + E^{-2}I.$$

Substituting for  $B_r^{(1)}$ ,  $r \geq 2$ , from Eq. (38), and evaluating  $\int_{C_1}$  term by term, yields

$$B_1^{(1)} = E^{-4}(1-b_1)^{-2} \int_{C_2} du \exp[-u + \gamma_0(u)] \times \{ \exp[u/E^2 p(1-b_1)] - 1 \} + E^{-2}I. \quad (39)$$

To leading order we can replace  $u$  by the saddle-point value  $u^*$  in the (order unity) factor in curly braces in Eq. (39). Combining the result with the perturbative contribution derived in Sec. IV yields the following implicit equation for  $b_1 \equiv B_1$ :

$$b_1 = \frac{1}{E^2(1-b_1)} + \frac{1}{p} \frac{1}{E^6(1-b_1)^5} + \frac{I}{E^2} \left\{ 1 + \frac{1}{E^2(1-b_1)^2} \left[ \exp \left( \frac{u^*}{E^2 p (1-b_1)} \right) - 1 \right] \right\}. \quad (40)$$

It remains to evaluate the integral  $I$ , Eq. (36). After the change of variable  $u = pz$ , the integral has the form, using (31) for  $\gamma_0(u)$ ,

$$I = p e^{-p} \int_{C_2} dz \exp[p\omega(z)],$$

where

$$\omega(z) = -z + \exp \left[ \frac{z}{E^2(1-b_1)} \right].$$

The saddle point  $z^* \equiv u^*/p$  is the solution of  $\partial\omega/\partial z = 0$ , i.e.,

$$z^* = E^2(1-b_1) \ln[E^2(1-b_1)],$$

and

$$\omega(z^*) = E^2(1-b_1) \{1 - \ln[E^2(1-b_1)]\}.$$

Integrating away from the saddle point along the steepest descent contour gives the final result, expressed in terms of  $\mu^2 = pE^2$ , as

$$I(\mu) = \chi(\mu) \left[ -i + \frac{2}{3\sqrt{\pi}} \frac{1}{\mu\sqrt{Q(\mu)}} \right], \quad (41)$$

where

$$Q(\mu) = 1 + \left[ 1 - \frac{\mu_c^2}{\mu^2} \right]^{1/2},$$

$$\chi(\mu) = \frac{\sqrt{\pi}}{2} e^{-p} \left[ \frac{2ep}{\mu^2 Q(\mu)} \right]^{\mu^2 Q(\mu)/2} \mu\sqrt{Q(\mu)},$$

and  $\mu_c^2$  is given below Eq. (30).

The density of states is obtained from (24), with  $b_1$  given by Eq. (40). For general values of  $\mu$  the final result is neither simple nor illuminating. To avoid encumbering the reader with more algebra, we content ourselves here with deriving the result in the limit  $\mu^2 \gg \mu_c^2$ , which serves to demonstrate the central point that nonperturbative terms lead to states outside the perturbative band, and particularly, states at arbitrarily large eigenvalue. In this limit one has  $Q(\mu) \rightarrow 2$  and

$$\ln\chi(\mu) \simeq \mu^2 \ln(ep/\mu^2), \quad \mu^2 \gg \mu_c^2. \quad (42)$$

In the same limit one can also replace  $b_1$  by zero in the right-hand side of Eq. (40) to obtain

$$\ln[-\text{Im}b_1(\mu)] \simeq \ln[-\text{Im}I(\mu)] \simeq \ln\chi(\mu). \quad (43)$$

Combining (24), (42), and (43) yields finally

$$\ln\rho(\mu) \simeq -\mu^2 \ln(\mu^2/ep), \quad \mu^2 \gg \mu_c^2. \quad (44)$$

As a final point we note that if one solves Eq. (40) for  $\mu = \mu_1$  such that  $\text{Im}b_1 = 0$ , one finds that the nonperturba-

tive term moves  $\mu_1$  off the real axis. Thus the density of states for any finite  $p$  covers the entire interval  $(-\infty, \infty)$ , the weight in the "tails" being given by (44).

## VI. CONCLUSION

We have computed the density of states of a random matrix with elements  $0, \pm 1$ , and mean connectivity  $p$ . In the limit  $p \rightarrow \infty$ , the "semicircular" distribution of Wigner<sup>14</sup> is recovered, with no weight outside the semicircle in the limit of an infinite matrix. The general features (sharp band edges, no weight outside the band) of the Wigner distribution are preserved order by order in perturbation theory in  $1/p$ . We have shown, however, that for any finite  $p$  nonperturbative terms lead to a small, but finite, density of states for any  $\mu$ , no matter how large.

Returning to dilute spin systems, we note that for a Gaussian spin model (spin weight function  $\exp[W(s)] = \exp[-s^2/2]$ ), the inverse susceptibility matrix is given *exactly* by  $\chi^{-1} = T\mathbf{I} - \mathbf{J}$ . If the couplings are rescaled by a factor  $1/\sqrt{p}$ , so that  $J_{ij}$  takes the values  $0, \pm 1/\sqrt{p}$ , and the limit  $p \rightarrow \infty$  taken, one recovers the semicircular distribution with band edges at  $\mu_c = \pm 2$ . In this limit, therefore, which corresponds to a nondilute, infinite-range, spin-glass model, the Gaussian spin model is well defined above a critical temperature  $T_c = 2$ . As soon as nontrivial dilution is introduced (via finite  $p$ ), however, and the  $\mathbf{J}$  eigenvalue distribution develops infinite tails, the Gaussian spin model becomes ill defined ( $\chi^{-1}$  has negative eigenvalues) at any finite temperature. For physical spin weights (e.g., the Ising model,  $\exp[W(s)] = \delta(s^2 - 1)$ , or the "s<sup>4</sup>" model,  $W(s) = -rs^2 - us^4$ ), nonlinear terms in the relation between  $\chi^{-1}$  and  $\mathbf{J}$  renormalize the eigenvalue distribution of  $\chi^{-1}$  so as to keep all eigenvalues positive above the critical temperature of the dilute system.<sup>11,12</sup> One of the goals of studying the simple, mean-field-like dilution models considered in this paper is the hope that they will lead to an understanding, within a soluble model, of how such renormalization effects take place. In particular it would be nice to know how the renormalized density of states [i.e.,  $\rho(\mu)$  for  $\chi^{-1}$ ] vanishes for  $\mu \rightarrow 0$ . This is particularly interesting for the especially simple case of the  $m$ -vector model in the limit  $m \rightarrow \infty$ . For this latter model the dynamics (assumed relaxational, with no conservation laws) is determined completely by the statics.<sup>17</sup> The presence of arbitrarily small eigenvalues of  $\chi^{-1}$  then leads to nonexponential relaxation at temperatures above the critical point of the dilute system, i.e., throughout the Griffiths phase.<sup>17</sup> The latter is expected to be a completely general phenomenon in random systems, and we hope that the techniques introduced in this paper may eventually lead to a quantitative understanding of the Griffiths's phase within the context of a soluble model.

## ACKNOWLEDGMENT

We would like to thank A. B. Harris, A. J. McKane, M. A. Moore, and P. Mottishaw for useful discussions, and A. B. Harris for a very helpful correspondence. One of us (G.J.R.) thanks the Science and Engineering Research Council for financial support.

\*Permanent address: Department of Theoretical Physics, The University, Manchester, M13 9PL, United Kingdom.

- <sup>1</sup>L. Viana and A. J. Bray, *J. Phys. C* **18**, 3037 (1985).
- <sup>2</sup>I. Kanter and H. Sompolinsky, *Phys. Rev. Lett.* **58**, 164 (1987); M. Mezard and G. Parisi (unpublished).
- <sup>3</sup>J. R. Banavar, D. Sherrington, and N. Surlas, *J. Phys. A* **20**, L1 (1987).
- <sup>4</sup>K. Y. M. Wong and D. Sherrington, *J. Phys. A* **20**, L785 (1987); **20**, L793 (1987).
- <sup>5</sup>Y. Fu and P. W. Anderson, *J. Phys. A* **19**, 1605 (1986).
- <sup>6</sup>M. Mezard and G. Parisi, *J. Phys. (Paris) Lett.* **46**, L771 (1985).
- <sup>7</sup>M. Mezard and G. Parisi, *J. Phys. (Paris)* **47**, 1285 (1985).
- <sup>8</sup>R. B. Griffiths, *Phys. Rev. Lett.* **23**, 17 (1969).
- <sup>9</sup>D. Dhar, in *Stochastic Processes: Formalism and Applications*, edited by G. S. Agarwal and S. Dattagupta (Springer, Berlin, 1983).
- <sup>10</sup>M. Randeria, J. P. Sethna, and R. G. Palmer, *Phys. Rev. Lett.* **54**, 1321 (1985).
- <sup>11</sup>A. J. Bray and M. A. Moore, *J. Phys. C* **15**, L765 (1982).
- <sup>12</sup>J. A. Hertz, L. Fleishman, and P. W. Anderson, *Phys. Rev. Lett.* **43**, 942 (1979).
- <sup>13</sup>See, e.g., M. L. Mehta, *Random Matrices* (Academic, New York, 1967).
- <sup>14</sup>E. P. Wigner, *Ann. Math.* **67**, 325 (1958).
- <sup>15</sup>C. De Dominicis and P. Mottishaw, *Europhys. Lett.* **3**, 87 (1987); P. Mottishaw (private communication).
- <sup>16</sup>Y. Kim and A. B. Harris, *Phys. Rev. B* **31**, 7393 (1985).
- <sup>17</sup>A. J. Bray, *Phys. Rev. Lett.* **59**, 586 (1987); A. J. Bray and G. J. Rodgers (unpublished).

# Spectra of Sparse Random Matrices

**Reimer Kühn**

Mathematics Department, King's College London, Strand, London WC2R 2LS, UK

26 March 2008

**Abstract.** We compute the spectral density for ensembles of sparse symmetric random matrices using replica, managing to circumvent difficulties that have been encountered in earlier approaches along the lines first suggested in a seminal paper by Rodgers and Bray. Due attention is paid to the issue of localization. Our approach is not restricted to matrices defined on graphs with Poissonian degree distribution. Matrices defined on regular random graphs or on scale-free graphs, are easily handled. We also look at matrices with row constraints such as discrete graph Laplacians. Our approach naturally allows to unfold the total density of states into contributions coming from vertices of different local coordination.

## 1. Introduction

Since its inception by Wigner in the context of describing spectra of excited nuclei [1], Random Matrix Theory (RMT) has found applications in numerous areas of science, including questions concerning the stability of complex systems [2], electron localisation [3], quantum chaos [4], Quantum Chromo Dynamics [5], finance [6, 7], the physics of glasses both at elevated [8, 9] and low [10, 11] temperatures, number theory [12], and many many more. For an extensive review describing many of the applications in physics see, e.g. [13].

In the present paper we revisit the problem of determining the spectral density for ensembles of sparse random matrices pioneered two decades ago in seminal papers by Bray and Rodgers [14, 15]. The problem has in recent years received much renewed interest in connection with the study of complex networks, motivated, for instance, by the fact that geometric and topological properties of networks are reflected in spectral properties of adjacency matrices defining the networks in question [16, 17]. Also, phenomena such as non-exponential relaxation in glassy systems and gels [15, 18] — intimately related to Lifshitz tails [19] and Griffiths' singularities in disordered systems [20] — as well as

Anderson localization of electronic [21] or vibrational [22] states have been studied in sparsely connected random systems, as finite dimensional versions of these problems have proven to be extremely difficult to analyse. A wealth of analytical and numerical results has been accumulated on these systems in recent years. Progress has, however, been partly hampered by the fact that full solutions of the Rodgers-Bray integral equation [14], in terms of which spectral densities of the sparse random matrices in question are computed, have so far eluded us. Asymptotic analyses for large average connectivities [14, 15], and other approximation schemes such as the single defect approximation (SDA) and the effective medium approximation (EMA) [23, 24, 17] or very recently [25], as well as numerical diagonalization (e.g. [26]) had to come in for help.

In what follows we describe some significant progress in the understanding of this problem, based upon advances in the statistical mechanical analysis of sparsely connected spin-glass like systems seen in the last couple of years [27, 28] — in the present context in particular the proposal of a stochastic population-dynamics algorithm [28] to solve the nonlinear integral equations appearing in the solution of these problems, and the recent generalization of these methods to systems with continuous degrees of freedom, such as models of sparsely connected vector spins [29], or finitely coordinated models for low-temperature phases of amorphous systems [30].

It is well known that the average spectral density of an ensemble  $\mathcal{M}$  of  $N \times N$  matrices  $M$  can be computed from the ensemble average of the imaginary part of their resolvent via

$$\overline{\rho_N(\lambda)} = \frac{1}{\pi N} \text{Im Tr } \overline{[\lambda_\varepsilon \mathbb{I} - M]^{-1}}, \quad (1)$$

in which  $\mathbb{I}$  is the  $N \times N$  unit matrix, and  $\lambda_\varepsilon = \lambda - i\varepsilon$ , the limit  $\varepsilon \rightarrow 0^+$  being understood. Following Edwards and Jones [31], one can express this result in terms of the Gaussian integral

$$Z_N = \int \prod_{i=1}^N \frac{du_i}{\sqrt{2\pi/i}} \exp \left\{ -\frac{i}{2} \sum_{i,j} u_i (\lambda_\varepsilon \delta_{ij} - M_{ij}) u_j \right\} \quad (2)$$

as

$$\overline{\rho_N(\lambda)} = -\frac{2}{\pi N} \text{Im } \frac{\partial}{\partial \lambda} \overline{\ln Z_N} = \frac{1}{N} \text{Re } \sum_{i=1}^N \overline{\langle u_i^2 \rangle}, \quad (3)$$

using the replica method to evaluate the average of the logarithm in (3) over the ensemble  $\mathcal{M}$  of matrices  $M$  under consideration. The ‘averages’  $\langle u_i^2 \rangle$  in (3) are evaluated with respect to the ‘Gaussian measure’ defined by (2).<sup>‡</sup> This has been the path taken in [14]; we shall initially follow their reasoning.

<sup>‡</sup> Note that we are using probabilistic notions in a loose, metaphorical sense, as the Gaussian measures used in these calculations are complex.

Disregarding the complex nature of the ‘Hamiltonian’ in the evaluation of (2), the mathematical problem posed in (2), (3) is analogous to the evaluation of an ‘internal energy of a disordered system with quenched disorder. Within the general class of finitely coordinated amorphous model systems considered in [30], the one represented by (2), (3) constitutes a particular sub-class, viz. that of harmonically coupled systems, for which the analysis was found to be *much* simpler than for systems involving anharmonic couplings. Indeed, while the solution of the latter required the self-consistent determination of probability distributions over infinite dimensional function-spaces, it was realized in [30] that solutions of harmonically coupled systems could be formulated in terms of superpositions of Gaussians, and that the self-consistency problem reduced to the (much simpler) problem of a self-consistent determination of the probability distribution of their variances.

It can be fairly argued that this last insight is, in fact, easier to obtain within a Bethe-Peierls or cavity type approach [28], in which (2) is recursively evaluated *for given instances* on graphs which are locally tree-like, ignoring correlations among subtrees — an approximation that becomes exact, e.g., for random graphs that remain finitely coordinated in the thermodynamic limit. This approach is taken in a separate publication [32], in which (finite) single-instances and promising algorithmic aspects of the problem are being highlighted.

Although [30] describes all technical details needed for a replica analysis of the present problem, we shall nevertheless reproduce the key steps here, both to keep the paper self-contained, and to point out along the way where the impasse in [14] arises, and how it is circumvented.

The remainder of the paper is organized as follows. In Sec. 2, we describe the replica analysis of the problem posed by (2), (3), specializing to matrices defined on Poissonian (Erdős-Renyi) random graphs. It has been known for some time [31, 14] that the replica-symmetric high-temperature solution — i.e., a solution preserving both, permutation-symmetry among replica, and rotational symmetry in the space of replica — is exact for problems of the type considered here. Accordingly, a representation that respects these symmetries is formulated in Sec. 2.1. It is at this point where our formulation departs from that of [14]. In Sec. 3 we present results for a variety of examples, and compare with numerical diagonalization results for large finite matrices to assess their quality. In sufficiently sparse graphs, one expects localized states to appear. The signatures of localization within our approach are discussed throughout Sec. 3, with inverse participation ratios (IPRs) as a diagnostic tool looked at in Sec. 3.2. A detailed investigation of Anderson localization for (discrete) Schrödinger operators on sparse random graphs will be reserved to a separate publication [33]. Matrices with bimodal instead of Gaussian random couplings are studied in Sec. 3.3. As the formal structure of

the self-consistency problem remains unaltered when the Poissonian random graphs are replaced by graphs with other degree distributions [30], we can exploit this fact to present results for regular and scale-free random graphs in Sec. 3.4. Modifications needed to treat matrices with row-constraints, such as discrete graph Laplacians are outlined in Sec. 3.5. Our approach naturally allows to unfold the total density of states into contributions coming from vertices of different local coordination, and we finally present an example of such an unfolding in Sec. 3.6. The final Sec. 4 contains a brief summary and an outlook on promising directions for future research.

## 2. Replica Analysis

### 2.1. General Formulation

Here we briefly outline the evaluation of (2), (3) for sparse symmetric matrices  $M$  of the form

$$M_{ij} = c_{ij}K_{ij} , \quad (4)$$

in which  $C = \{c_{ij}\}$  is a symmetric adjacency matrix of an undirected random graph (with  $c_{ii} = 0$ ), and the non-zero elements of  $M$  are specified by the  $K_{ij}$ , also taken to be symmetric in the indices. Within the present outline we restrict ourselves for the sake of simplicity to adjacency matrices of Erdős-Renyi random graphs, with

$$P(\{c_{ij}\}) = \prod_{i < j} p(c_{ij})\delta_{c_{ij},c_{ji}} \quad \text{and} \quad p(c_{ij}) = \left(1 - \frac{c}{N}\right)\delta_{c_{ij},0} + \frac{c}{N}\delta_{c_{ij},1} ,$$

exhibiting a Poissonian degree distribution with average coordination  $c$ . We note at the outset that formal results carry over without modification to other cases [30]. There is no need at this point to specify the distribution of the  $K_{ij}$ , but we shall typically look at Gaussian and bimodal distributions.

The average (3) is evaluated using replica  $\overline{\ln Z_N} = \lim_{n \rightarrow 0} \frac{1}{n} \ln \overline{Z_N^n}$ , starting with integer numbers of replica as usual. After performing the average over the distribution of the connectivities one obtains

$$\overline{Z_N^n} = \int \prod_{ia} \frac{du_{ia}}{\sqrt{2\pi/i}} \exp \left\{ -\frac{i}{2} \lambda_\varepsilon \sum_{i,a} u_{ia}^2 + \frac{c}{2N} \sum_{ij} \left( \left\langle \exp \left( iK \sum_a u_{ia} u_{ja} \right) \right\rangle_K - 1 \right) \right\} , \quad (5)$$

in which  $\langle \dots \rangle_K$  refers to an average over the distribution of the  $K_{ij}$ . A decoupling of sites is achieved by introducing the replicated density

$$\rho(\mathbf{u}) = \frac{1}{N} \sum_i \prod_a \delta(u_a - u_{ia}) , \quad (6)$$

with  $\mathbf{u}$  denoting the replica vector  $\mathbf{u} = (u_1, u_2, \dots, u_n)$ , and enforcing its definition via functional  $\delta$  distributions,

$$1 = \int \mathcal{D}\rho \mathcal{D}\hat{\rho} \exp \left\{ -i \int d\mathbf{u} \hat{\rho}(\mathbf{u}) \left( N\rho(\mathbf{u}) - \sum_i \prod_a \delta(u_a - u_{ia}) \right) \right\}. \quad (7)$$

This gives (using shorthands of the form  $d\rho(\mathbf{u}) \equiv d\mathbf{u}\rho(\mathbf{u})$  where useful)

$$\begin{aligned} \overline{Z_N^n} &= \int \mathcal{D}\rho \int \mathcal{D}\hat{\rho} \exp \left\{ N \left[ \frac{c}{2} \int d\rho(\mathbf{u}) d\rho(\mathbf{v}) \left( \left\langle \exp \left( iK \sum_a u_a v_a \right) \right\rangle_K - 1 \right) \right. \right. \\ &\quad \left. \left. - \int d\mathbf{u} i\hat{\rho}(\mathbf{u})\rho(\mathbf{u}) + \ln \int \prod_a \frac{du_a}{\sqrt{2\pi/i}} \exp \left( i\hat{\rho}(\mathbf{x}) - \frac{i}{2} \lambda_\varepsilon \sum_a u_a^2 \right) \right] \right\}, \quad (8) \end{aligned}$$

allowing to evaluate  $N^{-1} \ln \overline{Z_N^n}$  by a saddle point method. The stationarity conditions w.r.t. variations of  $\rho$  and  $\hat{\rho}$  read

$$i\hat{\rho}(\mathbf{u}) = c \int d\rho(\mathbf{v}) \left( \left\langle \exp \left( iK \sum_a u_a v_a \right) \right\rangle_K - 1 \right), \quad (9)$$

$$\rho(\mathbf{u}) = \frac{\exp \left( i\hat{\rho}(\mathbf{u}) - \frac{i}{2} \lambda_\varepsilon \sum_a u_a^2 \right)}{\int d\mathbf{u} \exp \left( i\hat{\rho}(\mathbf{u}) - \frac{i}{2} \lambda_\varepsilon \sum_a u_a^2 \right)}. \quad (10)$$

The way in which sites are decoupled constitutes the first point of departure between our treatment and that of [14] and subsequent analyses inspired by it (e.g. [34, 35]). In these papers the averaged exponential expressions in the exponent of (5),

$$f(\mathbf{u}_i \cdot \mathbf{v}_j) = f\left(\sum_a u_{ia} v_{ja}\right) = \left\langle \exp \left( iK \sum_a u_{ia} v_{ja} \right) \right\rangle_K - 1, \quad (11)$$

is expanded, and an infinite family of multi-replica generalizations of Edwards Anderson order parameters (and corresponding Hubbard-Stratonovich transformations) are used to decouple the sites, much as in the treatment of the dilute spin-glass problem by Viana and Bray [36]. The authors then use the expansion and the infinite set of self-consistency equations for the multi-replica generalizations of Edwards Anderson order parameters to construct a non-linear integral equation for a function  $g$  defined via a suitable ‘average’ of  $f$ ; see [14] for details. Our treatment in this respect is closer in spirit to the alternative approach of Kanter and Sompolinsky [37] who treat local field distributions (which in the general context of disordered amorphous systems discussed in [30] become distributions of local potentials) as the primary object of their theory.

However, the difference between our treatment and that of [14] is at this point still superficial. Indeed, we have the correspondence

$$i\hat{\rho}(\mathbf{u}) = cg(\mathbf{u}) \quad (12)$$

between our ‘conjugate density’  $\hat{\rho}$  and the function  $g$  of [14]. With this identification, (9) and (10) can be combined to give

$$g(\mathbf{u}) = \frac{\int d\mathbf{v} f(\mathbf{u} \cdot \mathbf{v}) \exp\left(cg(\mathbf{v}) - \frac{i}{2} \lambda_\varepsilon \mathbf{v}^2\right)}{\int d\mathbf{v} \exp\left(cg(\mathbf{v}) - \frac{i}{2} \lambda_\varepsilon \mathbf{v}^2\right)}, \quad (13)$$

which is the Rodgers-Bray integral equation for general distributions of non-zero bond strengths.

## 2.2. Replica Symmetry

To deal with the  $n \rightarrow 0$  limit in these equations, assumptions concerning the invariance properties of the solutions  $\rho(\mathbf{u})$  and  $\hat{\rho}(\mathbf{u})$  of (9) and (10) — alternatively of the solution  $g(\mathbf{u})$  of (13)— under transformations among the replica are required. It has been established for some time [31, 14] that the replica-symmetric high-temperature solution — i.e., a solution preserving both, permutation-symmetry among replica, and rotational symmetry in the space of replica — is exact for problems of the type considered here. It is here where the paths taken in the present paper and in [14] really bifurcate. In [14], the assumption  $g(\mathbf{u}) = g(u)$ , with  $u = |\mathbf{u}|$  is used to perform the angular integrals in  $n$ -dimensional polar coordinates in (13), resulting in an integral equation for  $g(u)$  in the  $n \rightarrow 0$ -limit. This integral equation has also been obtained using the supersymmetry approach [38]. It has, however, so far resisted exhaustive analysis or full numerical solution.

In the present paper we follow [30], and represent  $\rho$  and  $\hat{\rho}$  as superpositions of replica-symmetric functions, using the observation made in [30] that superpositions of Gaussians of the form

$$\rho(\mathbf{u}) = \int d\pi(\omega) \prod_a \frac{\exp\left[-\frac{\omega}{2} u_a^2\right]}{Z(\omega)}, \quad (14)$$

$$i\hat{\rho}(\mathbf{u}) = \hat{c} \int d\hat{\pi}(\hat{\omega}) \prod_a \frac{\exp\left[-\frac{\hat{\omega}}{2} u_a^2\right]}{Z(\hat{\omega})}, \quad (15)$$

would provide exact solutions for harmonically coupled systems. Note that these expressions do indeed preserve permutation symmetry among replica as well as rotational symmetry. In (15) the constant  $\hat{c}$  is to be determined such that  $\hat{\pi}$  is normalized,  $\int d\hat{\pi}(\hat{\omega}) = 1$ . We note that these representations make sense only for  $\text{Re } \omega > 0$  and  $\text{Re } \hat{\omega} > 0$ ; later on we shall find that these conditions are self-consistently met for solutions of the fixed point equations. Expressing (8) in terms of  $\pi$  and  $\hat{\pi}$ , we get

$$\overline{Z_N^n} = \int \mathcal{D}\pi \mathcal{D}\hat{\pi} \exp\{N[G_1[\pi] + G_2[\hat{\pi}, \pi] + G_3[\hat{\pi}]]\}. \quad (16)$$

As  $n \rightarrow 0$ , the functionals  $G_1$ ,  $G_2$  and  $G_3$  evaluate to

$$G_1[\pi] \simeq n \frac{c}{2} \int d\pi(\omega) d\pi(\omega') \left\langle \ln \frac{Z_2(\omega, \omega', K)}{Z(\omega)Z(\omega')} \right\rangle_K, \quad (17)$$

$$G_2[\hat{\pi}, \pi] \simeq -\hat{c} - n\hat{c} \int d\hat{\pi}(\hat{\omega}) d\pi(\omega) \ln \frac{Z(\hat{\omega} + \omega)}{Z(\hat{\omega})Z(\omega)}, \quad (18)$$

$$G_3[\hat{\pi}] \simeq \hat{c} + n \sum_{k=0}^{\infty} p_{\hat{c}}(k) \int \{d\hat{\pi}\}_k \ln \frac{Z_{\lambda}(\{\hat{\omega}\}_k)}{\prod_{\ell=1}^k Z(\hat{\omega}_{\ell})}, \quad (19)$$

in which we have introduced the shorthands  $\{d\hat{\pi}\}_k \equiv \prod_{\ell=1}^k d\hat{\pi}(\hat{\omega}_{\ell})$ , and  $\{\hat{\omega}\}_k = \sum_{\ell=1}^k \hat{\omega}_{\ell}$ , a Poissonian connectivity distribution

$$p_{\hat{c}}(k) = \frac{\hat{c}^k}{k!} \exp[-\hat{c}] \quad (20)$$

with average connectivity  $\langle k \rangle = \hat{c}$ , and the ‘partition functions’

$$Z(\omega) = \int du \exp\left[-\frac{\omega}{2}u^2\right] = \sqrt{2\pi/\omega}, \quad (21)$$

$$Z_{\lambda_{\varepsilon}}(\{\hat{\omega}\}_k) = \int \frac{du}{\sqrt{2\pi/i}} \exp\left[-\frac{1}{2}\left(i\lambda_{\varepsilon} + \{\hat{\omega}\}_k\right)u^2\right] = \left(\frac{i}{i\lambda_{\varepsilon} + \{\hat{\omega}\}_k}\right)^{1/2}, \quad (22)$$

$$Z_2(\omega, \omega', K) = \int dudv \exp\left[-\frac{1}{2}\left(\omega u^2 + \omega' v^2 - 2iKuv\right)\right] = \frac{2\pi}{\sqrt{\omega\omega' + K^2}}. \quad (23)$$

Note that the  $\mathcal{O}(1)$  contributions of  $G_2$  and  $G_3$  in the exponent of (8) cancel in their sum.

The stationarity condition of the functional integral (8) w.r.t variations of  $\rho$  and  $\hat{\rho}$  is reformulated in terms of stationarity conditions w.r.t variations  $\pi$  and  $\hat{\pi}$ ,

$$\hat{c} \int d\hat{\pi}(\hat{\omega}) \ln \frac{Z(\hat{\omega} + \omega)}{Z(\hat{\omega})Z(\omega)} = c \int d\pi(\omega') \left\langle \ln \frac{Z_2(\omega, \omega', K)}{Z(\omega)Z(\omega')} \right\rangle_K + \mu, \quad (24)$$

$$\hat{c} \int d\pi(\omega) \ln \frac{Z(\hat{\omega} + \omega)}{Z(\hat{\omega})Z(\omega)} = \sum_{k \geq 1} k p_{\hat{c}}(k) \int \{d\hat{\pi}\}_{k-1} \ln \frac{Z_{\lambda_{\varepsilon}}(\hat{\omega} + \{\hat{\omega}\}_{k-1})}{Z(\hat{\omega}) \prod_{\ell=1}^{k-1} Z(\hat{\omega}_{\ell})} + \hat{\mu} \quad (25)$$

with  $\mu$  and  $\hat{\mu}$  Lagrange multipliers to take the normalization of  $\pi$  and  $\hat{\pi}$  into account.

The conditions that (24) must hold for all  $\omega$  and similarly that (25) must hold for all  $\hat{\omega}$  can be translated [28] into

$$\hat{\pi}(\hat{\omega}) = \frac{c}{\hat{c}} \int d\pi(\omega') \left\langle \delta(\hat{\omega} - \hat{\Omega}(\omega', K)) \right\rangle_K, \quad (26)$$

$$\pi(\omega) = \sum_{k \geq 1} \frac{k}{\hat{c}} p_{\hat{c}}(k) \int \{d\hat{\pi}\}_{k-1} \delta(\omega - \Omega(\{\hat{\omega}\}_{k-1})), \quad (27)$$

in which  $\hat{\Omega}(\omega', K)$  and  $\Omega(\{\hat{\omega}\}_{k-1})$  are defined via

$$Z(\omega + \hat{\Omega}(\omega', K)) = \frac{Z_2(\omega, \omega', K)}{Z(\omega')} \Leftrightarrow \hat{\Omega}(\omega', K) = \frac{K^2}{\omega'}, \quad (28)$$

and

$$\Omega(\{\hat{\omega}\}_{k-1}) = i\lambda_\varepsilon + \sum_{\ell=1}^{k-1} \hat{\omega}_\ell , \quad (29)$$

respectively. Given that  $\pi$  is normalized, it follows from (26) that the same is true for  $\hat{\pi}$ , provided  $\hat{c} = c$ , so the fixed point equations take their final form as

$$\hat{\pi}(\hat{\omega}) = \int d\pi(\omega') \langle \delta(\hat{\omega} - \hat{\Omega}(\omega', K)) \rangle_K , \quad (30)$$

$$\pi(\omega) = \sum_{k \geq 1} \frac{k}{c} p_c(k) \int \{d\hat{\pi}\}_{k-1} \delta(\omega - \Omega(\{\hat{\omega}\}_{k-1})) . \quad (31)$$

These equations can be seen as special cases of the general framework derived in [30], when restricted to harmonically coupled random systems. In [30] it is shown that they hold — unmodified — for non-Poissonian degree distributions as well, as long as the average connectivity in these systems remains finite.

Note that for all  $\varepsilon > 0$ ,  $\pi$  and  $\hat{\pi}$  — self-consistently — have support in  $\text{Re } \omega > 0$  and  $\text{Re } \hat{\omega} > 0$  as required. The equations take a form that suggests solving them via a stochastic population-based algorithm, as described in Appendix A.

For the thermodynamic limit of the spectral density we obtain from (2), (3) and (16)-(23) that

$$\begin{aligned} \overline{\rho(\lambda)} &= \frac{1}{\pi} \text{Im} \sum_{k=0}^{\infty} p_c(k) \int \{d\hat{\pi}\}_k \frac{i}{i\lambda_\varepsilon + \{\hat{\omega}\}_k} \\ &= \frac{1}{\pi} \sum_{k=0}^{\infty} p_c(k) \int \{d\hat{\pi}\}_k \frac{\text{Re}(\{\hat{\omega}\}_k + \varepsilon)}{(\text{Re}(\{\hat{\omega}\}_k + \varepsilon))^2 + (\lambda + \text{Im} \{\hat{\omega}\}_k)^2} . \end{aligned} \quad (32)$$

This expression has a natural interpretation as a sum of contributions of local-densities of state of sites with connectivities  $k$ , weighted according to their probability of occurrence. Referring to (3), we may further identify the

$$\sigma_k^2 = \frac{1}{\pi} \text{Im} \frac{i}{i\lambda_\varepsilon + \{\hat{\omega}\}_k} \quad (33)$$

as realizations of the variance of (Gaussian) marginals on sites of coordination  $k$ .

With an eye towards disentangling singular (pure point) and continuous contributions to the spectral density, we find it useful to define

$$P(a, b) = \sum_k p_c(k) \int \{d\hat{\pi}\}_k \delta(a - \text{Re} \{\hat{\omega}\}_k) \delta(b - \text{Im} \{\hat{\omega}\}_k) , \quad (34)$$

with  $a \geq 0$  by construction. The density of states can then be expressed as an integral over  $P$ ,

$$\overline{\rho(\lambda)} = \int \frac{da db}{\pi} P(a, b) \frac{a + \varepsilon}{(a + \varepsilon)^2 + (b + \lambda)^2} . \quad (35)$$

Noting the singular nature of the above integrand in the limit  $\varepsilon \rightarrow 0$  for  $a = 0$ , we propose to isolate possible singular contributions to the spectral density by writing

$$P(a, b) = P_0(b)\delta(a) + \tilde{P}(a, b) . \quad (36)$$

This gives

$$\overline{\rho(\lambda)} = \int db P_0(b)\mathcal{L}_\varepsilon(b + \lambda) + \int_{a>0} \frac{da db}{\pi} \tilde{P}(a, b) \frac{a + \varepsilon}{(a + \varepsilon)^2 + (b + \lambda)^2} , \quad (37)$$

in which  $\mathcal{L}_\varepsilon$  denotes a Lorentzian of width  $\varepsilon$ . Our results below strongly suggest that, when the limit  $\varepsilon \rightarrow 0$  is taken — thereby  $\mathcal{L}_\varepsilon(x) \rightarrow \delta(x)$  — a non-zero value of

$$P_0(-\lambda) = \lim_{\varepsilon \rightarrow 0} \int db P_0(b)\mathcal{L}_\varepsilon(b + \lambda) \quad (38)$$

gives the contribution of the pure-point spectrum, originating from localized states, to the overall spectral density.

This concludes the general framework.

### 3. Results

In what follows, we report results for a variety of different ensembles of sparse random matrices, in order to explore the capabilities and limitations of our approach. In order to properly appreciate the results presented below, it is worth pointing out that within our stochastic population-dynamics based approach to solving the fixed point equations (30) and (31), the integrals (32), or (35), (37) are evaluated by *sampling* from a population. Denoting by  $\mathcal{N}$  the number of samples  $(a_i, b_i)$  taken, we have, e.g.,

$$\overline{\rho(\lambda)} \simeq \frac{1}{\mathcal{N}} \left[ \sum_{\substack{i=1 \\ a_i=0}}^{\mathcal{N}} \mathcal{L}_\varepsilon(b_i + \lambda) + \frac{1}{\pi} \sum_{\substack{i=1 \\ a_i>0}}^{\mathcal{N}} \frac{a_i + \varepsilon}{(a_i + \varepsilon)^2 + (b_i + \lambda)^2} \right] \quad (39)$$

as an approximation of (37). The  $\varepsilon \rightarrow 0$ -limit is clearly singular in the first contribution to (39). If  $b_i + \lambda \neq 0$  for all  $b_i$  in the sample, one obtains zero in the  $\varepsilon \rightarrow 0$ -limit, whereas one obtains a diverging contribution, if  $b_i + \lambda = 0$  for at least one  $b_i$  in the sample. The second alternative will quite generally be an event of probability zero, so a small regularizing  $\varepsilon > 0$  must be kept in order to ‘see’ this contributions (if it exists). In what follows, we shall refer to the two contributions to (37), as  $\overline{\rho_s(\lambda)}$  and  $\overline{\rho_c(\lambda)}$ , with

$$\overline{\rho_s(\lambda)} \simeq \frac{1}{\mathcal{N}} \sum_{\substack{i=1 \\ a_i=0}}^{\mathcal{N}} \mathcal{L}_\varepsilon(b_i + \lambda) , \quad \overline{\rho_c(\lambda)} \simeq \frac{1}{\pi\mathcal{N}} \sum_{\substack{i=1 \\ a_i>0}}^{\mathcal{N}} \frac{a_i + \varepsilon}{(a_i + \varepsilon)^2 + (b_i + \lambda)^2} . \quad (40)$$

The population-dynamics algorithm itself is run with a small regularizing  $\varepsilon > 0$  (as required in (2) to guarantee existence of the integral). While running the algorithm, we use  $\varepsilon = 10^{-300}$ , which is close to the smallest representable real number in double-precision arithmetic on the machines used for the numerics.

### 3.1. Poisson Random Graphs — Gaussian Couplings

Our first results pertain to sparse matrices defined on Poisson random graphs, with Gaussian couplings. The left panel of Fig. 1 shows spectral densities for the case of mean connectivity  $c = 4$ , having Gaussian random couplings with  $\langle K_{ij}^2 \rangle = 1/c$ . For this system we find an integrable power-law divergence of the form

$$\bar{\rho}(\lambda) \simeq 0.05|\lambda|^{-0.61}, \quad \lambda \rightarrow 0, \quad (41)$$

and a  $\delta$  peak at  $\lambda = 0$ , the latter originating from isolated sites in the ensemble. Results of numerical diagonalizations (using a sample of 500  $N \times N$  matrices with  $N = 2000$  are shown for comparison, and the agreement is excellent.

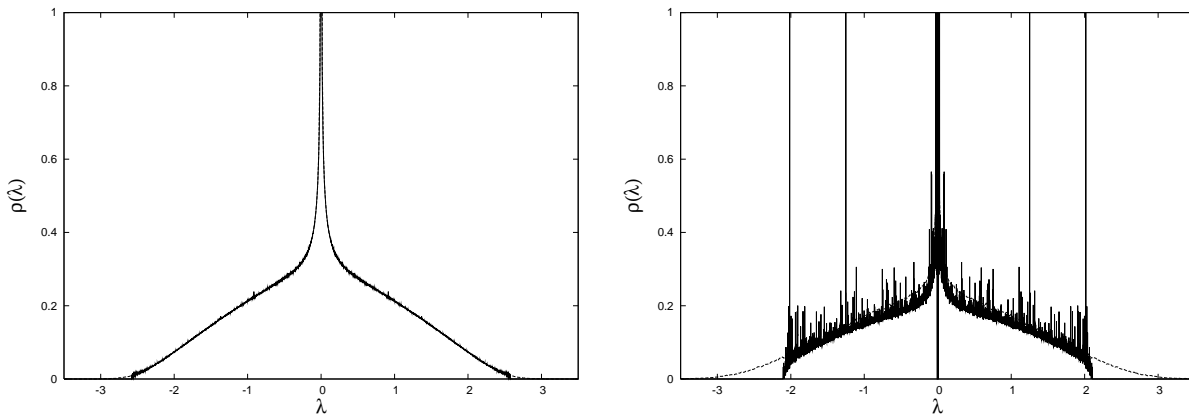


**Figure 1.** Spectral density for matrices defined on Poissonian random graphs with  $c = 4$  (left panel) and  $c = 2$  (right panel), having Gaussian random couplings with  $\langle K_{ij}^2 \rangle = 1/c$ . Full line: results obtained from the present theory; dashed line: results obtained from a sample of  $2000 \times 2000$  matrices. In both cases  $\varepsilon = 10^{-300}$  was used in the evaluation of (39).

The behaviour changes rather drastically if the average connectivity is reduced to  $c = 2$  — a value closer to the percolation threshold  $c_c = 1$ . In this case the spectral density shows strong fluctuations, when evaluated with the same small regularizer. These originate from  $\bar{\rho}_s$  in (40), and are related to the pure point spectrum associated with localized eigenstates coming from a collection of isolated finite clusters of all sizes in the ensemble. These exist for  $c = 4$  as well, but their contribution is too small to be easily notable when

combined with  $\overline{\rho}_c$  in (39). In addition, there is a central  $\delta$  peak as in the  $c = 4$ -case which appears to be separated from the main bands by a gap; see the second panel in Fig 2. The agreement with results of numerical diagonalization is fairly poor as it stands; in particular, exponential tails of localized states extending beyond the apparent edge of the central band are missed in this way. However, when (39) is evaluated with a regularizing  $\varepsilon = 10^{-3}$  comparable to the resolution of the  $\lambda$ -scan, the agreement is once more excellent as shown in Fig 2. It is worth noting in this context that numerical simulations, in which binning of eigenvalues is used to determine the spectral density *also imply a form of regularization*, and they do not distinguish continuous and singular contributions to the DOS if the distribution of the singular contributions is itself reasonably uniform.

When displayed on a logarithmic scale, the results clearly reveal two interesting features: (i) a localization transition at  $\lambda_c \simeq 2.295$ , characterised by a vanishing continuous contribution  $\overline{\rho}_c$  to (39) for  $|\lambda| > \lambda_c$ , and (ii) exponential (Lifshitz) tails [19] in the spectral density, related to localized states represented by the singular contribution  $\overline{\rho}_s$  to (39)), and exhibited only through regularization. We shall substantiate this analysis in the following sub-section by looking at the behaviour inverse participation ratios. The same phenomena are seen for  $c = 4$ , where  $\lambda_c \simeq 2.581$ .

### 3.2. Inverse Participation Ratios and Localization

In order to substantiate our identification of singular and continuous contributions to the spectral densities we look at Inverse Participation Ratios (IPRs) of eigenstates as obtained from numerical diagonalizations. Given eigenvectors  $\mathbf{v}$  of a (random) matrix, their IPRs are defined as

$$\text{IPR}(\mathbf{v}) = \frac{\sum_{i=1}^N v_i^4}{\left(\sum_{i=1}^N v_i^2\right)^2}. \quad (42)$$

As eigenvectors can always be chosen to be normalized, we see that IPRs remain of order 1 for localized states which have a few  $\mathcal{O}(1)$  eigenvector components — the extreme case being  $\text{IPR}(\mathbf{v}) = 1$  for  $v_i = \delta_{i,i_0}$  — whereas they are  $\mathcal{O}(N^{-1})$  for fully extended states for which  $v_i = \mathcal{O}(N^{-1/2})$  for all  $i$ .

Here we only produce a qualitative comparison for the two cases studied in the previous subsection, comparing IPRs computed for systems of size  $N = 100$  and  $N = 1000$ , and using scatter-plots of IPRs vs eigenvalues to exhibit the salient features. As clearly visible, there remains a substantial fraction of states at all  $\lambda$  in the  $c = 2$  case, which do *not* exhibit the  $N^{-1}$  scaling of IPRs expected for delocalized states; the tails, and a small central band in particular appear to be *dominated* by localized states. By contrast in the  $c = 4$  case there is a notable depletion of states with  $\mathcal{O}(1)$  IPRs, except for  $\lambda = 0$  and in the tails of

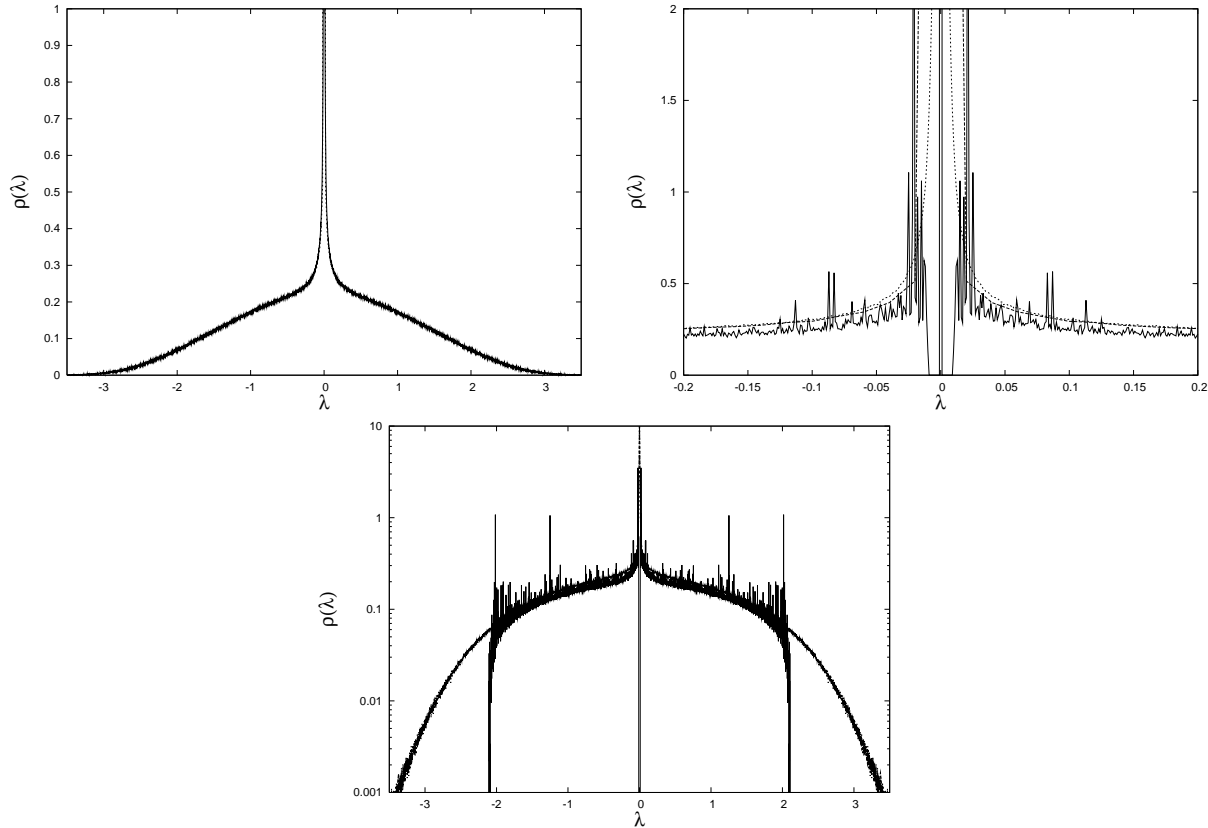


**Figure 2.** Upper left panel: Spectral density for matrices defined on Poissonian random graphs with  $c = 2$  as in the previous figure, but now evaluated with a regularizing  $\varepsilon = 10^{-3}$  in (39) (full line). At the resolution given the result is indistinguishable from the numerical simulation results (dashed line). Upper right panel: zoom into the central region comparing results obtained with the small regularizer, exhibiting a gap around the central peak (full line), with a larger regularizer  $\varepsilon = 10^{-3}$  (short dashed line) and with results of numerical diagonalization (long dashed line). The same comparison is made in the lower panel for a larger portion of the spectrum on a logarithmic scale. The regularized  $\varepsilon = 10^{-3}$ -results are on this scale indistinguishable from those of the numerical simulations. Note the localization transition and the Lifshitz tails as discussed in the main text.

the spectrum. These findings are entirely consistent with our identifications made in the previous subsection. We note that the role of regularization in identifying localized states has been pointed out before using heuristics related to the evaluation of *local* densities of state [22].

We shall return to this issue in greater quantitative detail in a separate paper devoted to Anderson localization in discrete random Schrödinger operators defined on sparse random graphs [33].

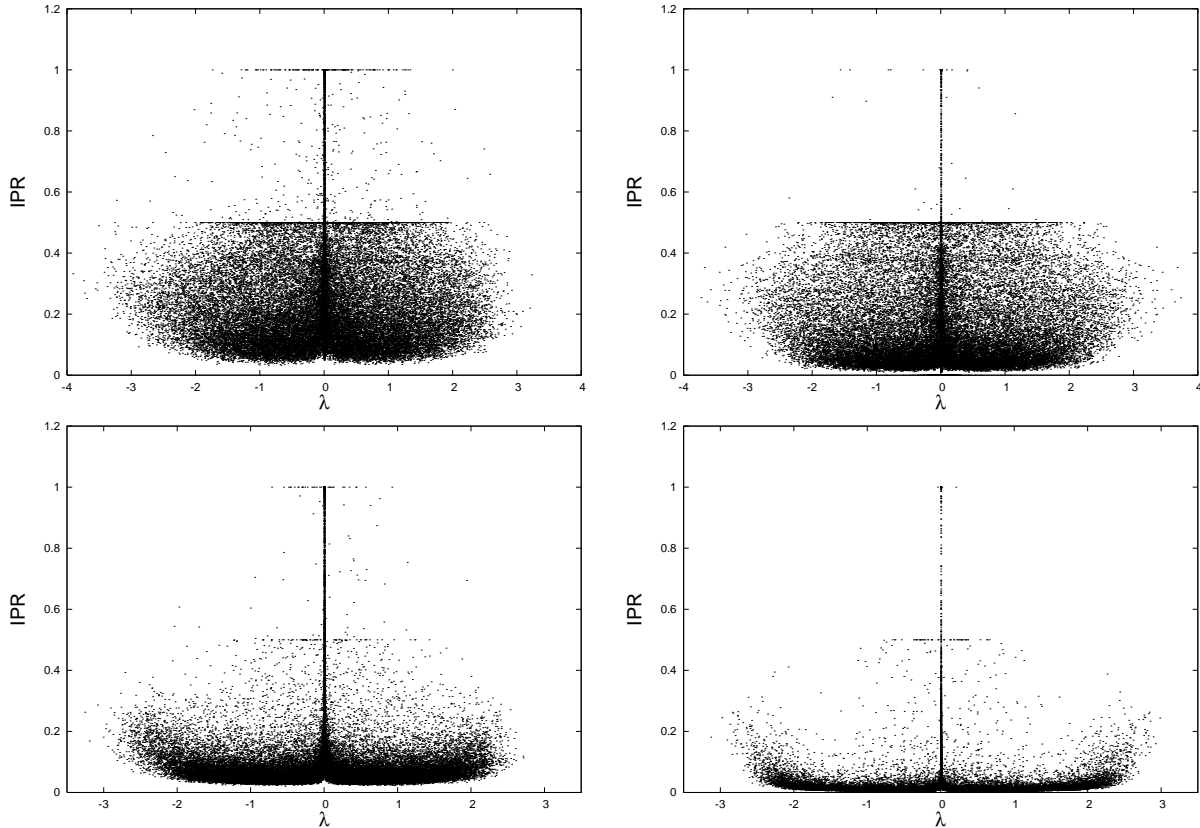


**Figure 3.** Scatterplots showing eigenvalue against IPRs for Poissonian random graphs with  $c = 2$  (first row) and  $c = 4$  (second row). The graphs in the left column correspond to  $N = 100$ , those in the right column to  $N = 1000$ .

### 3.3. Poisson Random Graphs — Bimodal Couplings

We can also look at coupling distributions different from Gaussian for the non-zero couplings, e.g. fixed  $K_{ij} = 1/\sqrt{c}$  or bi-modal  $K_{ij} = \pm 1/\sqrt{c}$ . As noted before [14], both give rise to the same spectral densities on large sparse (tree-like) graphs due to the absence of frustrated loops. It can also be seen as a consequence of the appearance of  $K^2$  in (28).

We choose a Poissonian random graph *at* the percolation threshold  $c = 1$  as an example that allows us to highlight both the strengths and the limitations of the present approach. It is known that all states will be localized for this system. In Fig 4 we compare results of a  $\lambda$ -scan with resolution  $\delta\lambda = 10^{-3}$ , using a regularizer  $\varepsilon = 10^{-4}$  for the scan. The smaller panels exhibit numerical diagonalization results, as well as a comparison between the two using a zoom into the region around  $\lambda = 1$ .

On the side of the strengths, we note that the spectral density obtained from our algorithm is able to display more details than can be exposed by simulation results obtainable at

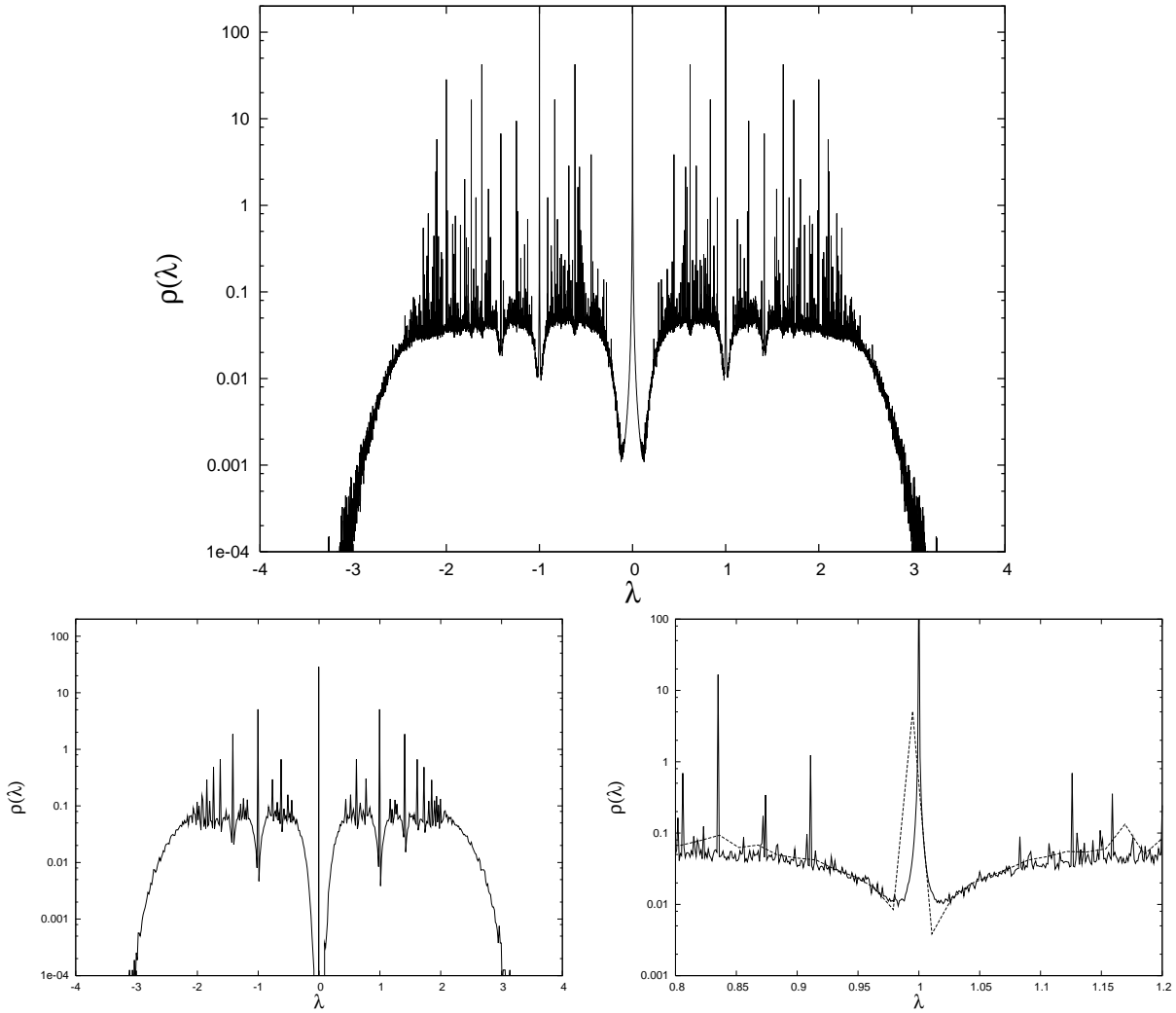


**Figure 4.** Comparison of spectral density for  $K_{ij} = \pm 1/\sqrt{c}$ , on a Poissonian random graph with  $c = 1$  as computed via the present algorithm (main panel) with results from numerical diagonalisation of  $N \times N$  matrices of the same type with  $N = 2000$  (lower left) and a direct comparison in the region around  $\lambda = 1$ .

reasonable effort. On the downside, one might note that the results for this system attain the status of semi-quantitative results, as they do depend on the chosen regularization, though in fairness it should be said that the same applies to the results obtained via numerical diagonalization where results vary with the binning resolution. In the present case this is due to the fact that the spectrum for most parts consists of a dense collection of  $\delta$  peaks [39]. A notable deficiency is the broadening of delta-peaks into Lorentzians of finite width, which creates artefacts around isolated delta-peaks, exemplified here by the peak at  $\lambda = 0$ . Since the origin of this deficiency is understood, more precise details can, if desired, be recovered by choosing a smaller regularizing  $\varepsilon$ .

### 3.4. Regular and Scale-Free Random Graphs

In the present section we consider matrices defined on regular and scale-free random graphs.

*3.4.1. Regular Random Graphs* Our theory applies unmodified to matrices defined on graphs with degree distributions other than Poissonian, as long as the *mean connectivity remains finite*. We use this fact to obtain spectra of matrices with Gaussian random couplings defined on regular random graphs with fixed connectivity  $c$ , choosing  $\langle K_{ij}^2 \rangle = 1/c$  for the couplings. Results for  $c = 4$  and  $c = 100$  are shown in Fig. 5. The  $c = 4$  results are compared with simulations, with results analogous to previous cases, including the presence of a localization transition at  $\lambda_c \simeq 2.14$

The second example is chosen as a test to see the semicircular law [40] reemerge in the limit of large (though finite) connectivity. This limit can also be extracted from the fixed point equations. It is somewhat easier to verify for results pertaining to single instances [32] than for the ensemble.

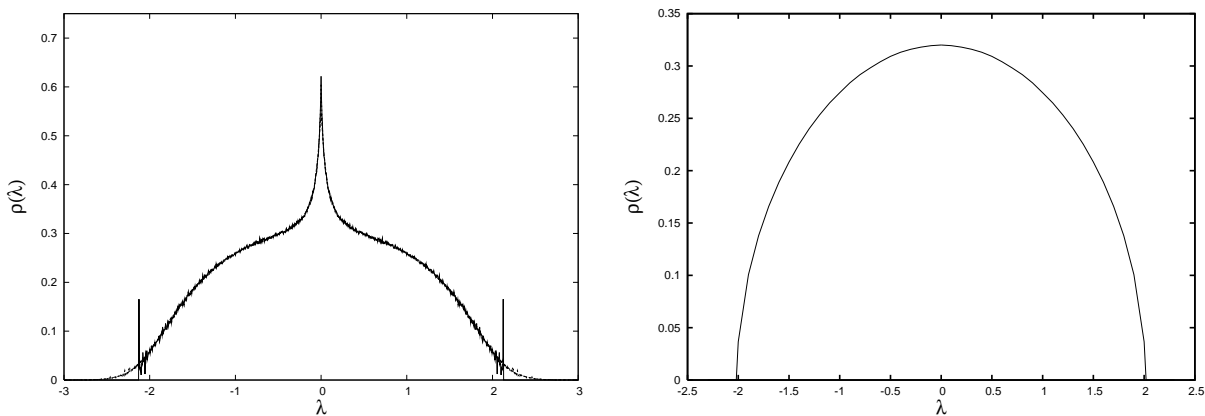


**Figure 5.** Spectral densities for a random graph with fixed connectivity  $c = 4$  (left), and on a random graph with fixed non-random connectivity  $c = 100$  (right).

*3.4.2. Scale-Free Graphs* We have also looked at a scale free graph with connectivity distribution given by  $p(k) = P_0 k^{-\gamma}$  with  $\gamma = 4$  and a lower cut-off at  $k = 2$ . Results shown in Fig. 6 reveal a continuous central band, and localized states for  $|\lambda| > \lambda_c \simeq 2.85$  much as in the other cases. For the present system, the tails in the spectral density follow a power law of the form  $\rho(\lambda) \sim \lambda^{1-2\gamma}$  [17, 41].

Comparison with exact diagonalization results is facilitated by a fast algorithm that allows to generate sparse graphs with arbitrary degree distribution [42].

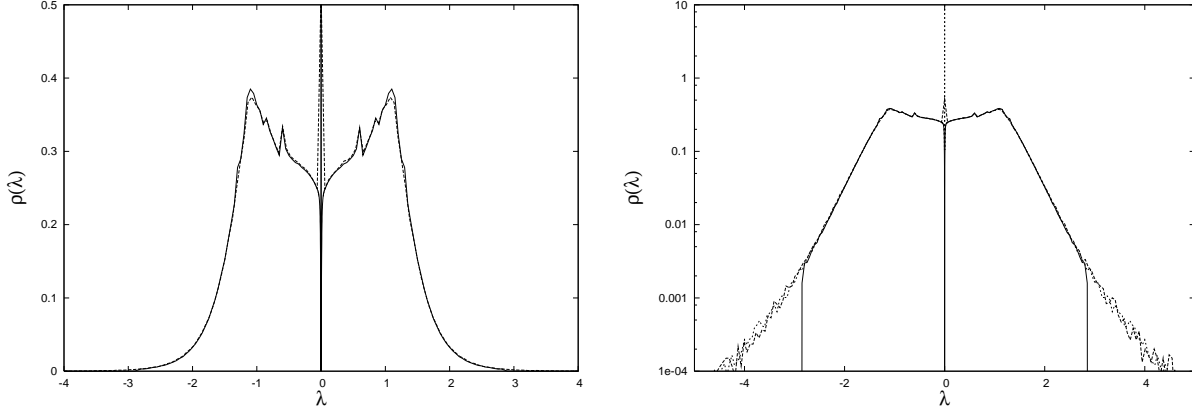


**Figure 6.** Spectral density for for  $K_{ij} = \pm 1/\sqrt{c}$  on a random graph with power-law degree distribution of average connectivity  $c \simeq 2.623$ . Left panel: results obtained with small regularizer (full line), and numerical diagonalization results from a sample of 500 matrices of dimension  $N = 2000$  (dashed line). Right panel: the same results displayed on a logarithmic scale, this time with results regularized at  $\varepsilon = 10^{-3}$  (short dashed line) included.

### 3.5. Graph Laplacians

Let us finally look at matrices row-constraints, such as related to discrete graph-Laplacians.

The discrete graph Laplacian of a graph with connectivity matrix  $C = \{c_{ij}\}$  has matrix elements

$$\Delta_{ij} = c_{ij} - \delta_{ij} \sum_k c_{ik} . \quad (43)$$

A quadratic form involving the Laplacian can be written in the form

$$\frac{1}{2} \sum_{ij} \Delta_{ij} u_i u_j = -\frac{1}{4} \sum_{ij} c_{ij} (u_i - u_j)^2 . \quad (44)$$

As before we shall be interested in more general matrices with zero row-sum constraint of the form

$$M_{ij} = c_{ij} K_{ij} - \delta_{ij} \sum_k c_{ik} K_{ij} . \quad (45)$$

To evaluate the spectral density within the present framework one would thus have to compute

$$\overline{Z_N^n} = \int \prod_{ia} \frac{du_{ia}}{\sqrt{2\pi/i}} \exp \left\{ -\frac{i}{2} \lambda_\varepsilon \sum_{i,a} u_{ia}^2 + \frac{c}{2N} \sum_{ij} \left( \left\langle \exp \left( \frac{iK}{2} \sum_a (u_{ia} - u_{ja})^2 \right) \right\rangle_K - 1 \right) \right\}$$

instead of (5). The required modification has, of course, been noted earlier [15, 43]. The resulting problem constitutes precisely (the harmonic variant of) the translationally invariant systems, for which the framework in [30] was developed in the first place. The general theory can be copied word for word, and the fixed point equations (30), (31) remain formally unaltered except for the change in  $Z_2(\omega, \omega', K)$  in (23), owing to the modified interaction term, which gives rise to a modified expression for  $\hat{\Omega}(\omega', K)$  in (28). We obtain

$$\hat{\Omega}(\omega', K) = \frac{K\omega'}{K - i\omega'} \quad (46)$$

instead of (28). Fig. 7 shows the spectrum of a Laplacian for a Poisson random graph with  $c = 2$ , comparing our solution (upper left panel) computed with  $\varepsilon = 10^{-3}$  with numerical diagonalization results in the upper right panel. We use  $K_{ij} \equiv 1/c$  for the non-zero matrix elements in this case. As in the other cases, we observe a localization transition, here at  $\lambda_c \simeq -3.98$ . Results obtained with a small regularizer  $\varepsilon = 10^{-300}$  exhibiting only the continuous part of the spectrum are shown in the lower panel.

### 3.6. Unfolding Spectral Densities

As a last item in this study we look at the possibility of unfolding the spectral density according to contributions of local densities of state, coming from vertices of different coordination, as suggested by Eq. (32). This method has been used in [30] to look at distributions of Debye-Waller factors in amorphous systems, unfolded according to local coordinations. In the present context it may provide an interesting diagnostic tool to help understanding localization phenomena.

Fig 8 exhibits the spectrum of the graph Laplacian shown in the previous figure along with its unfolding into contributions of local densities of state with different coordination. The present example clearly shows that — somewhat paradoxically — the well connected sites are the ones providing the dominant contributions to localized states in the lower band-edge Lifshitz tails. The clearly identifiable humps in the figure correspond from left to right to  $k = 9$ ,  $k = 8$ ,  $k = 7$ ,  $k = 6$ ,  $k = 5$ ,  $k = 4$ , and  $k = 3$ , which easily allows to identify the corresponding contributions to the spectral density, the contribution of  $k = 2$  gives rise to several notable humps in the spectral density, and together with the  $k = 1$  contribution is mainly responsible for the dip at  $\lambda = -1$ . The  $k = 0$  contribution is mainly responsible for the  $\delta$ -peak at  $\lambda = 0$  (which is broadened into a Lorentzian of width  $\varepsilon = 10^{-3}$  due to the regularization, as discussed earlier).

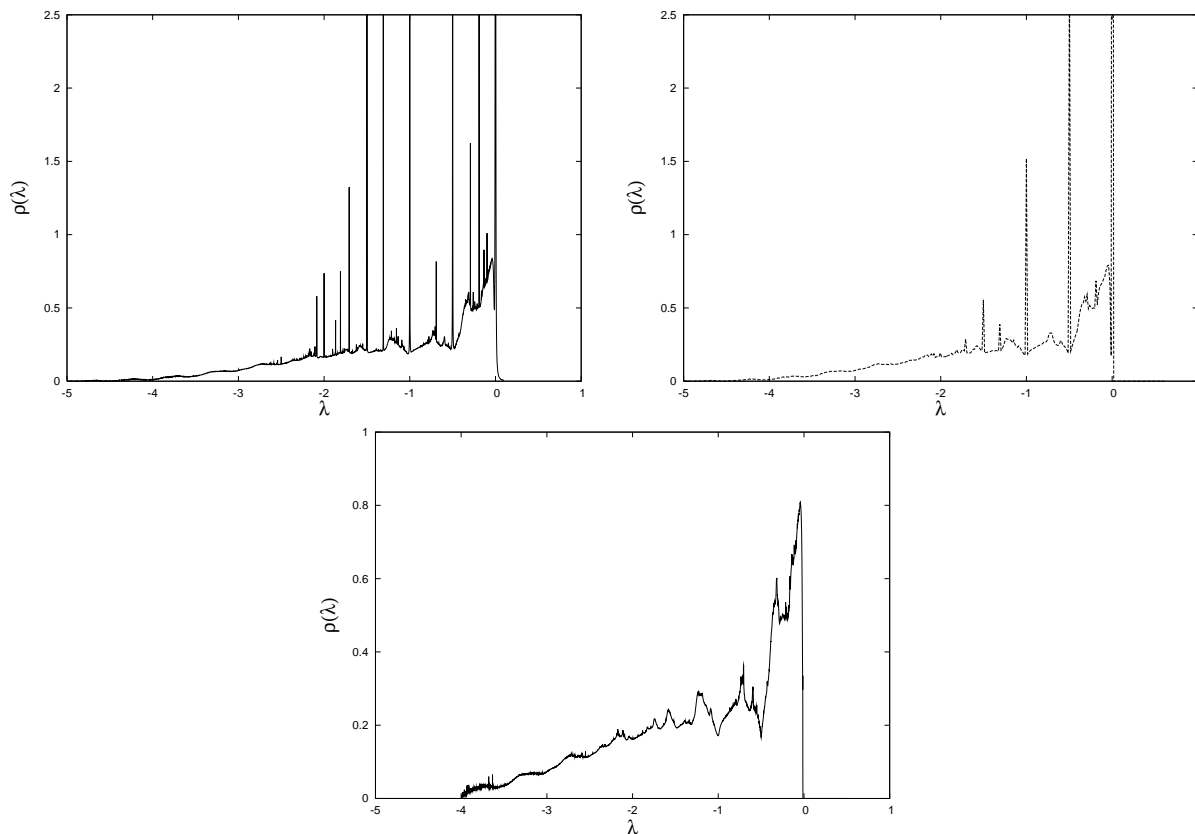


**Figure 7.** Spectral density for the Laplacian on a Poissonian random graph with  $c = 2$  as computed via the present algorithm. Upper left panel:  $\varepsilon = 10^{-3}$ -results; upper right panel: results from numerical diagonalisation of  $N \times N$  matrices of the same type with  $N = 2000$ . Lower panel: continuous part of the spectrum obtained using  $\varepsilon = 10^{-300}$  as a regularizer.

#### 4. Conclusions

In the present paper we have used a reformulation of the replica approach to the computation of spectral densities for sparse matrices, which allows to obtain spectral densities in the thermodynamic limit to any desired detail — limited only by computational resources. Our method is versatile in that it allows to study systems with arbitrary degree distributions, as long as they give rise to connectivity distributions with finite mean. A cavity approach that emphasises results on finite instances will appear elsewhere [32]. As expected (and well known), the Wigner semi-circle reemerges in the large  $c$  limit as discussed in [32]. Large and small  $\lambda$  asymptotics remain to be investigated. Our method allows to expose the separate contributions of localized and extended states to the spectral density, and thereby to study localization transitions. We shall explore this issue in greater detail in a separate publication. Indeed, with results for graph-Laplacians

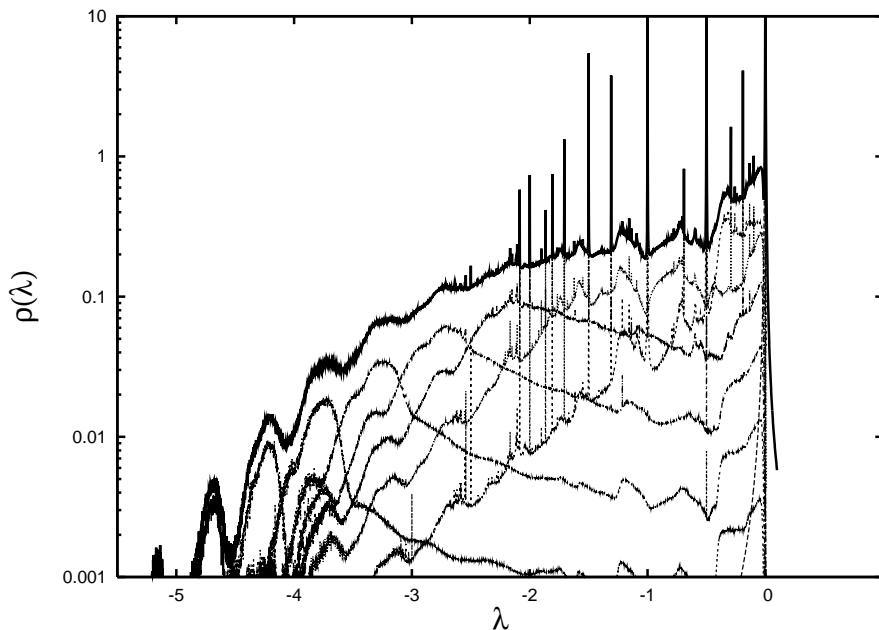


**Figure 8.** Spectral density for the Laplacian on a Poissonian random graph with  $c = 2$  (full upper line), shown together with its unfolding according to contributions of different coordination, as discussed in the main text.

in hand, the step towards a study of discrete random Schrödinger operators and Anderson localization in such systems is just around the corner [33]. A generalization to asymmetric matrices using both the cavity method and a replica approach for the ensemble along the lines of [44] is currently under investigation in our group [45]. Other problems we have started to look at are spectra of modular systems [46] and small world networks.

We believe our results to constitute an improvement over previous asymptotic results as well as over results obtained by closed form approximations. They may open the way to further interesting lines of research. Let us here mention just a few such examples: within RMT proper, one might wish to further investigate the degree of universality of level correlations in these systems [47]; one could refine the random matrix analysis of financial cross-correlations [7] by taking non-trivial degree distributions of economic interactions into account, or one might wish to look at finite connectivity variants of random reactance networks [48], taking e.g. regular connectivity 4 to compare with results of numerical simulations of such systems on two-dimensional square lattices.

**Acknowledgements** It is a pleasure to thank Güler Ergün, Jort van Mourik, Isaac Pérez-Castillo, Tim Rogers and Koujin Takeda for illuminating discussions. Jort van Mourik also kindly supplied instances of scale free-random graphs to allow comparison of ensemble results and results from numerical diagonalization in this case.

## Appendix A. Population Dynamics

The stochastic algorithm used to solve (30), (31) takes the following form. Populations  $\{\omega_i; 1 \leq i \leq N_p\}$  and  $\{\hat{\omega}_i; 1 \leq i \leq N_p\}$  are randomly initialized with  $\text{Re } \omega_i > 0$  and  $\text{Re } \hat{\omega}_i > 0$ .

Then the following steps are iterated

1. Generate a random  $k \sim \frac{k}{c} p_c(k)$ .
2. Randomly select  $k - 1$  elements from  $\{\hat{\omega}_i; 1 \leq i \leq N_p\}$ ; compute

$$\Omega = i\lambda_\varepsilon + \sum_{j=1}^{k-1} \hat{\omega}_{i_j} , \quad (\text{A.1})$$

and replace  $\omega_i$  by  $\Omega$  for a randomly selected  $i \in \{1, \dots, N_p\}$ .

3. Select  $j \in \{1, \dots, N_p\}$  at random, generate a random  $K$  according to distribution of bond strengths; compute

$$\hat{\Omega} = \frac{K^2}{\omega_j} \quad , \quad \left( \text{or } \hat{\Omega} = \frac{K\omega_j}{K - i\omega_j} \text{ for zero row-sums} \right) , \quad (\text{A.2})$$

and replace  $\hat{\omega}_i$  by  $\hat{\Omega}$  for a randomly selected  $i \in \{1, \dots, N_p\}$ .

4. return to 1.

This algorithm is iterated until populations with stable distributions of  $\{\hat{\omega}_i; 1 \leq i \leq N_p\}$  and  $\{\omega_i; 1 \leq i \leq N_p\}$  are attained.

A variant of this algorithm when implemented on instances of real graphs generates the belief-propagation or cavity equations for this problem, as studied in [32]. It can be derived directly in terms iterative evaluations of (2) on locally tree-like graphs.

## References

- [1] E. P. Wigner. On the Statistical Distribution of the Widths and Spacings of Nuclear Resonance Levels. *Proc. Cambr. Philos. Soc.*, 47:790–798, 1951.
- [2] R. M. May. Will a Large Complex System be Stable? *Nature*, 238:413–414, 1972.
- [3] D. J. Thouless. Maximum Metallic Resistance in Thin Wires. *Phys. Rev. Lett.*, 39:1167–1169, 1977.
- [4] O. Bohigas, M. J. Giannoni, and C. Schmit. Characterization of Chaotic Quantum Spectra and Universality of Level Fluctuation Laws. *Phys. Rev. Lett.*, 52:1–4, 1984.
- [5] J. Verbaarschot. The Spectrum of the QCD Dirac Operator and Chiral Random Matrix Theory: The Threefold Way. *Phys. Rev. Lett.*, 72:2531–2533, 1994.
- [6] L. Laloux, P. Cizeau, J.-P. Bouchaud, and M. Potters. Noise Dressing of Financial Correlation Matrices. *Phys. Rev. Lett.*, 83:1467–1470, 1999.
- [7] V. Plerou, P. Gopikrishnan, B. Rosenow, L. A. N. Amaral, and H. E. Stanley. Universal and Non-Universal Properties of Cross-Correlations in Financial Time Series. *Phys. Rev. Lett.*, 83:1471–1474, 1999.

- [8] A. Cavagna, I. Giardina, and G. Parisi. Analytic Computation of the Instantaneous Normal Modes Spectrum in Low Density Liquids. *Phys. Rev. Lett.*, 83:108–111, 1999.
- [9] K. Broderix, K.K. Bhattacharya, A. Cavagna, A. Zippelius, and I. Giardina. Saddles on the Potential Energy Landscape of a Lennard-Jones Liquid. *AIP Conf. Proceedings*, 553:23–27, 2001.
- [10] R. Kühn and U. Horstmann. Random Matrix Approach to Glassy Physics: Low Temperatures and Beyond. *Phys. Rev. Lett.*, 78:4067–4070, 1997.
- [11] R. Kühn. Universality in Glassy Low-Temperature Physics. *Europhys. Lett.*, 62:313–319, 2003.
- [12] J.P. Keating and N.C. Snaith. Random Matrix Theory and L-Functions at  $s = 1/2$ . *Comm. Math. Phys.*, 214:91–110, 2000.
- [13] T. Guhr, A. Müller-Groeling, and H. A. Weidenmüller. Random Matrix Theories in Quantum Physics: Common Concepts. *Phys. Rep.*, 299:190–425, 1998.
- [14] G. J. Rodgers and A. J. Bray. Density of States of a Sparse Random Matrix. *Phys. Rev. B*, 37:3557–3562, 1988.
- [15] A. J. Bray and G. J. Rodgers. Diffusion in a Sparsely Connected Space: A Model for Glassy Relaxation. *Phys. Rev. B*, 38:11461–11470, 1988.
- [16] R. Albert and A.-L. Barabási. Statistical Mechanics of Complex Networks. *Rev. Mod. Phys.*, 74:47–97, 2002.
- [17] S. N. Dorogovtsev, A. V. Goltsev, J. F. F. Mendes, and A. N. Samukhin. Spectra of Complex Networks. *Phys. Rev. E*, 68(4):046109, 2003.
- [18] K. Broderix, T. Aspelmeier, A.K. Hartmann, and A. Zippelius. Stress Relaxation of Near-Critical Gels. *Phys. Rev. E*, 64:021404, 2001.
- [19] O. Khorunzhiy, W. Kirsch, and P. Müller. Lifshitz Tails for Spectra of Erdős-Renyi Random Graphs. *Ann. Appl. Prob.*, 16:295–309, 2006, arXiv:math-ph/0502054.
- [20] R. B. Griffiths. Nonanalytic Behavior Above the Critical Point in a Random Ising Ferromagnet. *Phys. Rev. Lett.*, 23:17–19, 1969.
- [21] S. N. Evangelou. Spectral Density Singularities, Level Statistics. and Localization in a Sparse Random Matrix Ensemble. *Phys. Rev. Lett.*, 68:361–364, 1992.
- [22] S. Ciliberti, T. S. Grigera, V. Martín-Mayor, G. Parisi, and P. Verrocchio. Anderson Localization in Euclidean Random Matrices. *Phys. Rev. B*, 71:153104, 2005.
- [23] G. Biroli and R. Monasson. A Single Defect Approximation for Localized States on Random Lattices. *J. Phys. A*, 32:L255–L261, 1999.
- [24] G. Semerjian and L. F. Cugliandolo. Sparse Random Matrices: The Eigenvalue Spectrum Revisited. *J. Phys. A*, 35:4837–4851, 2002.
- [25] T. Nagao and G. J. Rodgers. Spectral Density of Complex Networks with a Finite Mean Degree. arXiv:cond-mat/08031042, 2008.
- [26] K.-I. Goh, B. Kahng, and D. Kim. Spectra and Eigenvectors of Scale-Free Networks. *Phys. Rev. E*, 64:051903, 2001.
- [27] R. Monasson. Optimization Problems and Replica Symmetry Breaking in Finite Connectivity Spin-Glasses. *J. Phys. A*, 31:513–529, 1998.
- [28] M. Mézard and G. Parisi. The Bethe Lattice Spin Glass Revisited. *Eur. Phys. J. B*, 20:217–233, 2001.
- [29] A.C.C. Coolen, N S Skantzou, I. Pérez-Castillo, C .J. Pérez-Vicente, J. P. L. Hatchett, B. Wemmenhove, and T. Nikolettopoulos. Finitely Connected Vector Spin Systems with Random Matrix Interactions. *J. Phys. A*, 38:8289–8317, 2005.
- [30] R. Kühn, J. van Mourik, M. Weigt, and A. Zippelius. Finitely Coordinated Models for Low-Temperature Phases of Amorphous Systems. *J. Phys. A*, 40:9227–9252, 2007.
- [31] S. F. Edwards and R. C. Jones. The Eigenvalue Spectrum of a Large Symmetric Random Matrix. *J. Phys. A*, 9:1595–1603, 1976.

- [32] T. Rogers, I. Pérez-Castillo, R. Kühn, and K. Takeda. Cavity Approach to the Spectral Density of Sparse Symmetric Random Matrices. *arXiv:cond-mat/0803.1553*, 2008.
- [33] R. Kühn and J. van Mourik. Localization in Random-Schrödinger Operators on Sparse Random Graphs. *work in progress*, 2008.
- [34] G. J. Rodgers, K. Austin, B. Kahng, and D. Kim. Eigenvalue Spectra of Complex Networks. *J. Phys. A*, 38:9431–9437, 2005.
- [35] D. Kim and B. Kahng. Spectral densities of scale-free networks. *arXiv:cond-mat/0703055*.
- [36] L. Viana and A. J. Bray. Phase Diagrams for Dilute Spin Glasses. *J. Phys. C*, 18:3037–3051, 1985.
- [37] I. Kanter and H. Sompolinsky. Mean-Field Theory of Spin-Glasses with Finite Coordination Number. *Phys. Rev. Lett.*, 58:164–167, 1987.
- [38] Y. V. Fyodorov and A. D. Mirlin. On the Density of States of Sparse Random Matrices. *J. Phys. A*, 24:2219–2223, 1991.
- [39] O. Golinelli. Statistics of Delta Peaks in the Spectral Density of Large Random Trees. *arXiv:cond-mat/0301437*, 2003.
- [40] E. P. Wigner. On the Distribution of the Roots of Certain Symmetric Matrices. *Ann. Math.*, 67:325–327, 1958.
- [41] M. Mihail and C. Papadimitriou. On the Eigenvalue Power Law. *Lect. Notes Comput. Sci.*, 2483:254–262, 2002.
- [42] J. van Mourik and Y. Kabashima. The Polynomial Error Probability for LDPC Codes. *arXiv:cond-mat/0310177*, 2003.
- [43] J. Ståring, B. Mehlige, Y. V. Fyodorov, and J. M. Luck. Random symmetric Matrices with a Constraint: The Spectral Density of Random Impedance Networks. *Phys. Rev. E*, 67:047101, 2003.
- [44] F. Haake, F. Izrailev, N. Lehmann, D. Saher, and H.-J. Sommers. Statistics of Complex Levels of Random Matrices for Decaying Systems. *Z. Phys. B*, 88:359–370, 1992.
- [45] K. Anand and T. Rogers. *work in progress*. 2008.
- [46] G. Ergün and R. Kühn. Spectra of Sparsely Connected Modular Random Matrices. *to be published*, 2008.
- [47] A. D. Mirlin and Y. V. Fyodorov. Universality of Level Correlation Function of Sparse Random Matrices. *J. Phys. A*, 24:2273–2286, 1991.
- [48] Y. V. Fyodorov. Spectral Properties of Random Reactance Networks and Random Matrix Pencils. *J. Phys. A*, 32:7429–7446, 1999.